Divergent metabolism between *Trypanosoma congolense* and *Trypanosoma brucei* results in differential drug sensitivity

P. C. Steketee[1*], E. A. Dickie[2], J. Iremonger[1], K. Crouch[2], E. Paxton[1], S. Jayaraman[1], O. A. Alfituri[1], G. Awuah-Mensah[3], R. Ritchie[2], A. Schnaufer[4], H. P. de Koning[5], C. Gadelha[3], B. Wickstead[3], M. P. Barrett[2,6] and L. J. Morrison[1]

[1]The Roslin Institute, Royal (Dick) School of Veterinary Studies, University of Edinburgh, Edinburgh, UK

[2]Wellcome Centre foar Integrative Parasitology, Institute of Infection, Immunity and Inflammation, University of Glasgow, Glasgow, UK

[3]School of Life Sciences, University of Nottingham, Nottingham, UK

[4]Institute of Immunology and Infection Research, University of Edinburgh, Edinburgh, UK

[5]Institute of Infection, Immunity and Inflammation, University of Glasgow, Glasgow, UK

[6]Glasgow Polyomics, University of Glasgow, UK

*Corresponding author: Pieter.Steketee@ed.ac.uk

Abstract

Animal African Trypanosomiasis (AAT) is a debilitating livestock disease prevalent across sub-Saharan Africa, a main cause of which is the protozoan parasite *Trypanosoma congolense*. In comparison to the well-studied *T. brucei*, there is a major paucity of knowledge regarding the biology of *T. congolense*. Here, we use a combination of omics technologies and novel genetic tools to characterise core metabolism in *T. congolense* mammalian-infective bloodstream-form parasites, and test whether metabolic differences compared to *T. brucei* impact upon drug sensitivity. Like *T. brucei*, glycolysis plays a major part in *T. congolense* energy metabolism. However, the rate of glucose uptake is significantly reduced in *T. congolense*, with cells remaining viable when cultured in concentrations as low as 2 mM. Instead of pyruvate, the primary glycolytic endpoints are succinate, malate and acetate. Comparative transcriptomics analysis showed higher levels of activity associated with the mitochondrial pyruvate dehydrogenase complex, acetate generation and the succinate shunt in *T. congolense*. However, based on omics analysis and chemical inhibition, there does not appear to be significant levels of oxidative phosphorylation. Stable-isotope labelling of glucose enabled the comparison of carbon usage between *T. brucei* and *T. congolense*, highlighting differences in nucleotide and fatty acid metabolism. To validate the metabolic similarities and differences, both species were treated with pharmacological inhibitors, confirming a lack of essential electron transport chain activity in *T. congolense,* but increased sensitivity to inhibition of mitochondrial pyruvate import. Strikingly, *T. congolense* exhibited significant resistance to inhibitors of fatty acid synthesis, including a 780-fold greater EC_{50} against the lipase and fatty acid synthase inhibitor Orlistat, compared to *T. brucei*. These data highlight that bloodstream form *T. congolense* diverges from *T. brucei* in key areas of metabolism, with several features that are intermediate between bloodstream- and insect-stage *T. brucei*. These results have implications for drug development, mechanisms of drug resistance and host-pathogen interactions.

Introduction

The hemoflagellate protozoan parasite *Trypanosoma congolense* is a primary causative agent of animal African trypanosomiasis (AAT), which can also be caused by *T. vivax* and *T. brucei* [1]. AAT accounts for livestock deaths in excess of 3 million annually with up to 120 million cattle at risk [2-4]. Thus, AAT is one of the most important livestock diseases across sub-Saharan Africa.

Current methods of AAT control centre around chemotherapy and prophylaxis (reviewed in [3]), but the very few available veterinary trypanocidal drugs have been used extensively for decades, resulting in resistance and inadequate protection against AAT [5-7]. As such, there is a dire need for the development of new and improved chemotherapeutics to manage AAT [3, 8].

Most of our biological understanding of African trypanosomes derives from studies on *T. brucei*, subspecies of which, *T. b. gambiense* and *T. b. rhodesiense,* cause Human African Trypanosomiasis (HAT) [9]. The ability to culture both procyclic (PCF; tsetse fly) and bloodstream (BSF; mammalian) forms of *T. brucei in vitro*, combined with its tractability with respect to genetic manipulation, have enabled extensive study of this species on a molecular level [10, 11]. In stark contrast, very few *T. congolense* strains are amenable to continuous bloodstream form (BSF) culture, with a single strain (IL3000) used in most studies [12]. Whilst genetic modification is possible in *T. congolense* PCF stage, routine BSF transfection has only recently become possible [13-15]. Additionally, although *T. congolense* exhibits a superficially similar morphology and life cycle to *T. brucei* [16, 17] emerging evidence increasingly suggests that *T. brucei, T. congolense* and *T. vivax* exhibit some profound differences at the genomic level [18-22], including in genes and phenotypes of direct relevance to infection biology and disease epidemiology. However, there is a lack of understanding to what extent these genetic differences translate into biological differences, including with respect to metabolism.

Understanding metabolism is critical to identifying how pathogens survive and thrive in the varying host environments they encounter, as well as being a means of elucidating drug targets, modes of drug action and mechanisms of drug resistance [23-25]. *T. brucei* metabolism has been extensively studied, aided by the application of technologies such as liquid chromatography-mass spectrometry (LC-MS) and nuclear magnetic resonance (NMR) spectroscopy (reviewed in detail by [26, 27]), which enable global profiling of the cellular metabolome.

The BSF stage of *T. brucei* utilizes the high levels of glucose available in the mammalian bloodstream, and depends almost exclusively on the glycolytic pathway to generate ATP [28]. The first seven steps of glycolysis are encompassed by a specialized organelle, the glycosome, which maintains its own ATP/ADP and NAD/NADH balance, allowing glycolysis to proceed at an extraordinarily high rate in comparison to other eukaryotic cells [29]. The endpoint of glycolysis, pyruvate, is a primary waste product of *T. brucei*, and excreted from the cell in large quantities. As a result, only small amounts of pyruvate are further metabolized in the mitochondrion to acetyl-CoA by pyruvate dehydrogenase (PDH), with

acetate the main excretory metabolite in this secondary, yet essential pathway [30]. The acetyl-CoA generated from this pathway is utilized, at least partially, for the *de novo* synthesis of fatty acids [31]. Indeed, both BSF and PCF *T. brucei* are highly sensitive to the lipase and fatty acid synthase inhibitor Orlistat [32].

Conversely, in the absence of blood meals, glucose is scarce in the tsetse fly midgut [33], and the main energy source of PCF *T. brucei* is L-proline, the catabolism of which leads to production of acetate, succinate and L-alanine through a more developed and active mitochondrion (including an active respiratory chain capable of generating ATP, as opposed to the inactive respiratory chain in BSF *T. brucei* [34]). Until recently, it was thought that PCF *T. brucei* did not exhibit active TCA metabolism, although recent data have shown that TCA intermediates such as succinate and 2-oxoglutarate can stimulate PCF *T. brucei* growth. [35-37].

Among the glycolytic enzymes, *T. brucei* expresses three isoforms of phosphoglycerate kinase, which catalyze the conversion of 1,3-bisphosphoglycerate to 3-phosphoglycerate [38]. These are developmentally regulated, with the major isoform in BSF parasites present in the glycosome (PGK-C), whilst the primary PCF isoform is found in the cytosol (PGK-B) [39]. The localization of PGK-B in the PCF cytosol is thought to result in an ATP/ADP imbalance in the glycosome, which is rectified by upregulating the glycosomal “succinate shunt”, a pathway that includes the ATP-generating phospho*enol*pyruvate carboxykinase (PEPCK)- and pyruvate phosphate dikinase (PPDK)-mediated conversion of phospho*enol*pyruvate (PEP) to oxaloacetate and pyruvate respectively [39, 40]. The succinate shunt, combined with amino acid metabolism, results in the excretion of high levels of succinate in PCF *T. brucei* [41].

Stable isotope labelling data has revealed that BSF *T. brucei* utilize D-glucose to a greater extent than first realized, with heavy carbons disseminating into amino acid, lipid and nucleotide metabolism [42]. This study also showed that some of the succinate and malate excreted from BSF parasites originates from glycolysis and, unexpectedly, inhibition of PEPCK is lethal at this life-cycle stage [42]. It has also been shown that acetate production is essential to BSF *T. brucei*, in particular for the synthesis of fatty acids (FAs) [30]. However, acetate excretion, as well as that of succinate and malate, is negligible in BSF *T. brucei* compared to that of pyruvate and L-alanine.

In contrast to *T. brucei*, the literature on metabolism in *T. congolense* is scarce. More than half a century ago it was suggested that BSF *T. congolense* has a significantly lower rate of glucose consumption compared to BSF *T. brucei* [43]. Furthermore, pyruvate is not the main glycolytic end product and instead, acetate and succinate are excreted at high levels,

indicative of metabolism more akin to PCF *T. brucei* [43]. Further work has revealed additional differences that support this hypothesis [44-46]. For example, BSF *T. congolense* primarily expresses cytosolic PGK-C, rather than glycosomal PGK-B [46]. Microscopy has also revealed a more developed mitochondrion in BSF *T. congolense*, with visible cristae, suggesting that mitochondrial energy metabolism could play a more prominent role in BSF *T. congolense* [47]. The high levels of acetate excretion first shown by Agosin & Von Brand [43] are consistent with this hypothesis. However, other studies have shown that BSF *T. congolense* is sensitive to inhibitors of Trypanosome Alternative Oxidase (TAO), including salicylhydroxamide (SHAM); and is insensitive to cyanide, suggesting that, as for BSF *T. brucei*, TAO is the sole terminal oxidase, responsible for reoxidising glycerol 3-phosphate, in BSF *T. congolense* [48-51]. Notably, nitroblue tetrazolium staining of BSF *T. congolense* does indicate the presence of NADH dehydrogenase (complex I) activity [48]. However, to date, no studies have assessed BSF *T. congolense* sensitivity to chemical inhibition of the electron transport chain, or the F_1F_0-ATPase.

Post-genomic technologies allow for the generation of large datasets that enable analysis of cellular processes on a systems scale, including metabolomics and transcriptomics. Integration of these data can provide a detailed snapshot of cell metabolism at the transcript and metabolite levels and help to dissect differences between species or conditions in unprecedented detail [52]. Furthermore, this knowledge can aid in predication and understanding of drug efficacy and mode of action

This study aimed to generate the first comprehensive overview of the metabolome of bloodstream-form *T. congolense* IL3000 parasites, allowing a global metabolic comparison of differences between *T. congolense* and *T. brucei*. Glycolytic metabolism in BSF *T. congolense* appears to be similar to PCF *T. brucei*, particularly in terms of metabolic outputs and gene expression. However, there are pronounced differences in parasite reliance on exogenous amino acids as well as carbon dissemination into pathways involved in nucleotide and lipid metabolism, as shown by stable isotope-labelled metabolomics. Using these data, we further validated these metabolic differences in *T. congolense* by pharmacological inhibition, which highlighted increased sensitivity to inhibition of mitochondrial pyruvate uptake, as well as significant resistance to inhibition of fatty acid synthesis, tested using inhibitors of fatty acid synthase and acetyl-coA synthetase. Taken together, these results suggest that *T. congolense* and *T. brucei* differ in some fundamental aspects of their core metabolism, which has important implications in terms drug sensitivity, and therefore, development of novel chemotherapeutics.

Results

Comparative RNA-sequencing of *T. congolense* and *T. brucei*

To permit direct comparison of BSF *T. congolense* and *T. brucei* at the transcriptome level, RNAseq analysis was carried out on parasites cultured *in vitro* and trypanosome samples isolated from infected mice at first peak parasitaemia (*ex vivo*) (Fig 1). Samples were prepared using *T. congolense* (strain IL3000, *in vitro* and *ex vivo*) and pleomorphic *T. brucei* (strain STIB 247; *in vitro* and *ex vivo*), to assess similarities and differences between trypanosomes grown in culture and those from an infection (Fig 1A and 1B), and to compare and contrast the transcriptome across the species (Fig 1C and 1D). Sequencing data were aligned to the respective genome sequence with a mean overall alignment rate of 88.0 ± 2.3% and 94.1 ± 0.7% for *T. brucei* and *T. congolense* reads, respectively. Resultant files were sorted and filtered for quality, and to minimize artefacts from multigene families, only uniquely aligned reads were used for downstream analyses. Read counts were normalised using transcripts per million (TPM) [53]. Orthologues were inferred between the species using Orthofinder [54], in order to compare directly TPM values for 1-to-1 orthologues, as well as sum-of-TPM values for groups containing families of paralogues (e.g. hexose transporters). These normalised read counts are henceforth referred to as orthoTPM values (S1 Table). The Orthofinder dataset (S2 Table) consisted of 6,677 orthogroups (denoted with the prefix “TbTc”), of which 5,398 (80.84%) were 1-to-1 orthologues. The Orthofinder tool was also used to predict genes only present in one of the two species (S2 Table). There are several metabolic genes that are not present in the *T. congolense* genome, including putative delta-4 and delta-6 desaturases (Tb927.10.7100 & Tb11.v5.0580), a succinate dehydrogenase subunit (SDH11; Tb927.8.6890) and guanine deaminase (Tb927.5.4560, Tb05.5K5.200 & Tb11.v5.0409), in addition to mitochondrial pyruvate carrier 1 (MPC1; Tb927.9.3780) (S2 Table).

Differences between four sample groups were assessed based on orthoTPM values (Fig 1; full dataset in S1 Table). There was a strong intra-species correlation between the *in vitro* and *ex vivo* conditions at the transcriptome level (*T. congolense* Pearson correlation coefficient, $\rho = 0.765$, Fig 1A; *T. brucei* $\rho = 0.803$, Fig 1B), showing that *in vitro*-derived BSF *T. congolense* and *T. brucei* closely resemble parasites isolated from infections at the transcriptome level. However, correlations between species even in the same condition were lower, implying transcriptional differences between the species (*ex vivo*: $\rho = 0.651$, Fig 1C; *in vitro*: $\rho = 0.687$, Fig 1D).

To compare data from this study to BSF *T. congolense* transcriptomics data generated by Silvester *et al*. (generated at ascending and peak parasitaemia [55]), TPM values for each

191 annotated *T. congolense* gene were compared directly (S1 Fig, S3 Table). There was good
192 correlation between both *in vitro* and *ex vivo T. congolense* BSF datasets and the data from
193 Silvester *et al.* (ρ > 0.8, S1 Fig), with the highest correlation being between the *ex vivo* and
194 ascending data as expected (ρ = 0.897, S1 Fig), albeit the correlation between the
195 'ascending' and 'peak parasitaemia' in Silvester *et al*. was higher (ρ = 0.979, S1 Fig).

196 *T. congolense* metabolite consumption and output

197 Global metabolite (metabolomics) analysis of *in vitro* culture supernatant samples provides a
198 detailed insight into the metabolic inputs and outputs of cultured cells [56]. However, high
199 levels of medium components can often mask subtle but significant changes in culture
200 medium composition over time. To counteract this, a modified culture medium was designed
201 for *T. congolense* strain IL3000, based on previous published medium formulations (SCM-3;
202 for details see Materials and Methods) [14, 15].

203 A time course was initiated in this medium. BSF *T. congolense* IL3000 cells during
204 exponential growth phase were inoculated into fresh medium (0 h time point). Culture
205 supernatant samples were collected at 0, 8, 24, 32, 48 and 56 hours (n = 4 at each time
206 point) and metabolites extracted for LC-MS analysis.

207 A total of 290 putative metabolites were detected across all samples (207 after removing
208 putative metabolites that did not map to metabolic pathways, e.g. peptides and medium
209 components), of which 37 were matched to an authentic standard to confidently predict their
210 identity (S4 Table).

211 80 of the 206 putative metabolites were significantly altered across the dataset (false
212 discovery rate-adjusted $P < 0.05$; one-way repeated measures ANOVA; Fig 2A and S4
213 Table). To analyse metabolites undergoing similar changes, K-means clustering with
214 Pearson correlation coefficient as the similarity metric was used, highlighting seven clusters
215 with two clusters of particular interest: one containing metabolites that accumulated over
216 time, and the other containing metabolites depleted over time (Fig. 2A). Log_2 fold change
217 (Log_2 FC) between the first and final time points (0 and 56 h, respectively) was also
218 calculated for each metabolite (S4 Table).

219 Glucose, the primary energy source for *T. brucei*, whilst clearly consumed, was not fully
220 depleted after 56 hours in *T. congolense* culture (Log_2 FC: -0.76; Fig 2A and 3A), in contrast
221 to *T. brucei*, where 10 mM glucose is consumed by the same time-point [56]. Ribose,
222 glucosamine, inosine and threonine were similarly depleted in *T. congolense* culture (Log_2
223 FC: -0.78, -0.97, -2.82 and -0.89, respectively).

In contrast, a number of metabolites accumulated in the medium (Fig 2A). The most significant of these were guanine (Log_2 FC: 6.34; Fig 2A and 5A), succinate (Log_2 FC: 5.60; Fig 2A & 3B) and (S)-malate (malate, Log_2 FC: 1.37; Fig 2A and 3B). Interestingly, pyruvate (Log_2 FC: 0.24; Fig 3B) was not excreted at the high levels relative to starting concentration consistently observed in BSF *T. brucei* culture, in both HMI-11 and in Creek's Minimal medium (CMM) [56]. Succinate and malate appear to be the primary glycolytic outputs from BSF *T. congolense*, similar to PCF *T. brucei*. Elevated levels of 2-oxoglutarate and a metabolite putatively identified as 2-oxoglutaramate were observed, which potentially originate from alanine aminotransferase activity using L-glutamate and L-glutamine, respectively, as substrates [42, 57]. Moreover, a significant build-up of *N*6-Acetyl-L-lysine (Log_2 FC: 6.30) was observed (Fig 2B). Whilst the low molecular weight of acetate means it could not be detected by the LC-MS platform used here, concentrations of this molecule were measured directly using an acetate assay in samples taken at the same time points from four independent cultures, which confirmed high levels of acetate excretion by BSF *T. congolense* (Fig 3F).

Other notable observations included the depletion of several putative lysophosphatidylcholine species at 56 hours (Fig 2A; S4 Table), coincident with increased medium levels of *sn*-glycero-3-phosphocholine, choline and choline phosphate, indicating lyso-phospholipase activity where the charged headgroup moiety of a lyso-species is cleaved from its bound fatty acid [58]. In addition, tryptophan (Log_2 FC: -0.74; Fig 6B; S4 Table) was significantly consumed ($P = 0.042$), in contrast with cysteine (Log_2 FC: -0.07; $P > 0.05$), despite the latter being essential to *T. brucei* [59] (S4 Table).

The Log_2 metabolite fold changes after 56 hours of culture of *T. congolense* were compared to those of *T. brucei* grown in HMI-11 (Fig 2B) [56]. A total of 90 metabolites were identified in both datasets, with some showing divergence between the two species (Fig 2B). Several metabolites only accumulated in *T. brucei* supernatant, in particular pyruvate, D-glycerate, 2-oxoglutarate and 12-hydroxydodecanoic acid (Fig 2B). Conversely, succinate, N6-acetyl-L-lysine, 4-hydroxy-4-methylglutamate, N6,N6,N6-trimethyl-L-lysine and choline only accumulated in *T. congolense* supernatant (Fig 2B). Whilst cystine (Fig 2B; 12) was depleted in *T. brucei* samples, this metabolite remained unchanged in those from *T. congolense*.

In summary, whilst core elements of metabolism have been conserved between BSF *T. congolense* and *T. brucei*, several pronounced differences in *T. congolense* metabolism were identified based solely on metabolic input and output in *in vitro* culture. An integrated analysis of the metabolomic and transcriptomic datasets was then undertaken in order to further define the metabolic differences between the two species.

Energy metabolism

As described above, RNA sequencing and culture supernatant metabolomics provided initial indications that *T. congolense* energy metabolism, specifically with respect to glucose usage, diverges substantially from that characterized in *T. brucei* BSFs (simplified map of glycolysis depicted in Fig 3G).

To dissect metabolic differences at the transcriptome level, pathway analysis was carried out using the TrypanoCyc database [60], which contains 186 manually curated pathways covering 422 genes or groups of multi-copy genes (S5 Table). These analyses showed broadly similar levels of gene expression of glycolytic components between BSF *T. brucei* and *T. congolense* (Fig 3G and 3I). However, the *T. brucei ex vivo* samples displayed a more distinct expression profile, with low transcript abundances for most glycolytic components compared to all sample groups. This is most likely the result of cells being sampled near peak parasitaemia, and so having a higher proportion of tsetse-transmissible, quiescent short stumpy forms – consistent with this there was elevated expression of stumpy markers such as the PAD array (TbTc_0074), PIP39 (TbTc_0700) and reduced expression of RBP10 (TbTc_0619) (S1 Table) [61-63].

Transcripts associated with gluconeogenesis, the succinate shunt, and the acetate generation pathway were upregulated in BSF *T. congolense* under both *in vitro* and *ex vivo* conditions compared to BSF *T. brucei*. Key examples of this are pyruvate phosphate dikinase (PPDK), phosphoenolpyruvate carboxykinase (PEPCK), glycosomal malate dehydrogenase (gMDH) and two subunits of pyruvate dehydrogenase (PDH) (Fig 3I). PPDK was previously reported to be expressed in BSF *T. congolense*, but not BSF *T. brucei* [44], and it may be assumed that the enzyme serves a similar function in BSF *T. congolense* as it does in PCF *T. brucei*; in a mainly glycolytic role to maintain ATP/ADP balance in the glycosome. The high levels of glycosomal MDH expressions in BSF *T. congolense* contrasts with BSF *T. brucei*, where gMDH expression is reported to be mostly absent, and cytosolic MDH (cMDH) is the major isoform [64]. The RNAseq analysis also supports a previous study showing high levels of glycerol kinase expression in BSF *T. congolense* [45]. The most recent PacBio assembly of the *T. congolense* genome indicates that the parasite encodes five copies of PEPCK in tandem array (TcIL3000.A.H_000300300, TcIL3000.A.H_000300400, TcIL3000.A.H_000300500, TcIL3000.A.H_000300600 & TcIL3000.A.H_000300700; compared to one copy in *T. brucei* – Tb927.2.4210; [65]), whilst there are only three copies of glycerol kinase in *T. congolense* (compared to five in *T. brucei*).

To confirm that the elevated levels of succinate and malate seen in *T. congolense* spent medium samples originated from glucose, LC-MS analysis using ^{13}C-U-D-glucose was carried out on intracellular metabolites from cell pellet extracts. Stable isotope analysis has provided valuable insights into *T. brucei* central carbon metabolism [42], and generating *T. congolense* datasets enabled comparative analysis of glucose catabolism (albeit with an unavoidable difference in medium supplementation of goat serum for *T. congolense*, rather than foetal bovine serum for *T. brucei*).

BSF *T. congolense* was grown for 48 hours in a custom medium (Steketee's congolense medium; SCM-6; S6 Table), containing a total D-glucose concentration of 10 mM in a 1:1 ratio of D-glucose:^{13}C-U-D-glucose. Following metabolite extraction, LC-MS analysis was undertaken and the majority of glycolytic intermediates were detected, including ^{13}C-labels (Fig 3H). Moreover, labelling ratios of downstream metabolites were largely similar to that of intracellular glucose, and the number of carbons found to be labelled in each metabolite matched that which would be expected in the BSF *T. brucei* glycolytic pathway (i.e. three ^{13}C atoms in all metabolites downstream of glyceraldehyde 3-phosphate and glycerol-3-phosphate). Similar to *T. brucei*, a high percentage of 3-carbon labelled fructose-1,6-bisphosphate (FBP) (34.8%) was observed in *T. congolense* (Fig 3H), probably a result of the "reverse" aldolase reaction occurring in the glycosome [42]. Importantly, two-carbon labelling was observed in several acetylated compounds (N-acetylornithine & N-acetyl-L-lysine; Fig 3H), confirming that acetyl groups used to generate these metabolites originate from D-glucose. Although acetyl-CoA, the product of pyruvate oxidation, was not detected for technical reasons, labelling of acetylated metabolites indicate that glucose-derived pyruvate is used to generate acetyl-CoA and subsequently acetate in the mitochondrion, similar to other trypanosomatids. Taken together, these data indicate that the flow of carbon atoms for glycolytic components in *T. congolense* is very similar to that in *T. brucei*. However, the metabolic outputs differ drastically from BSF *T. brucei* and appear to be more similar to PCF *T. brucei*.

To determine whether the elevated succinate in supernatants originated from glucose catabolism, metabolite labelling was corrected for the 1:1 (50%) ratio of natural glucose to ^{13}C-U-D-glucose, which equated to a mean percentage labelling of 43.1% (the value is less than 50% due to D-glucose in the serum). All glycolytic metabolites up to pyruvate showed >90% labelling when corrected (for glucose 6-phosphate and fructose-1,6-bisphosphate, both 3-carbon and 6-carbon labels were taken into account), although glycerol and glycerol 3-phosphate exhibited 57.2% and 64.4% labelling, respectively, as these metabolites can also be obtained from catabolism of lipid precursors. Moreover, 40.1% (93.0% corrected) labelling was detected in L-alanine, suggesting that the alanine aminotransferase reaction

that utilizes pyruvate to generate 2-oxoglutarate and L-alanine in both BSF and PCF *T. brucei*, also occurs in BSF *T. congolense* [42, 66]. For both succinate and malate, 3 carbons are derived from glucose and these metabolites showed 33.6% (78.1% corrected) and 26.0% (60.3% corrected) labelling, respectively. These results suggest that glucose is not the only source of intracellular succinate and malate in *T. congolense*. However, these values were higher than those reported in *T. brucei* (70% and 52% for malate and succinate, respectively [42]).

Whilst PCF *T. brucei* exhibit citric acid (TCA) cycle activity, this pathway is not used to catabolize glucose [35]. Similarly, no citric acid cycle intermediate isotopologues (e.g. citrate) were found when BSF *T. congolense* were incubated with ^{13}C-U-D-glucose, although small amounts of 2-carbon labelled succinate and malate were observed (Fig 3H). This is similar to BSF *T. brucei* [42], indicating that, like *T. brucei*, *T. congolense* does not appear to couple glycolysis to TCA metabolism and instead directs high amounts of pyruvate through pyruvate dehydrogenase (PDH) into acetyl-CoA and acetate. Taken together, these data suggest that BSF *T. congolense* both from *in vitro* cultures and *in vivo* infection metabolically resemble an intermediate between BSF and PCF *T. brucei*, with moderate glycolytic capacity and significant levels of succinate shunt activity (glycosomal, rather than mitochondrial; S1 Table) as well as a highly active mitochondrial acetate generating pathway.

Previous work has shown that reduction of glucose concentrations in BSF *T. brucei* culture from 10 mM to 5 mM leads to decreased cellular motility, reduction in growth and cell body rounding morphology within 8 hours [67]. Given that glucose was not substantially depleted in *T. congolense* cultures after 56 h, we tested the effect of reduced glucose concentrations on *T. congolense* viability. Unlike *T. brucei*, *T. congolense* was able to maintain a growth rate equal to controls at concentrations as low as 2 mM (Fig 4A) when continuously passaged with no observable change in morphology or motility. To test whether glucose uptake was essential in *T. congolense*, cells were incubated with D-glucose in addition to varying concentrations of 2-deoxy-D-glucose (2DG), which can be internalised, but not metabolised further than 2-deoxy-D-glucose 6-phosphate, thereby inhibiting glycolysis (Fig 4B). Incubation of *T. congolense* in medium supplemented with 2DG (in addition to 10 mM glucose) led to growth defects in a dose dependent manner, likely due to 2DG being outcompeted by glucose at lower concentrations (Fig 4B). Although the growth defect was minor in the presence of 1 mM 2DG, there was a more pronounced reduction with 5 mM 2DG. When equimolar concentrations of glucose and 2DG were used, growth was repressed and cell death occurred within 48 hours (Fig 4B). *T. congolense* viability was also tested in SCM-6 in the presence of N-acetyl-D-glucosamine (GlcNAc), a sugar that inhibits glucose uptake [68] (S2 Fig). In the presence of 60 mM GlcNAc with 10 mM glucose, there was a

365 moderate, yet significant (P < 0.0001 at 96 h, *t*-test of cell densities) growth defect in *T.*
366 *congolense* (S2 Fig). Viability was further reduced when the same concentration GlcNAc
367 was used alongside 2 mM glucose (P < 0.0001 at 96 h, *t*-test of cell densities), the lowest
368 concentration *T. congolense* could tolerate (S2 Fig). The rate of glucose consumption was
369 measured by assaying glucose concentrations in cell culture supplemented with 4 mM
370 glucose, and shown to be 47.17 ± 27.91 $nmol^{-1}$ min^{-1} 10^8 cells in *T. congolense*, significantly
371 lower than the rate (132.18 ± 16.31 $nmol^{-1}$ min^{-1} 10^8 cells) in *T. brucei* (n = 4, P = 0.0039; *t*-
372 test).

373 To further probe glycolytic metabolism in BSF *T. congolense*, several targets were selected
374 for RNAi-mediated knock-down, using a tetracycline-inducible *T. congolense* line expressing
375 T7 polymerase and Tet repressor under puromycin selection (TcoSM [69]). Given that the
376 majority of both malate and succinate appear to originate from glucose catabolism, the effect
377 of reducing expression levels of two proteins involved in the succinate shunt, PEPCK and
378 PPDK (TcIL3000.A.H_000922100 – both expressed at high levels in *T. congolense*; Fig 3I),
379 was tested in separate experiments (Fig 4C, D). RNAi was induced by addition of 1 µg/mL
380 tetracycline, and cell growth in culture and transcript abundance measured by qPCR were
381 monitored every 24 hours (Fig 4C, D). Creek et al showed that PEPCK is essential in BSF *T.*
382 *brucei*, even though the levels of succinate generated through this pathway are negligible
383 [42]. In BSF *T. congolense*, RNAi targeting the five copies of PEPCK reduced overall
384 *PEPCK* transcript abundance by approximately 50% (mean transcript levels of 60%, 46%
385 and 63% compared to uninduced controls at 24, 48 and 72 h post-induction, respectively;
386 Fig 4E), leading to a small but non-significant reduction in growth rate (Fig 4C (P=0.0689, *t*-
387 test at the 96 h time-point). PPDK expression is not detected in BSF *T. brucei* but is
388 expressed in the PCF stage [44]. Knock-down of PPDK in *T. congolense* did not affect
389 parasite viability or growth rate (Fig 4D), although similar levels of transcript knockdown
390 were observed (mean transcript levels of 67%, 64% and 50% compared to uninduced
391 controls at 24, 48 and 72 h post-induction, respectively; Fig 4F).

392 RNAi was also used to knock down expression of the hexose transporter (HT) array,
393 specifically those matching the THT1 and THT2 array in *T. brucei*
394 (TcIL3000.A.H_000260500, TcIL3000.A.H_000260600, TcIL3000.A.H_000794500,
395 TcIL3000.A.H_000794600, TcIL3000.A.H_000794700.1), which has been shown to
396 significantly restrict growth of BSF *T. brucei* [70]. Whilst growth rate was unaffected in BSF
397 *T. congolense* (Fig 4G), induction of HT RNAi led to a reduction in transcript abundance at
398 all time points (mean transcript levels of 83%, 75%, 68% and 65% compared to uninduced
399 controls at 24, 48, 72 and 96 h post-induction, respectively; Fig 4H). Glucose uptake was
400 decreased (mean reduction of 37% in uptake compared to uninduced controls after 72 h; Fig

4I), suggesting that either lower levels of glucose are sufficient for energy generation in *T. congolense*, or the parasite can utilize other carbon sources for ATP production. These alternatives sources could include serum components such as fatty acids or amino acids, both of which trypanosomatids have been reported to utilise [71, 72].

PCF *T. brucei* express most components of the electron transport chain (ETC) to generate ATP through oxidative phosphorylation, in contrast to BSF *T. brucei*, which do not detectably express any ETC components with the exception of the reversed ATPase and alternative oxidase [73]. As mentioned previously, BSF *T. congolense* is thought to express a complex I NADH dehydrogenase, but it is not known whether BSF *T. congolense* has capacity for oxidative phosphorylation. Transcriptomics analysis of the ETC was attempted, using a gene list generated by Zikova and colleagues [73], but no significant patterns could be discerned (S1 Table, S3 Fig).

Nucleotide metabolism

Metabolomic analysis of BSF *T. congolense* culture supernatants indicated a significant uptake of exogenous ribose, a contributor to nucleotide metabolism via uptake, or via the pentose phosphate pathway (PPP; Fig 5A and Fig 2A). Whilst guanosine was not detected in the supernatant, significant accumulation of guanine (Fig 5B) was observed, suggesting either excretion of this metabolite, or, hydrolysis of guanosine through parasite-secreted hydrolases/nucleosidases (previously identified in BSF *T. brucei* secretomes [74, 75]). This mechanism would enable uptake of guanine and other nucleobases through nucleobase transporters, for which multiple orthologues have been identified in the *T. congolense* genome [18] through homology with known *T. brucei* nucleobase transporters TbNT8.1 and TbNBT1 [76, 77]. In addition, there was an accumulation of xanthine, a product of xanthosine hydrolysis, and depletion of inosine, an important nucleoside composed of hypoxanthine and ribose (Fig 5C and 5D). The nucleoside cytidine and the nucleobase hypoxanthine were also detected, but appeared to remain unchanged during the time course, although the latter was a medium supplement potentially added in excess (S4 Table). It is noteworthy that only a single nucleoside transporter gene (TbTc_1072; *T. congolense* gene IDs: TcIL3000.A.H_000665800 and the pseudogene TcIL3000.A.H_000679300; S2 Table) can be identified in *T. congolense*, a syntenic homologue of TbNT10 [18], functionally characterized as a P1-type purine nucleoside transporter [78], and is thus unlikely to transport cytidine [79].

Purine salvage is an essential process in trypanosomatids, as they lack the *de novo* synthesis pathway for the purine ring [80], and previous analysis of cell pellets to investigate intracellular nucleotide metabolism utilizing ^{13}C-U-D-glucose in BSF *T. brucei* showed purine

436 salvage pathways incorporating 5-carbon labelled ribose derived from glucose [42] (Fig. 5F).
437 Whilst the ribose incorporated into these nucleosides originates almost exclusively from
438 glucose in *T. brucei* (Fig 5F), *T. congolense* appears to use far less glucose-derived ribose
439 to make purine nucleosides such as adenosine, guanosine and inosine (Fig 5F).

440 Transcriptomics analyses indicated upregulation of genes associated with generation of
441 adenosine nucleotides (Fig 5G; red vertical bar), especially in *ex vivo T. congolense*, as well
442 as hypoxanthine-guanine phosphoribosyltransferase and uracil phosphoribosyltransferase.
443 Upregulation of nucleoside hydrolases and phosphoribosyltransferases supports previous
444 theories based upon genome content that *T. congolense* has a capacity for nucleobase
445 uptake [18].

446 The purines guanosine and inosine, which incorporate glucose-derived ribose in *T. brucei*,
447 were almost entirely unlabelled in *T. congolense* (Fig 5F). However, the phosphorylated
448 nucleosides GMP, GDP and GTP all incorporate glucose-derived carbon atoms, presumably
449 through ribose. Given the labelling patterns seen in adenosine, one possible explanation
450 could be conversion of AMP to inosine monophosphate (adenosine monophosphate
451 deaminase; TbTc_0145), IMP to xanthosine monophosphate (IMP dehydrogenase;
452 TbTc_1648) and XMP to GMP (GMP synthase; TbTc_1452). However, only one of these
453 enzymes, GMP synthase, was expressed at higher abundance in *T. congolense* (Log_2 fold
454 change: 1.56 and 2.02 for *ex vivo* and *in vitro*, respectively). Overall, incorporation of
455 glucose-derived carbons into purine nucleosides is reduced in *T. congolense* compared to *T.*
456 *brucei*. It should be noted that in both experiments, there was no ribose supplementation in
457 the media

458 Of the pyrimidines, uracil and its derivatives were detected during the glucose labelling
459 experiment (S4 Fig). Uracil is known to be the main pyrimidine salvaged by other
460 kinetoplastids including *T. brucei* [81-83]. Whilst the majority of the uridine, UMP, UDP and
461 UTP pools incorporate glucose-derived ribose (five ^{13}C labels), 5-carbon isotopologues of
462 these pyrimidines were reduced in abundance in *T. congolense* compared to *T. brucei*.
463 Instead, 2-carbon labelled isotopologues appeared to comprise the majority of uridine, uracil
464 and their nucleotides (S4 Fig).

465 Whilst uracil biosynthesis is not essential in *T. brucei* [84], the uracil pool in *T. congolense*
466 appears to derive almost entirely from glucose, when corrected for 50% glucose labelling
467 (76% in *T. congolense* vs 44% in *T. brucei* [42]; S4 Fig), suggesting that this species
468 predominantly synthesizes uracil from orotate to UMP (orotate
469 phosphoribosyltransferase/orotidine 5-phosphate decarbocylase; TbTc_0735) and from
470 UMP to uracil (uracil phosphoribosyltransferase; TbTc_4220), as can occur in *T. brucei* [42].

Both these genes are expressed at higher abundance in *T. congolense*, both *in vitro* and *ex vivo,* compared to *T. brucei* (Fig 5G, S1 Table), which could explain the increased isotopologue labelling. Uridine nucleosides (UMP, UDP, UTP) all show a similar pattern, with significant 2-carbon labelling, as well as moderate levels of 5-carbon labelling from incorporation of glucose-derived ribose (S4 Fig).

These data indicate that, at least under the growth conditions used here, BSF *T. congolense* favours purine nucleoside salvage in lieu of biosynthesis, in addition to *de novo* synthesis of orotate, uracil and uridine nucleosides. However, the difference in serum requirements for the two organisms is a confounding factor to the interpretation of this difference.

Amino acid metabolism

It is well established that trypanosomatid parasites scavenge amino acids, key nutrients for survival, from their hosts [85, 86]. Therefore, comparative analyses of *T. congolense* and *T. brucei* amino acid metabolism were undertaken. Whilst the majority of amino acids were detected during the supernatant time course, relative abundances in the medium did not vary greatly after 56 hours of *in vitro* culture (Fig 6A–C, S4 Table). The greatest reductions were observed in threonine (Log_2 FC after 56 hours: -0.89; Fig 6A), tryptophan (Log_2 FC: -0.74; Fig 6B), glutamine (Log_2 FC: -0.39), asparagine (Log_2 FC: -0.35) and phenylalanine (Log_2 FC: -0.35). Interestingly, cysteine, an essential factor for the *in vitro* culture of *T. brucei*, was not significantly consumed by 56 hours (Log_2 FC: -0.07; Fig 6C). However, at least low-level exogenous cysteine is still required to sustain parasite growth *in vitro*, as viability was significantly affected in the absence of cysteine (for both 1.5 mM and 1 mM vs 0 mM cysteine, $P < 0.0001$, *t*-test of cells densities at 96 h; S5 Fig). Experiments were carried out to test the essentiality of all other individual amino acids (with the exception of glutamine, known to be an important amino donor in trypanosomatid metabolism). Using the minimal medium SCM-6, cell viability was monitored for 72 hours in the absence of specific amino acids. Removal of the following amino acids from culture medium led to defects in growth over 72 hours: asparagine, histidine, isoleucine, leucine, methionine, proline, serine, tyrosine and valine (Fig 6D–G). Whilst aspartate appeared to be depleted in spent culture supernatants (S4 Table), this also occurred in the medium only control. Furthermore, removal of aspartate did not lead to reduced cell viability or growth rate in culture (Fig 6F). Long term culture was impossible without the addition of phenylalanine and threonine, leading to a final culture formulation, SCM-7 (S6 Table) containing a total of 14 amino acids. Therefore, BSF *T. congolense* appears to require a higher number of amino acids than BSF *T. brucei*, at least *in vitro*, with CMM containing only 8 amino acids in total, including cysteine and glutamine [56]. To further probe amino acid metabolism, pathway analysis was carried out on the transcriptome (S6 Fig) and metabolome (Fig 6; S6, S7 Fig).

BSF *T. brucei* utilizes exogenous L-glutamine as the primary source of intracellular glutamate and 2-oxoglutarate and produce significant levels of glutamine-derived succinate [42, 85] (Fig 6I). Given the high levels of succinate excreted by *T. congolense*, stable isotope labelling was used to determine the contribution of L-glutamine to this pool. *T. congolense* was incubated for 48 hours with 1 mM ^{13}C-U-L-glutamine and cell pellets analysed by LC-MS. Results indicated the presence of biochemical activities consistent with those observed in *T. brucei*. Significant glutamine-derived carbon labelling was detected after 48 h incubation for succinate (41.3%, 48.5% corrected), glutamate (76.1%, 89.2% corrected), 2-oxoglutarate (80.5%, 94.3% corrected) and succinate semialdehyde (94.7% corrected; Fig 6I). As would be anticipated, labelling of glutathione (86.1%) and trypanothione (98.4%) from glutamine through glutamate were also observed (S7 Fig). No labelling of malate or aspartate was seen in this study, despite the use of high concentrations of ^{13}C-U-L-glutamine compared to the equivalent study performed in *T. brucei* with a 50:50 ratio of ^{13}C-U-L-glutamine [85].

The apparent essentiality of several amino acids was also investigated using stable isotope labelling. Proline is an essential carbon source for PCF but not BSF *T. brucei* [87]. However, removal of proline from BSF *T. congolense* medium led to reduced growth (Fig 6F). RNAi-mediated knock-down of proline metabolism (specifically pyrroline-5-carboxylate dehydrogenase, TbP5CDH) in PCF *T. brucei* has highlighted the requirement of proline metabolism for mitochondrial function [87]. Indeed, both P5CDH (TbTc_1695) and proline dehydrogenase (TbTc_1591) expression were upregulated in *ex vivo T. congolense*, compared to *T. brucei*, suggesting that proline catabolism was more active (S1 Table and S6 Fig). However, ^{13}C-U-L-proline labelling showed that this amino acid did not contribute to the biosynthesis of other metabolites (S8 Fig). Therefore, the apparent requirement for proline in BSF *T. congolense* may be for the purposes of polypeptide synthesis only.

As in *T. brucei*, glucose-derived carbon usage was detected in several amino acids in *T. congolense* (S6A Fig). Aspartate (a precursor for pyrimidine nucleotide biosynthesis) and alanine (a by-product of a pyruvate-utilising aminotransferase reaction) (S6A Fig) exhibited 3-carbon isotopologues derived from ^{13}C-U-D-glucose. However, in *T. brucei*, a small proportion of L-asparagine labelling was observed (1.2% 3-carbon labelling) [42], whilst none was observed in *T. congolense* (S6A Fig). The metabolism of asparagine has not been studied in African trypanosomes; given the reduction of cell growth in the absence of this amino acid (Fig 6F), labelling with ^{13}C-U-L-asparagine was performed, but no other labelled metabolites were detected (S8 Fig). This indicates that, as with proline, protein synthesis is the sole role of asparagine in *T. congolense*. The reduced expression of asparagine synthetase (TbTc_4894; TcIL3000.A.H_000497800), which converts aspartate to asparagine

(S6 Fig), suggests that BSF *T. congolense* may rely upon scavenging of exogenous asparagine.

Serine was also shown to be essential to *T. congolense* (Fig 6F), in contrast to minimal culturing requirements for *T. brucei* [56]. ^{13}C-U-L-serine labelling indicated that *T. congolense* L-serine metabolism mirrors that of *T. brucei* in several aspects, such as *de novo* sphingolipid biosynthesis, with 70.0% 2-carbon labelling of sphinganine and downstream labelling of ceramide and sphingomyelin species (S8 Fig). Similarly, phosphatidylserine decarboxylase activity was evidenced at both transcript and metabolite levels, with 40.1% 2-carbon labelling of glycerol-phospho-ethanolamine (S1 Table; S8 Fig). However, L-serine also has a minor role in S-adenosyl-L-homocysteine detoxification, where serine-derived carbon ultimately contributes to cysteine biosynthesis. In *T. congolense*, serine-derived carbon labelling can be detected in cystathionine (18.1%) and cysteine (16.7%), through to glutathione (4.1%) and trypanothione disulfide (3-carbon labelled, 6.8%; 6-carbon labelled, 0.02%; S7 Fig). Therefore, the inability to exclude L-serine from *T. congolense in vitro* culture media may primarily be attributable to lipid metabolism and an increased demand for serine-derived cysteine, potentially over exogenously obtained cysteine, depending on bioavailability. Indeed, metabolomics analysis of culture medium indicates that the ability of *T. congolense* to take up cysteine from its environment may be lower than in *T. brucei* (Fig 6C).

Although L-cysteine is primarily a source of sulphur for trypanosomatids, we also investigated the carbon contribution of this amino acid in *T. congolense*, and in particular, whether L-cysteine-derived carbon atoms contribute to the biosynthesis of glutathione and trypanothione. ^{13}C-U-L-cysteine stable isotope labelling experiments were performed (S7 and S8 Fig). Direct replacement of the 1.5 mM L-cysteine present in SCM with ^{13}C-U-L-cysteine led to high levels of labelling in glutathione and trypanothione disulfide (S7B Fig). This indicates that *T. congolense* can readily take up and metabolize exogenous cysteine, even though abundance of the amino acid is not reduced significantly over 56 hours of parasite *in vitro* culture. Although no clear pattern could be observed in transcriptomic analysis of the trypanothione biosynthesis pathway, both trypanothione synthase (TRYS; TbTc_1359) and trypanothione reductase (TRYR; TbTc_4239) were expressed at high levels in *in vitro T. congolense* cells relative to *ex vivo* cells, indicating that under *in vitro* conditions, cells may be subjected to higher levels of oxidative stress (S7C Fig).

Fatty acid metabolism in *T. congolense*

Lipids have a variety of crucial roles in trypanosomes, as a major constituent of membranes and under certain conditions, for energy [72]. BSF *T. brucei* require large quantities of

578 myristic acid in particular, for the synthesis of glycosylphosphatidylinositol (GPI) that anchors
579 the parasite's major surface glycoprotein antigens [88]. To do this, BSF *T. brucei* both
580 synthesises and scavenges myristic acid. Glucose labelling experiments in *T. brucei* have
581 shown that myristic acid is partially synthesized from glucose-derived carbon through acetyl-
582 CoA, using a system of fatty acid elongases [89] (Fig 7A). However, no fatty acid carbon
583 labelling was detected after incubation of *T. congolense* with ^{13}C-U-D-glucose (Fig 7A).
584 Carbon dissemination was also investigated from threonine, which is used as a source of
585 acetate, and thus, lipids [90] (Fig 7B). Similarly, no saturated lipid carbon labelling was
586 observed, suggesting that *T. congolense* either uses alternative sources of carbon for lipid
587 biosynthesis, or does not rely on acetate as a source of lipids in the same way as *T. brucei*
588 [30].

589 While acetate/acetyl-CoA metabolism is highly active at the level of gene expression in *T.*
590 *congolense* compared to *T. brucei* (Fig 7C), consistent with metabolic data, expression of
591 acetyl-CoA synthetase (TbTc_0318), a key enzyme in lipid biosynthesis from acetate, is
592 reduced in both *ex vivo* and *in vitro T. congolense* (Fig 7C). Furthermore, an acetyl-CoA
593 thioesterase (TbTc_5515) that is involved in ATP synthesis-uncoupled acetate production in
594 PCF *T. brucei* [91] is also expressed at lower levels in *T. congolense* (Fig 7B). Other
595 enzymes involved in fatty acid biosynthesis, namely acetyl-CoA carboxylase (TbTc_0754),
596 β-ketoacyl-CoA synthase (TbTc_3372) and β-ketoacyl-CoA reductase (TbTc_1241), were all
597 expressed at lower abundance in *T. congolense* than *T. brucei*, in particular in *ex vivo* cells
598 (Fig 7C). Of the four elongases, ELO1 (TbTc_0159) and ELO2 (TbTc_1882) were expressed
599 at equal levels in BSF *T. congolense*, compared to BSF *T. brucei* (S1 Table). Whilst
600 expression of ELO3 (TbTc_0235) appeared to be reduced in *T. congolense* (Log_2 fold
601 change of -1.98 and -1.62 compared to *T. brucei* for *in vitro* and *ex vivo*, respectively; S1
602 Table), *T. congolense* cells expressed higher levels of ELO4 (TbTc_0737) in both *in vitro*
603 and *ex vivo* conditions, compared to *T. brucei* (Log2 fold change: 1.39 and 1.38 for *in vitro*
604 and *ex vivo* comparisons, respectively)

605 The variation in observed gene expression associated with the sterol pathway appeared to
606 correlate with sample condition rather than species (Fig 7C). However, *T. congolense*
607 transcripts for genes involved in lanosterol synthesis were reduced, especially under *in vitro*
608 conditions (squalene synthase, SQase, TbTc_2577; squalene monooxygenase, SM,
609 TbTc_3357; lanosterol synthase, LSS, TbTc_4540; Fig 7C).

610 Fatty acid oxidation was recently confirmed to be an energy source for *T. brucei* residing in
611 adipose tissue [72]. Transcripts associated with this pathway were less abundant in *T.*
612 *congolense* compared to *T. brucei* under both conditions (Fig 7C), suggesting this may not

be an energy-generating pathway in glucose-rich culture medium, or under the *in vivo* conditions from which they were sampled. However, capacity for ATP generation from fatty acid oxidation should not be ruled out.

Exploiting differences in metabolism for pharmacological intervention

Differences in metabolism between *T. congolense* and *T. brucei* have implications for differential drug efficacy between the two species. To validate our findings in key areas of metabolism, pharmacological inhibition was attempted for specific targets in trypanosome metabolism, in order to compare inhibitory concentrations (EC_{50}).

To assess whether areas of mitochondrial metabolism were more essential in BSF *T. congolense* than in BSF *T. brucei*, both species were treated with FCCP, an uncoupling agent that depolarises the mitochondrial membrane. However, there was no difference in sensitivity between the species (EC_{50}: 13.0 ± 5.0 µM and 12.6 ± 5.3 µM for *T. brucei* and *T congolense*, respectively; Table 1). Given both metabolic and transcriptomic data indicated no increased electron transport chain activity, we also treated with the complex III inhibitor antimycin A, with again no significant differences seen between the species (Table 1). In addition, there was no change in sensitivity to azide, an inhibitor of ATP hydrolysis by the F_1-ATPase (Table 1). However, *T. congolense* appeared to be more resistant to rotenone, a complex I NADH dehydrogenase inhibitor (Table 1). Previous data inferred complex I activity in BSF *T. congolense* based on nitroblue tetrazolium staining [48]. Rotenone resistance could indicate NADH dehydrogenase activity of a rotenone-insensitive NADH dehydrogenase, such as the inner membrane space-facing NDH2 [92]. *T. congolense* also showed enhanced sensitivity to salicylhydroxamic acid (SHAM), an inhibitor of the trypanosome alternative oxidase (TAO; Table 1). Taken together, these data indicate that, like *T. brucei*, *T. congolense* does not rely on oxidative phosphorylation for ATP production, as indicated by transcriptomics analysis, and that, as previously reported, TAO is the terminal oxidase [48, 51].

Metabolomics and transcriptomics data indicated that *T. congolense* direct pyruvate towards mitochondrial metabolism, with high transcript levels in PDH and enzymes involved in acetate generation, compared to *T. brucei* (Fig 3 and 7). We therefore hypothesised *T. congolense* to be more sensitive to inhibition of mitochondrial pyruvate uptake and to investigate this further, we tested drug sensitivities for UK5099, an inhibitor of mitochondrial pyruvate transport [93]. As expected, *T. congolense* (EC_{50}: 82.1 µM) was significantly more sensitive (P = 0.0091, unpaired t-test) to UK5099 compared to *T. brucei* (130.0 µM; Table 1).

Whilst acetate generation appears to be important in *T. congolense*, our data suggest that the acetate does not appear to be utilised for the biosynthesis of fatty acids, in contrast to

what has been shown for *T. brucei*. To probe this further, we compared drug sensitivity of the two species with compounds targeting fatty acid synthesis (Fig 8). Indeed, *T. congolense* was significantly more resistant than *T. brucei* to an acetyl-CoA synthetase inhibitor (ACS inhibitor; 1-(2,3-di(thiophen-2-yl)quinoxalin-6-yl)-3-(2-methoxyethyl)urea, [94]; Fig 8A; Table 1), indicating that acetyl-CoA synthetase is far less essential to this species. ACS is essential to both BSF and PCF *T. brucei* [30, 95], thus indicating a key metabolic difference between the species.

We next compared drug sensitivity to Orlistat, an inhibitor of fatty acid synthase and phospholipase [32]. Here, a striking difference was found, with *T. congolense* exhibiting significant resistance (780-fold increase in EC_{50}) to the compound compared to *T. brucei* (Fig 8B; Table 1), providing further evidence that *T. congolense* primarily relies on fatty acid scavenging, instead of synthesis, as predicted by the combination of metabolomics and transcriptomics.

Discussion

The protozoan parasite *T. congolense* is a principal cause of AAT, but crucially, *T. brucei* remains the dominant model for laboratory-led studies of African trypanosomes, even in the face of mounting evidence that *T. brucei* and *T. congolense* differ profoundly in many facets of their biology. In order to facilitate the identification and development of potential drug targets for *T. congolense*, a detailed understanding of the fundamental cellular metabolism, leading to an understanding of both the differences and commonalities between *T. congolense* and *T. brucei*, would be a significant step forward.

Thus, this study aimed to generate a detailed comparison of metabolism in *T. congolense* and *T. brucei*, through a combination of metabolomics, transcriptomics and gene knockdown approaches. Transcriptomic data was generated from *T. congolense* and *T. brucei* with parasite samples isolated from both *in vitro* culture and purified from *in vivo* murine infections (*ex vivo*). Crucially, there were high levels of correlation between *ex vivo* and *in vitro T. congolense* samples, indicating that the cultured form of the parasite closely resembles the *in vivo* situation, at a transcriptomic level. In contrast, there was lower inter-species correlation between *T. brucei* and *T. congolense.*

Our data demonstrate that BSF *T. congolense*, while possessing some metabolic similarities with BSF *T. brucei* (as expected), differs substantially in several core components, including in having a reduced reliance on glucose, excretion of distinct glycolytic end products (acetate, malate and succinate in *T. congolense* compared to pyruvate in *T. brucei*), and increased gene expression and metabolic signatures of specific mitochondrial pathways, in

682 particular pyruvate to acetate conversion. Additionally, we show increased reliance on
683 exogenous substrates such as ribose for nucleotide synthesis as demonstrated by reduced
684 glucose-derived carbon labelling in nucleoside species in addition to upregulation of
685 hydrolases and phosphoribosyltransferases. Furthermore, while there is overlap in amino
686 acid utilisation (e.g. glutamine), *T. congolense* relies on more exogenous amino acids than
687 *T. brucei*. Surprisingly, this included serine which, in the case of *T. congolense*, appears to
688 be important in the transsulfuration pathway that is geared towards trypanothione
689 biosynthesis. This may also explain the observed decreased reliance on exogenous L-
690 cysteine. Unlike *T. brucei*, *T. congolense* also requires asparagine and proline for viable *in*
691 *vitro* culture, although carbon usage from these amino acids is minimal. Finally, *T.*
692 *congolense* exhibits increased acetate/acetyl-CoA metabolism compared to *T. brucei*,
693 despite a reduction in fatty acid biosynthesis through the classical trypanosomatid pathways
694 involving acetyl-CoA synthase, acetyl-CoA carboxylase, β-ketoacyl-CoA synthase and β-
695 ketoacyl-CoA reductase, the expression of which are reduced in *T. congolense* (both in *ex*
696 *vivo* and *in vitro* conditions). This is further underlined by lack of glucose-derived 2-carbon
697 labelling of fatty acids, most notably myristic acid, a key GPI anchor component of variant
698 surface glycoproteins of *T. brucei*. However, fatty acid elongase 4, previously shown to
699 extend exogenously scavenged arachidonic acid (C22:4) to docosatetraenoic acid (C22:4)
700 [96], is upregulated under *in vitro* conditions, compared to *T. brucei*, which may indicate a
701 reliance on long-chain polyunsaturated fatty acids. These findings are shown in a summary
702 figure of *in vitro* transcriptomics data (Fig 9)

703 Analyses of culture supernatants showed that 10 mM glucose was not substantially depleted
704 after *T. congolense* cultures reached high cell density, as would be expected from an
705 equivalently dense *T. brucei* culture [56]. *T. brucei* requires at least 5 mM glucose in culture
706 [67], whereas BSF *T. congolense* were viable and maintained doubling times in levels as low
707 as 2 mM. Furthermore, confirming conclusions from one previous study on BSF *T.*
708 *congolense* [43], the primary metabolic outputs *in vitro* were (S)-malate, succinate and
709 acetate, in contrast to *T. brucei*, in which the main output is pyruvate, which is excreted in
710 large amounts [42, 56]. Interestingly, we observed a reproducible reduction in pyruvate
711 levels in *T. congolense* supernatants over time, before abundance of this metabolite
712 returned to levels similar to those observed in negative controls. A recent study in PCF *T.*
713 *brucei* demonstrated that these parasites can re-metabolize glycolytic end products such as
714 pyruvate and succinate [37]. Stable isotope labelling patterns in catabolic products derived
715 from glucose do not support cyclical TCA activity, nor re-uptake of excreted metabolites in
716 BSF *T. congolense*. However, it would be of interest to determine whether this species can
717 recycle the aforementioned metabolites.

718 *T. congolense* exhibits high levels of expression in genes involved in the glycosomal
719 succinate shunt (PEPCK, glycosomal malate dehydrogenase and fumarate hydratase; Fig
720 9). In *T. brucei* these phenotypes are associated with PCF rather than BSF; thus, to further
721 dissect glycolytic metabolism, RNAi was employed to investigate the essentiality of PPDK
722 and PEPCK in *T. congolense*. In *T. brucei*, PPDK is only expressed in the PCF stage, and is
723 absent in the BSF stage. In contrast, BSF *T. congolense* expresses PPDK at both transcript
724 (Fig 3) and protein [44] levels, although our initial analyses suggest that the protein is not
725 essential for growth *in vitro*. PEPCK was previously found to be essential in BSF *T. brucei*
726 [42]; though in BSF *T. congolense*, PEPCK knock-down only led to a mild reduction in
727 growth rate. Previous studies in PCF *T. brucei* demonstrated that individual null mutants of
728 PEPCK and PPDK showed no change in growth rate, with moderate reductions in glycolytic
729 flux [40]. However, a PEPCK/PPDK null mutant did exhibit reduced growth rates, with further
730 data showing that PPDK functions in a glycolytic direction and contributes to glycosomal
731 ATP/ADP balance [40]. Further work is required to establish the roles of PEPCK and PPDK
732 in BSF *T. congolense*. Gene knock-out has not been previously attempted for *T. congolense*,
733 and consistent with other studies RNAi penetrance does not appear as efficient as in *T.*
734 *brucei* [69]. Techniques such as CRISPR/Cas9 and conditional knock-out would greatly
735 enhance our capabilities to study this parasite.

736 Whilst the major PGK isoform in BSF *T. brucei* is expressed in the glycosome, a previous
737 study suggested that the major isoform of phosphoglycerate kinase in BSF *T. congolense*
738 lacks the glycosomal targeting signal present in *T. brucei*, and is thus expressed in the
739 cytosol, akin to PCF *T. brucei* [46]. This has significant implications for glycosomal ADP/ATP
740 balance, as the expression of cytosolic PGK in BSF *T. brucei* is lethal [39]. Taken together,
741 these data suggest that *T. congolense* appears to carry out glycolytic metabolism in the
742 same fashion as PCF, not BSF *T. brucei*, including in *ex vivo* cells.

743 Whilst 2-deoxy-D-glucose does cause *T. congolense* death *in vitro* and supplementation of
744 cultures with GlcNAc also has a detrimental impact on viability, knock-down of the glucose
745 transporter array did not affect growth, even though glucose uptake appeared to be reduced
746 by 37% subsequent to 72 h of RNAi induction. These experiments highlight a crucial
747 difference between BSF *T. congolense* and *T. brucei* in a pathway that has become a
748 metabolic paradigm in the latter species. Whilst *T. brucei* requires high levels of glucose to
749 sustain a significant glycolytic flux, *T. congolense* remains viable in significantly lower
750 glucose concentrations, with a reduced flux, more similar to PCF *T. brucei*. However,
751 glucose remains an essential carbon source in this species, as growth is abolished in the
752 absence of glucose. Of particular interest is whether the parasite generates the majority of
753 ATP from this reduced glucose intake, or if it can thrive on other carbon sources such as

amino acids or even fatty acids. If the latter, this adaptation could be due to the reduced bioavailability of glucose in the ruminant host bloodstream. Blood concentrations of glucose in humans are approximately 5.5 mM [97]. Glucose concentrations in ruminants are typically lower (2–4 mM [98-100]), and primary sources of energy are typically volatile fatty acids in the form of acetic, propionic and butyric acid [101, 102]. To date, products of volatile fatty acid metabolism, such as 2-methylcitrate and 2-methyl-cis-aconitase, have not been reported in *T. congolense*. As such, the ability of *T. congolense* to utilise other products only available in adult ruminant blood merits further investigation.

RNAseq analyses of *T. congolense* indicate high levels of expression of mitochondrial pathways associated with glucose catabolism, specifically acetate and acetyl-CoA metabolism involving pyruvate dehydrogenase, acetate:succinate CoA transferase and succinyl-CoA synthetase (Fig 9). Given that the large amounts of acetate generated by the parasite appear not to be required for fatty acid synthesis, these findings could suggest significant reliance on mitochondrial substrate level phosphorylation for growth, similar to PCF *T. brucei* cultured in glucose-rich medium [103, 104]. Interestingly, *T. congolense* does not appear to encode a homologue of MPC1, and therefore likely relies on MPC2 for pyruvate transport into the mitochondrion. The lack of multiple pyruvate transporters combined with the importance of mitochondrial pyruvate catabolism likely explains the increased sensitivity of *T. congolense* to UK5099, a mitochondrial pyruvate transport inhibitor, compared to *T. brucei*.

Our data are consistent with the absence of oxidative phosphorylation, based on transcriptomics and lack of sensitivity to chemical inhibition, compared to *T. brucei*. Interestingly, a previous study reported NADH dehydrogenase (complex I) activity in *T. congolense*, offering the possibility of ATP generation via complex V [48]. However, there was no change in rotenone sensitivity in *T. congolense*, suggesting that the NADH dehydrogenase activity may originate from a rotenone-insensitive NADH dehydrogenase such as NDH2, known to be important for acetate production in BSF *T. brucei* [92, 105, 106].

Rather than oxidative phosphorylation, we propose it is likelier that considerable ATP production occurs in the acetate:succinate CoA transferase – succinyl-CoA synthetase (SCS) cycle, which would explain the high levels of acetate generated by *T. congolense*, in addition to increased sensitivity to inhibition of mitochondrial uptake of pyruvate, the key metabolic precursor. Given that 2-oxoglutarate dehydrogenase complex expression appears to be less than, or equal to, that in *T. brucei* (under *in vitro* culturing conditions, Fig 9), it is likely that SCS activity occurs in the acetate-generating pathway rather than in the TCA cycle, which is not thought to be fully functional in BSF African trypanosomes [35], although

789 recent data have challenged this paradigm in PCF *T. brucei* [37]. The mechanisms proposed
790 here bear some similarities to the scheme proposed by Dewar and colleagues for stumpy-
791 form *T. brucei* metabolism, which also exhibit increased mitochondrial metabolism compared
792 to BSF *T. brucei* [107].

793 In *T. brucei*, carbon atoms from glucose disseminate through multiple pathways in the cell
794 [42] and, using stable isotope-labelled glucose, our data demonstrate that this pattern is also
795 seen in *T. congolense*, in particular through the glycolytic pathway, suggesting some of the
796 key metabolic differences observed are quantitative, rather than qualitative. However, there
797 were key differences in glucose-derived carbon usage. In particular, a reduction in labelling
798 was observed in purine nucleotides in *T. congolense*. In both species, carbon labelling is
799 likely due to generation of ribose phosphate sugars via the PPP and these data suggest that
800 *T. congolense* does not obtain its ribose through the pentose phosphate pathway (from
801 glucose), to the same extent that *T. brucei* does. Interestingly, *T. congolense* appears to
802 express higher levels of APRT1 (cytosolic) compared to APRT2 (glycosomal) to synthesise
803 adenosine (Fig 5). This discrepancy could underpin the reduced fraction of glucose-derived
804 purine labelling, with a reliance on ribose from alternative sources (for example,
805 exogenously).

806 Whilst the majority of pyrimidine labelling is 5-carbons in *T. brucei*, indicating labelled ribose,
807 there is decreased 5-carbon labelling and higher abundance of 2-carbon labelling in *T.*
808 *congolense*, likely through uridine generated from aspartate through orotate, again
809 highlighting a reduction in glucose-derived ribose, but conversely, an increase in glucose-
810 derived UMP and its derivatives.

811 There was also a reduced abundance of glucose-derived fatty acid labelling in *T. congolense*
812 relative to *T. brucei*. Coupled with a decreased abundance of acetyl-CoA synthetase mRNA,
813 these results suggest that *T. congolense* may scavenge exogenous lipids in favour of
814 carrying out fatty acid biosynthesis, for which it must break down extracellular lipids to their
815 constituent parts. Indeed, supernatant metabolomics showed accumulation of both choline
816 and choline phosphate, with a corresponding decrease in the LysoPC lipids, which appears
817 to indicate activity of the phospholipases which *T. congolense* is known to secrete [58, 108].
818 It is unknown whether *T. congolense* is able to generate cytosolic acetyl-CoA for fatty acid
819 biosynthesis through the action of citrate lyase, although transcript abundance of this gene
820 was reduced compared to *T. brucei*. Analysis of drug sensitivity supports these conclusions,
821 as *T. congolense* is significantly less sensitive to acetyl-CoA synthetase inhibition, as well as
822 Orlistat, and inhibitor of fatty acid synthase, suggesting that fatty acid scavenging (e.g. lipid
823 or fatty acid transporters) could be a viable therapeutic target for this species.

BSF *T. brucei* growth in CMM required only cysteine and glutamine when supplemented with FBS gold, although a further 6 amino acids (Tyr, Phe, Trp, Leu, Met and Arg) were required when supplemented with standard FBS [56]. As part of this study, 14 amino acids essential for *T. congolense* growth were identified. Tryptophan and arginine, essential to *T. brucei*, were not required to sustain *T. congolense* growth in 10% goat serum. Conversely, several amino acids considered not essential to *T. brucei* were crucial for *T. congolense* growth *in vitro* (Asp, His, Ile, Pro, Ser and Val). Proline is a well-established carbon source for PCF *T. brucei* [87]. However, based on stable isotope labelling experiments, this amino acid is solely used for protein synthesis in BSF *T. congolense*, as there was no evidence of carbon dissemination from proline into the metabolome (likewise for asparagine). Unlike BSF *T. congolense*, BSF *T. brucei* must be able to synthesise sufficient amounts of these amino acids from alternative sources, or obtain them from the serum supplement.

One metabolic area of interest in trypanosomatids is trypanothione biosynthesis, a crucial pathway for parasite response to oxidative stress. Indeed, trypanothione synthase, as well as proteins involved in the trypanothione biosynthesis pathway, such as ornithine decarboxylase (targeted by Eflornithine), have long been considered prime chemotherapeutic targets due to their absence from other organisms [109]. Whilst cysteine was previously known to be a main carbon contributor to trypanothione synthesis in *T. brucei* along with glutamine and methionine [85], we show here that L-serine, an amino acid essential to *T. congolense*, also contributes to the generation of this metabolite. Interestingly, L-cysteine was not significantly depleted from *T. congolense* culture supernatants and future work should ascertain whether the presence of L-serine in medium can compensate for reduced L-cysteine levels in *T. congolense* culture.

The data presented here have led to the generation of a novel semi-defined medium for culturing the strain IL3000, which must be further optimized for the culture of multiple strains of *T. congolense*. Of interest is the peculiar requirement of adult bovine or goat serum for *in vitro* culture of *T. congolense*, rather than foetal bovine serum (FBS) which is typically used to culture *T. brucei* [15, 59]. Whilst this study made no attempts to adapt *T. congolense* to FBS-supplemented medium (indeed, even in SCM-7, growth rate is drastically reduced in the presence of FBS after 2-3 passages), this is of crucial importance, as it would allow the study of multiple species of African trypanosome under the same *in vitro* conditions. Analysis of metabolism presented here indicates that this phenomenon is likely to centre on the lipid requirements of *T. congolense*, although it remains to be seen if this requirement is for energy generation or synthesis of lipids in general. Furthermore, adult ruminant serum composition drastically differs from that of non-ruminants and of foetal ruminants [101, 102],

and this likely has significant implications on the extracellular environment faced by livestock trypanosomes.

The information presented here is a significant step in laying the foundation for fundamental understanding of metabolism for an important livestock parasite. Understanding essential areas of metabolism in both *T. brucei* and *T. congolense* enables the development of drugs effectively targeting both species. Conversely, understanding the key differences between the two species aids in dissecting drug mechanisms of action and resistance, as well as enabling a greater understanding of host-pathogen dynamics.

Materials and Methods

Compounds and reagents

All compounds were obtained from Sigma/Merck with the exception of: Orlistat (Cambridge Bioscience), oligomycin A (VWR International), diminazene aceturate (Cambridge BioScience) and FCCP (Abcam).

Cell lines and *in vitro* culture

In all cases, *T. congolense* strain IL3000 [48] was used (originally received from Theo Baltz, University of Bordeaux). For RNAi experiments a *T. congolense* IL3000 single marker line, TcoSM, was used [69]. For *in vitro* experiments, cells were grown at 34°C, 5% CO_2 and routinely cultured in either TcBSF3 [14] or HMI-93 [15], in both cases without a serum plus supplement, with 20% goat serum (Gibco). For global metabolite analysis of culture supernatant, an experimental medium (SCM-3) was used with the following components: 77 mM NaCl, 1.5 mM $CaCl_2$, 4.5 mM KCl, 0.8 mM $MgSO_4$, 36 mM $NaHCO_3$, 25 mM HEPES, 0.05 mM bathocuproinedisulfonic acid, 0.22 mM 2-mercaptoethanol, 50 U/mL penicillin/streptomycin, 2.5 mM glucose, 1 mM pyruvate, 10 % goat serum, 10% TcBSF3 [14], 1 mM each of L-cysteine and L-glutamine, and 100 µM L-tyrosine, L-phenylalanine, L-tryptophan, L-leucine, L-methionine and L-arginine. BSF *T. congolense* in exponential growth phase were centrifuged at 1,500 × *g* for 10 minutes, washed with PBS and inoculated into this medium (0 h time point).

For stable isotope labelling experiments, as well as experiments involving the removal or addition of specific medium components, a custom medium, Steketee's Congolense Medium-6 (SCM-6) was used (S6 Table). The final medium formulation based on this study's findings, SCM-7, is provided in S6 Table. This medium is essentially HMI-93, although i) vitamins (with the exception of folate) were removed, ii) D-glucose concentrations were modified depending on experimental procedure, but was routinely kept at 10 mM, iii) goat serum levels were reduced to 10% and, iv) of the 20 amino acids, 14 were added. Increasing

the temperature to 37°C led to a detrimental effect on cell viability after several passages, as previously reported [15].

For experiments involving *T. brucei*, either the monomorphic Lister 427 (*in vitro* experiments and growth curves) or pleomorphic STIB 247 (RNAseq experiments, both *in vitro* and *ex vivo* sample groups) strains were used. Lister 427 cells were grown in HMI-11 [110], whilst STIB 247 were grown in modified HMI-9 containing 1.1% methylcellulose and 20% serum plus (Sigma) [111, 112]. In both cases, cells were incubated at 37°C, 5% CO_2.

For both species, cell counts were carried out using a haemocytometer, and in the case of *T. congolense*, cells were mechanically detached from the culturing plasticware by pipetting prior to counting. Growth curves were routinely carried out in 2 mL samples incubated in 24-well plates, resuspended using a P1000. For detachment of cells from flasks, 10 mL plastic pipettes were used. In cases where cells were harvested for experiments other than those involving metabolomics, cells could also be detached by replacing the medium with PBS for incubating at room temperature for several minutes, prior to vigorously tapping the flask to detach parasites.

RNAi experiments using TcoSM were carried out in HMI-93 in 20 mL cultures. Cells were seeded at 7×10^5 cells/mL and RNAi induction was initiated with the addition of 1 µg/mL tetracycline (Sigma) and 1×10^7 cells were isolated every 24 hours for RNA analysis (outlined below) before cells were passaged

Ethics statement

All animal experiments were performed in accordance with the Animals (Scientific Procedures) Act 1986 and the University of Glasgow care and maintenance guidelines. All animal protocols and procedures were approved by The Home Office of the UK government and the University of Glasgow Ethics Committee.

Animal experiments

Adult female CD-1 mice (20–30 g body weight; Charles River Laboratories) were infected with 5×10^4 wild-type *T. brucei* STIB 247 or 1×10^5 wild-type *T. congolense* IL3000 by intraperitoneal injection. Parasitaemia was monitored daily by venesection of the lateral tail vein [113]. At first peak of parasitaemia (>10^7 cells/mL) mice were euthanised and blood isolated. Parasites of both species were purified from blood by anion exchange using DEAE cellulose [114]. Purified cells were counted, and a total of 1×10^8 cells were centrifuged for 10 minutes at 1,500 × *g* prior to RNA extraction.

RNA extraction

For RNAseq experiments, 10^8 cells were isolated either from *in vitro* culture or from mouse infections. RNA was extracted using the QIAgen RNeasy kit (Qiagen) with an on-column DNase treatment step. Sample concentrations were analysed by Nanodrop and QuBit, and concentrations adjusted to 37 ng/µL of which 80 µL (2.96 µg) was submitted for RNAseq.

For RNAi time course experiments, cell pellets (10^7 cells) were resuspended in 1 mL TRIzol (Invitrogen) and stored at -80°C. Samples were thawed, 200 µL chloroform was added, samples were shaken vigorously for 15 seconds and incubated at room temperature for 3 minutes, prior to centrifugation at 12,000 × *g* for 15 minutes, 4°C. The aqueous layer was transferred to a fresh tube and 500 µL isopropanol and 1 µL Glycoblue (Invitrogen) were added. Samples were mixed by inverting, incubated at room temperature for 10 minutes and centrifuged at 12,000 × *g* for 10 minutes at 4°C. RNA pellet was washed in ice-cold 75% ethanol and centrifuged at 12,000 × *g* for 10 minutes at 4°C. After air-drying, RNA was resuspended in 20 µL RNase-free water and concentration adjusted to 100 ng/µL. DNase treatment was carried out using the Ambion TURBO DNase kit (Applied Biosystems) as per manufacturer's instructions.

Metabolomics sample preparation

For metabolomics analysis of supernatants, 10 mL *T. congolense* cultures were incubated in T25 flasks in relevant media. Cells were centrifuged at 1,500 × *g* for 10 minutes, washed with PBS, resuspended in relevant media and density adjusted to 1×10^5 cells/mL. At each time-point, 500 µL medium was transferred to a 1.5 mL eppendorf tube and briefly quenched in a dry ice/ethanol bath, before centrifuging at 1,500 × *g* for 10 minutes at 4°C. A 5 µL aliquot was then transferred to a new eppendorf containing 200 µL metabolite extraction solvent (chloroform:methanol:water in a 1:3:1 ratio) and samples vortexed at 4°C for one hour. Samples were centrifuged for 5 minutes at 13,000 × *g* (4°C) and supernatants transferred to new eppendorfs. Samples were stored at -80°C prior to analysis.

For analysis of intracellular metabolites, cells were grown to a final density of 2×10^6 cells/mL and a total of 10^8 cells isolated. Cells were quenched in 50 mL falcon tubes to 4°C using a dry ice/ethanol bath (stirred and measured by thermometer) and all subsequent steps were carried out at 4°C. Cells were centrifuged at 1,500 × *g* for 10 minutes and if supernatant samples were required in addition to cell pellets, 5 µL was transferred to an eppendorf containing 200 µL extraction solvent. Cells were resuspended in residual medium before transfer to eppendorf tubes. Cells were then centrifuged (1,500 × *g*, 5 minutes) and washed twice with ice-cold phosphate buffered saline (PBS) before resuspension in 200 µL extraction solvent (chloroform:methanol:water in a 1:3:1 ratio). Samples were vortexed at

4°C for 1 hour, and then centrifuged for 5 minutes at 13,000 × *g*. Supernatants were transferred to clean eppendorf tubes. For all experiments, a quality control sample was generated by pooling 10 µL from each sample and samples were stored under argon gas at -80°C.

Primers and plasmids

RNAi experiments were carried out using a *T. congolense* single marker line, TcoSM [69] that expresses Tet repressor and T7 polymerase, maintained in 0.5 µg/mL puromycin, and gene specific RNAi constructs were introduced with a *T. congolense* specific plasmid, p3T7-TcoV [69]. Primers carrying a HindIII (5'-AAGCTT-forward) or an FseI (5'-GGCCGGCC-reverse) restriction site were used to amplify *TcoPEPCK*, *TcoPPDK* and *TcoHT* (S7 Table). Gene fragments were amplified using a HiFi polymerase master mix (NEB) and cloned into pGEM-T easy (Promega) and sequenced to confirm correct sequence identity of each fragment. The constructs were then digested with HindIII and FseI and ligated into the p3T7-TcoV vector using T4 DNA ligase (Promega). The final plasmid was linearised with NotI before purification by ethanol precipitation prior to electroporation into TcoSM cells.

Transfections/electroporations

T. congolense IL3000 electroporation experiments and selection experiments were performed as developed by [69]. A total of 4×10^7 cells were used per transfection, including a negative (buffer only) control. A transfection buffer previously published for use with *T. brucei* was used for *T. congolense* transfections [115]. Cells were centrifuged at 1,500 × *g* for 10 minutes, pellets resuspended in residual medium and transferred to eppendorf tubes for a further centrifugation step. Cells were subsequently washed in transfection buffer prior to final resuspension in 100 µL buffer per transfection. Up to 12 µg linearised plasmid DNA was added to an electroporation cuvette (Sigma), and 100 µL cells were subsequently added. Electroporation was carried out using a Nucleofector II (Lonza) programme Z-001. Transfected cells were then incubated overnight in 25 mL warm medium in the absence of selective antibiotics, prior to their addition and plating out at dilutions of 1:50, 1:100 and 1:200 in 96-well plates. Antibiotics were added at the following concentrations: Puromycin: 0.5 µg/mL; Neomycin (G418): 0.4 µg/mL. Clones were retrieved after 7-10 days, and these were maintained in 0.25 µg/mL puromycin and 0.2 µg/mL G418.

Drug sensitivity assays

Drug sensitivity assays were carried out using the alamar blue method developed by Raz and colleagues [116]. Briefly, Compounds were diluted to 2× starting concentration in SCM-6 (with 10% goat serum for *T. congolense* IL3000 or 10% FBS for *T. brucei* Lister 427) and 200 µL was transferred to the first well of a solid white flat-bottomed 96-well plate. 100 µL

995 medium was then added to 23 further wells and compounds were diluted 1:2 over this series
996 of wells, with the exception of the last well, for a negative control. Subsequently, 100 µL cells
997 were added at 2× starting density (4×10^4 cells/mL for *T. brucei* and 5×10^5 cells/mL for *T.*
998 *congolense*). Plates were incubated for 48 hours (37°C or 34°c for *T. brucei* and *T.*
999 *congolense*, respectively, 5% CO_2 in both cases), prior to addition of 20 µL resazurin sodium
1000 salt (0.49 mM in 1× PBS, pH 7.4) to each well. Plates were then incubated for a further 24
1001 hours before measurements of cell viability.

1002 Reduction of the resazurin salt was measured as a function of cell viability. Fluorescence of
1003 each plate was read using a Cytation 5 imaging reader (BioTek) and GEN5 software.
1004 Parameters were as follows: $\lambda_{excitation}$ = 540 nm and $\lambda_{emission}$ = 590 nm. Raw values were
1005 plotted against concentrations (converted to Log_{10} values) and normalised (0% defined as
1006 smallest mean in the dataset; 100% defined as largest mean in the dataset) using Graphpad
1007 Prism version 8.4.0. EC_{50} values for each compound were calculated using a non-linear
1008 sigmoidal dose-response curve. Each assay was performed in duplicate and each EC_{50}
1009 value represents a mean of three independent experiments.

1010 ## Real-time quantitative PCR (RT-qPCR)

1011 RNA was extracted as described above, and reverse transcription was carried out in 20 µL
1012 using 1 µg RNA, using a high capacity cDNA kit (Applied Biosystems). Primers for RT-qPCR
1013 analysis were designed using Primer 3 [117], and primer efficiency was tested using serial
1014 dilutions of *T. congolense* IL3000 genomic DNA by plotting Ct value against Log_{10}(DNA
1015 concentration). Real-time PCR was carried out using the SensiFAST SYBR Hi-ROX kit
1016 (Bioline, BIO92005). Briefly, a 20 µL reaction was set up using 10 µL SYBR mix, RT
1017 template and 400 nM of each primer. Cycling conditions were: 96°C, 120 seconds, followed
1018 by 40 cycles of 95°C for 5 seconds, 62°C for 10 seconds and 72°C for 20 seconds.
1019 Previously published endogenous control primers for TcoTERT were used for within sample
1020 normalisation [118], and normalised transcript level was calculated using the delta delta Ct
1021 method [119].

1022 ## Glucose uptake assays

1023 For analysis of wild-type *T. congolense* and *T. brucei* glucose uptake, cells were seeded in
1024 10 mL cultures of SCM-6 at an initial density of 2×10^5 cells/mL (four cultures per species),
1025 with 10 mM glucose added separately at the start of the experiment. Upon the addition of
1026 glucose, 1 mL supernatant was immediately centrifuged (1,500 × *g*, 10 minutes) and
1027 supernatant stored at -80°C. This process was repeated at 12, 15, 18, 21 and 24 h, and cell
1028 density measured by haemocytometer. A medium-only control (4 replicates) was also
1029 incubated alongside *in vitro* cultures. Glucose concentration of each supernatant sample

was analysed using the Glucose (GO) assay kit (GAGO-20; Sigma) in a 96-well format. Briefly, 40 µL supernatant sample (diluted if necessary) was incubated with 80 µL assay reagent for 30 minutes at 37°C, after which 80 µL 12 N sulphuric acid was added and absorbance measured at 540 nm using a spectrophotometer. A standard curve was also run to calculate glucose concentration. Rate of glucose consumption was calculated using a custom script [57].

For glucose consumption of the TcoHT RNAi line, the Glucose Uptake-Glo kit (Promega) was used. RNAi was induced for 72 hours prior to carrying out the assay. Cells were centrifuged, washed in PBS and resuspended in assay buffer (77 mM NaCl, 1.5 mM $CaCl_2$-$2H_2O$, 4.5 mM KCl, 0.8 mM $MgSO_4$-$7H_2O$, 36 mM $NaHCO_3$, 25 mM HEPES and 0.02 mM bathocuproinedisulfonic acid), as it was determined *T. congolense* viability is reduced in PBS alone. Density was adjusted to 10^8 cells/mL, and three 100 µL replicates of each sample were added to wells of a black flat-bottomed 96-well plate. The uptake reaction was started by the addition of 50 µL 1 mM 2-deoxy-D-glucose. Plate was shaken for 15 minutes at 34°C prior to addition of 25 µL stop buffer, 25 µL neutralisation buffer and 100 µL pre-prepared 2DG6P detection reagent. Plates were shaken in between addition of the buffers. Finally, the plate was read with 0.3–1 second integration on a luminometer (Cytation 5 Imaging reader, BioTek). Wild-type *T. congolense*, and *T. congolense* supplemented with glucose were used as controls, in addition to cells without 2-deoxy-D-glucose and assays in the absence of cells.

Metabolomics – Liquid chromatography mass spectrometry

Hydrophilic interaction liquid chromatography (HILIC) was carried out by Glasgow Polyomics (Glasgow, UK), using a Dionex UltiMate 3000 RSLC system (Thermo Fischer Scientific) coupled to a ZIC-pHILIC column (150 mm × 4.6 mm, 5 µm column, Merch Sequant). The column was maintained at 30°C and samples were eluted with a linear gradient (20 mM ammonium carbonate in water and acetonitrile) over 26 minutes with a flow rate of 0.3 mL/minute.

Sample injection volume was 10 µL and samples were maintained at 4°C before injection. A Thermo Orbitrap Exactive (Thermo Fischer Scientific) was used to generate mass spectra, and was operated in polarity switching mode with the following settings: Resolution: 50,000; AGC: 106; m/z range: 70–1,400; sheath gas: 40; auxiliary gas: 5; sweep gas: 1; probe temperature: 150°C; capillary temperature: 275°C. Samples were run in both positive and negative polarity with the following ionisation: source voltage +4.5 kV, capillary voltage +50 V, tube voltage +70 kV and skimmer voltage +20 V for positive mode; source voltage -3.5 kV, capillary voltage -50 V, tube voltage -70 V and skimmer voltage -20 V for negative mode.

Mass calibration was performed for each polarity immediately prior to each analysis batch. The calibration mass range was extended to cover small metabolites by inclusion of low-mass contaminants with the standard Thermo calmix masses (below *m/z* 1400), $C_2H_6NO_2$ for positive ion electrospray ionisation (PIESI) mode (*m/z* 76.0393) and $C_3H_5O_3$ for negative ion electrospray ionisation (NIESI) mode (*m/z* 89.0244). To enhance calibration stability, lock-mass correction was also applied to each analytical run using these ubiquitous low-mass contaminants. A set of authentic standards was run prior to the sample set for each experiment.

Metabolomics data analysis

RAW spectra were converted to mzXML files (mzML files for fragmentation data) using XCMS for untargeted peak detection [120]. The resultant files were further processed using mzMatch [121] for peak matching and annotation, resulting in a tabular output that was analysed using IDEOM with default settings [122]. For stable-isotope assisted metabolomics experiments, mzMatch output (in .peakml format) was analysed using mzMatch-ISO to extract all carbon isotopologue abundances from putative metabolites [123]. Data analysis of stable isotope-labelled metabolomics was based on a 48 hour time-point in all experiments. Data was further analysed using Microsoft Excel or Metaboanalyst v4.0 [124]. The mzXML files from all metabolomics analyses are available in Metabolights.

RNA sequencing and data processing

RNA sequencing was carried out by Edinburgh Genomics (Edinburgh, UK). Libraries were prepared from 8 samples (4× *T. brucei*, 4× *T. congolense*) using the TruSeq Stranded mRNA kit (Illumina) and 2 × 75 bp paired-end sequencing was carried out using a HiSeq 4000 system (Illumina). Sequencing reads were aligned to the corresponding genome sequence using HiSat2 (--no-spliced-alignment) [125]. For *T. brucei*, the TREU 927 reference genome sequence was used (v34.0 from TriTrypDB [126]), whilst a PacBio assembly of *T. congolense* IL3000 was used for *T. congolense* [65]. The resulting SAM files were converted to BAM files using samtools [127], and subsequently filtered for quality and primary alignment (-q 1 -F 0x100), the latter to reduce the effects of multimapping. Read counts were extracted from the filtered BAM files using HTSeq-count (-s reverse -f bam -t CDS -i ID -m union -a 0 --nonunique all).

For all samples, transcripts per million (TPM) values for each gene were calculated manually using Microsoft Excel as follows: 1) Reads per kilobase (RPK) were calculated by dividing the read counts by the length of gene in kilobases; 2) All RPK values in a sample were summed and divided by 1 million as a scaling factor; 3) Each RPK value was divided by the scaling factor to yield TPM values [53]. To compare transcript abundances between the two

species, Orthofinder [54] was used to infer orthologue genes or gene groups. Default parameters were used to compare the TriTrypDB v34.0 TREU 927 annotated proteins and the PacBio *T. congolense* IL3000 annotated proteins (S2 Table). A custom MATLAB (version R2019a) was used to combine the Orthofinder dataset and the TPM values for 1-to-1 orthologues, as well as "sum of TPM" values for groups containing multiple genes, where TPM value for each gene was summed, resulting in a final dataset (S1 Table). Raw RNA-seq data is deposited at GEO. Transcriptomics data were cross-referenced with the TrypanoCyc database (vm-trypanocyc.toulouse.inra.fr/; [60]) to enable pathway analysis of the data.

Computation

Figures were generated using Graphpad Prism version 8.4.0 (www.graphpad.com) with the exception of scatter plots and heatmaps, which were generated using R [128]. Heatmaps were generated using the R packages pheatmap and ComplexHeatmap [129]; scatter plots were generated using GGplot2 and GGally; and pathway maps were generated with Inkscape v1.0.

Acknowledgements

The authors would like to thank the following people: Steve Kelly, Paul Michels & Simon Young for very useful discussion. We thank Anne-Marie Donachie for help with *in vivo* experiments. In addition, the authors would like to thank the following institutes: Glasgow Polyomics for LC-MS work, Edinburgh Genomics for RNAseq, MRC PPU DNA Sequencing and Services, Dundee, for plasmid sequencing. LM, PS, EP, HdK and MPB were funded by BBSRC grant BB/N007492/1, and LM, PS, EP, RR and MPB by BB/S00243X/1. CG and BW were funded by University of Nottingham Strategic Support Funds (Wellcome Trust), and GAM by Sir Halley Stewart Medical Research Grant (R410). This article is based on research funded in part by the Bill & Melinda Gates Foundation (Investment ID OPP1176784) and with UK aid from the UK Government (Project 300504) through GALVmed. The findings and conclusions contained within are those of the authors and do not necessarily reflect positions or policies of the Bill & Melinda Gates Foundation or the UK Government. The Roslin Institute is core funded by the BBSRC (BS/E/D/20002173).

Figure legends

Figure 1: Overview of comparative transcriptomics analysis of *T. brucei* and *T. congolense*, isolated from *ex vivo* and *in vitro* conditions. RNAseq data from *T. congolense* (IL3000) and *T. brucei* (STIB247) in both *in vitro* and *ex vivo* (from mouse

infections) conditions was aligned to the species' respective genome sequence and read counts were normalised by the transcripts per million (TPM) method. To directly compare the species, a pseudogenome was generated using the Orthofinder tool [54]. TPM values from the 4 sample groups were plotted against each other to analyse correlation between conditions (A and B) and between species in the same conditions (C and D). Correlation was assessed using both Spearman's rank correlation (ρ) and Pearson correlation (ρ; Pearson's *r*) coefficients.

Figure 2: Analysis of supernatant metabolites after *T. congolense* culture. A heatmap covering the 80 putative medium components judged to be significantly altered after 56 hours of *in vitro* cell culture containing *T. congolense* strain IL3000, as calculated by a one-way repeated measures ANOVA ($P < 0.05$). Peak abundances were log transformed and mean centred and metabolites were clustered based on Pearson correlation. Two clusters of interest were identified, which are shown in a larger format on the right. Metabolites in the top cluster were observed to increase significantly over time, whilst those in the bottom cluster decreased. Metabolite names follow by [*] were matched to an authentic standard. B) Comparison of metabolite changes in medium supernatants after 56 hours between *T. brucei* [56] and *T. congolense* (S4 Table). Relative changes in metabolite abundance were calculated as Log_2 fold change of 56 h vs 0 h. Key differences are highlighted numerically: 1, guanine; 2, N6-acetyl-L-lysine; 3, succinate; 4, 4-hydroxy-4-methylglutamate; 5, N6,N6,N6-trimethyl-L-lysine; 6, choline; 7, 2-oxoglutarate; 8, L-1-pyrroline-3-hydroxy-5-carboxylate; 9, D-glycerate; 10, pyruvate; 11, 12-hydroxydodecanoic acid; 12, L-cystine; 13, diacetyl; 14, [PC (18:0)] 1-octadecanoyl-sn-glycero-3-phosphocholine; 15, LysoPC(17:0); 16, [PC (16:0)] 1-hexadecanoyl-sn-glycero-3-phosphocholine; 17, inosine; 18, [PC (16:1)] 1-(9Z-hexadecenoyl)-sn-glycero-3-phosphocholine; 19, [FA trihydroxy(18:1)] 9S,12S,13S-trihydroxy-10E-octadecenoic acid; 20, inosine.

Figure 3: Energy metabolism in *T. congolense*. A-E) Supernatant metabolomics analysis of metabolites involved in glycolytic metabolism in *T. congolense*. Grey bars indicate a negative medium control incubated for 56 hours. F) A commercial kit was used to measure acetate concentration during *T. congolense* culture, with supernatant samples analysed at the same time points as the supernatant metabolomics experiment. G) A simplified overview of the glycolytic pathway. Typically, the succinate shunt is only active in PCF *T. brucei*, with low levels of activity in BSF *T. brucei*. Numbers refer to the following proteins: 1, glucose transporters; 2, hexokinase; 3, glucose 6-phosphate isomerase; 4, phosphofructokinase; 5, aldolase; 6, triosephosphate isomerase; 7, glycerol 3-phosphate dehydrogenase; 8, glycerol kinase; 9, glyceraldehyde 3-phosphate dehydrogenase; 10, phosphoglycerate kinase; 11, phosphoglycerate mutase and enolase; 12, phosphenolpyruvate carboxykinase; 13, malate

dehydrogenase; 14, fumarate hydratase; 15, NADH-dependent fumarate reductase; 16, pyruvate kinase; 17, alanine aminotransferase; 18, pyruvate dehydrogenase complex; 19, acetate:succinate CoA-transferase and acetyl-CoA thioesterase. H) Tracing glucose derived carbon usage through glycolytic metabolism. *T. congolense* were incubated with a 50:50 mix of ^{12}C-D-glucose:^{13}C-U-D-glucose before cell pellets were isolated for metabolomics analysis. Results were compared to those generated in *T. brucei* by Creek and colleagues [42]. Colours indicate the number of ^{13}C atoms in each metabolite. I) Comparative analysis of transcript level activity of glycolysis in *T. brucei* and *T. congolense* from both *in vitro* and *ex vivo* conditions. Gene IDs: HK1 & 2, hexokinase, TbTc_0341; GPI, glucose 6-phosphate isomerase, TbTc_1840; PFK, phosphofructokinase, TbTc_1399; ALDA, aldolase, TbTc_0358; TPI, Triosephosphate isomerase, TbTc_1075; GPDH, glycerol 3-phosphate dehydrogenase, TbTc_2722; GK, glycerol kinase, TbTc_0392; GAPDH, glyceraldehyde 3-phosphate dehydrogenase, TbTc_0377; PGK, phosphoglycerate kinase, TbTc_6030; PGKA, phosphoglycerate kinase A, TbTc_0241; PGKB/C, phosphoglycerate kinase B & C, TbTc_0240, ENO1, enolase, TbTc_0465; ENO2, enolase, putative, TbTc_3614, PK1, pyruvate kinase 1, TbTc_0372; FBPase, fructose-1,6-bisphosphatase, TbTc_1967; PEPCK, phosphoenolpyrvuate carboxykinase, TbTc_0348; gMDH, glycosomal malate dehydrogenase, TbTc_0642, FH, fumarate hydratase, TbTc_0242; Frd, NADH-dependent fumarate reductase, TbTc_0141; PPDK, pyruvate phosphate dikinase, TbTc_1304; AAT, alanine aminotransferase, TbTc_0675; PDH E1α, pyruvate dehydrogenase E1 alpha subunit, TbTc_4169; PDH E1β, pyruvate dehydrogenase E1 beta subunit, TbTc_5437.

Figure 4: *In vitro* analysis of glycolytic metabolism. To further probe glycolytic metabolism in *T. congolense*, novel RNAi technology was employed to knock-down key glycolytic and gluconeogenic steps. A) *T. congolense* remains viable in reduced glucose concentrations. A growth defect was only observed when glucose concentrations were reduced to <2 mM. B) Supplementation with increased concentrations of 2-deoxy-D-glucose leads to *T. congolense* cell death (red dotted line indicates detection limit by haemocytometer). C) Growth analysis of RNAi-mediated knock-down of PEPCK in *T. congolense* IL3000 single marker induced with 1 µg/mL tetracycline. D) Growth analysis of RNAi-mediated knock-down of PPDK in *T. congolense* IL3000 single marker induced with 1 µg/mL tetracycline. E-F) Transcript abundance over time, following tetracycline-mediated RNAi induction of PEPCK and PPDK. G) Knock-down of the entire glucose transporter (HT) array does not affect *in vitro* cell viability. H) Normalised HT mRNA abundance over time after RNAi induction. I) Changes in glucose uptake in RNAi-induced cells were detected via an enzyme-linked luminescence assay coupled to 2-deoxy-D-glucose uptake over a period

of 30 minutes. The assay was carried out 72-hours post-induction. Of the three RNAi lines, 2 showed a significant reduction in glucose uptake capability (*$P < 0.05$; ***$P < 0.001$)

Figure 5: Nucleotide metabolism in *T. congolense*. Supernatant analysis of *T. congolense in vitro* cultures showing changes in abundance of D-ribose (A), guanine (B), xanthine (C) and inosine (D) over 56 hours. Grey bar indicates a negative medium control group E) Simplified overview of purine salvage and synthesis in trypanosomatids adapted from [130]. Numbers indicate the following enzymes: 1, APRT; 2, AD; 3, HGPRT; 4, IMPD; 5, HGXPRT; 6, GMPR; 7, GMPS; 8, HGPRT. Red cross indicates guanine deaminase, which is not encoded/annotated in the *T. congolense* genome. F) Comparison of glucose-derived purine carbon labelling in *T. congolense* and *T. brucei* [42]. Colours indicate the number of ^{13}C atoms in each metabolite. D) Comparative RNAseq analysis of *T. congolense* and *T. brucei* under both *in vitro* and *ex vivo* conditions. Gene IDs from top to bottom: P121-PWY (adenine/adenosine salvage): IMPDH1, inosine-5'-monophosphate dehydrogenase, TbTc_1648; ADSS, adenylosuccinate synthetase, TbTc_1142; APRT-1, cytosolic adenine phosphoribosyltransferase, TbTc_3522; HGPRT, hypoxanthine-guanine phosphoribosyltransferase, TbTc_0726; GMPR, GMP reductase, TbTc_4627; HGXPRT, hypoxanthine-guanine-xanthine phosphoribosyltransferase, TbTc_3696; APRT-2, glycosomal adenine phosphoribosyltransferase, TbTc_5918; ADSL, adenylosuccinate lyase, TbTc_1986. PWY0-162 (pyrimidine biosynthesis): DHODH, dihydroorotate dehydrogenase (fumarate), TbTc_0620; PYR1A-B, glutamine hydrolysing carbomoyl phosphate synthase, TbTc_1631; PYR2, aspartate carbamoyltransferase, TbTc_1630; PYR3, dihydroorotase, TbTc_3801; CTPS, cytidine triphosphate synthase, TbTc_0920; OMPDC/OPRT, orotidine-5-monophosphate decarboxylase/orotate phosphoribosyltransferase, TbTc_0735; CMF40a, nucleoside diphosphate kinase, TbTc_5784. PWY0-163 (pyrimidine salvage): UP, uridine phosphorylase, TbTc_5794; CDA, cytidine deaminase, TbTc_3318; UPRT, uracil phosphoribosyltransferase, TbTc_4220; NDPK, nucleoside diphosphate kinase, TbTc_0593; CMF40a, nucleoside diphosphate kinase, TbTc_5784; NDPK3, nucleoside diphosphate kinase 3, TbTc_2560.

Figure 6: Amino acid metabolism in *T. congolense* IL3000. A-C) Analysis of indicated amino acids in *T. congolense* IL3000 culture supernatants over a 56 h time course. Grey bars indicate a negative medium control group. D-F) Growth curves in SCM-6 excluding one amino acid at a time, to determine those essential to *T. congolense* viability. In each experiment, full SCM-6 was used as a positive control. Legends indicate which amino acid was removed in each experiment. G) Growth analysis of SCM-6 and SCM-7, the latter containing only amino acids deemed essential, compared to HMI-93 [110]. H) Simplified map of intracellular glutamine metabolism. Numbers refer to the following enzymes: 1,

glutaminase; 2, glutamate decarboxylase; 3, 4-aminobutyrate aminotransferase; 4, succinate semialdehyde dehydrogenase; 5, glutamate dehydrogenase; 6, 2-oxoglutarate dehydrogenase; 7, Succinyl-CoA synthetase; 8, isocitrate dehydrogenase; 9 & 10, aconitase. I) Carbon utilisation from L-glutamine was analysed in *T. congolense* (100% ^{13}C-U-L-glutamine) and compared to that in *T. brucei* (50:50 ratio of L-glutamine and ^{13}C-U-L-glutamine) [85].

Figure 7: Fatty acid metabolism in *T. congolense*. A) Glucose-derived ^{13}C carbon labelling of saturated fatty acids in *T. congolense* and *T. brucei* [42]. Colours correspond to the number of ^{13}C labels detected in each metabolite. B) L-threonine-derived saturated fatty acid 13C labelling in T. congolense. Fatty acid systematic names and numbers: lauric acid: dodecanoic acid, C12:0; myristic acid: tetradecanoic acid, C14:0; palmitic acid: hexadecanoic acid, C16:0; nonadecyclic acid: nonadecanoic acid, C19:0. C) Transcriptomics analysis of acetate and lipid metabolism. Gene names and IDs: ACH, acetyl-CoA hydrolase, TbTc_5515; ACS, acetyl-CoA synthetase, TbTc_0318; AKCT, 2-amino-3-ketobutyrate-CoA ligase, TbTc_6236; TDH, L-threonine 3-dehydrogenase, TbTc_5991; PDHe1α, pyruvate dehydrogenase E1 α subunit, TbTc_4169; PDHe1β, pyruvate dehydrogenase E1 β subunit; SCSα, succinyl-CoA synthetase α subunit, TbTc_0813; PPDK, pyruvate phosphate dikinase, TbTc_1304; PDHe2, dihydrolipoamide acetyltransferase, TbTc_1015; PDHe3, pyruvate dehydrogenase E3, TbTc_4765; PYK1, pyruvate kinase, TbTc_0372; BKR, β-ketoacyl-ACP reductase, TbTc_1241; BKS, β-ketoacyl synthase, TbTc_3372; ACC, acetyl-CoA carboxylase, TbTc_0754; HMGCL, hydroxymethylglutaryl-CoA lyase, TbTc_6160; FPPS, farnesyl pyrophosphate synthase, TbTc_5375; LSS, lanosteral synthase, TbTc_4540; MVK, mevalonate kinase, TbTc_3761; SM, squalene monooxygenase, TbTc_3357; MDD, mevalonate diphosphate decarboxylase, TbTc_0546; SMT, sterol 24-c methyltransferase, TbTc_0387; CYP51A1, lanosterol 14α demethylase, TbTc_4837; SQase, squalene synthase, TbTc_2577; SPPS, solanesyl-diphosphate synthase, TbTc_3025; IDI, isopentenyl-diphosphate delta-isomerase, TbTc_1099; PTase, prenyltransferase, TbTc_1352; GGTase-IIβ, geranylgeranyl transferase type II β subunit, TbTc_0680; SCP2, 3-ketoacyl-CoA thiolase, TbTc_4024; PMVK, phosphomevalonate kinase, TbTc_3039; HMGR, 3-hydroxy-3-methylglutaryl-CoA reductase, TbTc_3189; LACS5, fatty acyl-CoA synthetase, TbTc_0099; ACSL_0688, long-chain-fatty-acid-CoA ligase, TbTc_0688; ECHD, enoyl-CoA hydratase, TbTc_3283; ACS3/ACS4, fatty acyl-CoA synthetase 3 & 4, TbTc_0101; ACS1, fatty acyl-CoA synthetase 1, TbTc_0100; ACS2, fatty acyl-CoA synthetase 2, TbTc_0102; ECI_4184, 3,2-trans-enoyl-CoA isomerase, TbTc_4184; ACSL_2381, long-chain-fatty-acid-CoA ligase, TbTc_2381; TFEα1, enoyl-CoA hydratase/enoyl-CoA isomerase, TbTc_3362; SCP2, 3-

ketoacyl-CoA thiolase, TbTc_4024; ECI_0360, 3,2-trans-enoyl-CoA isomerase, TbTc_0360; ACAD, acyl-CoA dehydrogenase, TbTc_4954.

Figure 8: Pharmacological inhibition of fatty acid synthesis in *T. brucei* and *T. congolense*. Dose-response curves to determine differential sensitivity of the two species of parasite to inhibition of an ACS inhibitor (panel A) and Orlistat (B).

Figure 9: Summary of *T. congolense* and *T. brucei in vitro* transcriptome. Log_2 fold change *T. congolense*/*T.brucei*) was calculated for each gene (for ratio changes, see the key on the bottom-left). Dashed lines represent transport processes. Genes: 1, hexose transporters, TbTc_0095; 2, hexokinase, TbTc_0341; 3, glucose-6-phosphate isomerase, TbTc_1840; 4, phosphofructokinase, TbTc_1399; 5, fructose-1,6-bisphosphatase, TbTc_1967; 6, aldolase, TbTc_0358; 7, triosephosphate isomerase, TbTc_1075; 8, glycerol-3-phosphate dehydrogenase, TbTc_2722; 9, glycerol kinase, TbTc_0392; 10, glyceraldehyde 3-phosphate dehydrogenase, TbTc_0377; 11, phosphoglycerate kinase, TbTc_0240; 12, phosphoglycerate mutase, TbTc_5039; 13, enolase, TbTc_0465; 14, pyruvate kinase 1, TbTc_0372; 15, alanine aminotransferase, TbTc_0675; 16, pyruvate phosphate dikinase, TbTc_1304; 17, Phosphoenolpyruvate carboxykinase, TbTc_0348; 18, glycosomal malate dehydrogenase, TbTc_0642; 19, glycosomal fumarate hydratase, TbTc_0242; 20, glycosomal NADH-dependent fumarate reductase, TbTc_0140; 21, glucose-6-phosphate dehydrogenase, TbTc_0931; 22, 6-phosphogluconolactonase, TbTc_4165; 23, 6-phosphogluconate dehydrogenase, TbTc_2025; 24, ribulose-5-phosphate epimerase, TbTc_4356; 25, ribose 5-phosphate isomerase, TbTc_3090; 26, transketolase, TbTc_1701; 27, transaldolase, TbTc_1823; 28, ribokinase, TbTc_5212; 29, malic enzyme, TbTc_0296; 30, Mitochondrial pyruvate carrier 2, TbTc_2668; 31, FAD-dependent glycerol-3-phosphate dehydrogenase, TbTc_2282; 32, NADH dehydrogenase (NDH2), TbTc_5033; 33, Alternative oxidase, TbTc_6589; 34, mitochondrial fumarate hydratase, TbTc_0243; 35, mitochondrial NADH-dependent fumarate reductase, TbTc_0141; 36, mitochondrial malate dehydrogenase, TbTc_0256; 37, citrate synthase, TbTc_0486; 38, aconitase, TbTc_5765; 39, isocitrate dehydrogenase, TbTc_0510; 40, 2-oxoglutarate dehydrogenase E1 component, TbTc_2864; 41, 2-oxoglutarate dehydrogenase E1 component, TbTc_3111; 42, 2-oxoglutarate dehydrogenase E2 component, TbTc_3057; 43, succinyl-CoA synthetase α, TbTc_0813; 44, succinyl-CoA ligase β, TbTc_3392; 45, glutamine synthetase, TbTc_2226; 46, glutamate dehydrogenase, TbTc_0872; 47, pyruvate dehydrogenase E1 α subunit, TbTc_4169; 48, pyruvate dehydrogenase E1 β subunit, TbTc_5437; 49, dihydrolipoamide acetyltransferase, TbTc_1015; 50, pyruvate dehydrogenase complex E3, TbTc_4765; 51, L-threonine 3-dehydrogenase, TbTc_5991; 52, 2-amino-3-ketobutyrate coenzyme A ligase, TbTc_6236; 53, Acetyl-CoA hydrolase (ACH), TbTc_5515; 54, Succinyl-CoA:3-ketoacid

coenzyme A transferase (ASCT), TbTc_0236; 55, Acyl carrier protein, TbTc_5262; 56, beta-ketoacyl-ACP synthase, TbTc_3372; 57, beta-ketoacyl-ACP reductase, TbTc_1241; 58, Trans-2-enoyl-ACP reductase 1, TbTc_5269; 59, acetyl-CoA synthetase, TbTc_0318; 60, acetyl-CoA carboxylase, TbTc_0754; 61, Fatty acid elongase (ELO1), TbTc_0159; 62, Fatty acid elongase (ELO2), TbTc_1882; 63, Fatty acid elongase (ELO3), TbTc_0235; 64, elongation of very long chain fatty acids protein (ELO4), TbTc_0737; 65, aspartate aminotransferase, TbTc_0799; 66, aspartate carbamoyltransferase, TbTc_1630; 67, dihydroorotase, TbTc_3801; 68, dihydroorotate dehydrogenase, TbTc_0620; 69, orotidine-5-phosphate decarboxylase/orotate phosphoribosyltransferase, TbTc_0735; 70, uracil phosphoribosyltransferase, TbTc_4220; 71, Adenine phosphoribosyltransferase (APRT-2), TbTc_3522; 72, inosine-adenosine-guanosine-nucleoside hydrolase, TbTc_4998; 73, adenosine kinase, TbTc_1024; 74, AMP deaminase, TbTc_5808; 75, hypoxanthine-guanine phosphoribosyltransferase (HGPRT), TbTc_0726; 76, inosine-guanine nucleoside hydrolase, TbTc_0808; 77, inosine-5'-monophosphate dehydrogenase, TbTc_1648; 78, Hypoxanthine-guanine-xanthine phosphoribosyltransferase (HGXPRT), TbTc_3696; 79, GMP reductase, TbTc_4627; 80, GMP synthase, TbTc_1452. Abbreviations: PUFA, polyunsaturated fatty acid.

S1 figure: comparative analysis of published *T. congolense* RNAseq data and data generated in this study. Scatter matrix of *T. congolense* datasets from this study compared to ascending and peak parasitaemia *in vivo* transcriptomics data generated by Silvester and colleagues [55]. TPM values were calculated for each gene in the *T. congolense* genome and Log_2 TPM was plotted. Lower panels: Scatter plots of individual comparisons of the 4 datasets. Red dots correspond to genes associated with glycolysis; Diagonal panels: sample names; Upper panels: Pearson correlation coefficients for comparisons of entire datasets (black), glycolytic pathway ("Glyc", green) and proteins with predicted transmembrane domains ("Trans", red).

S2 figure: Growth of *T. congolense* IL3000 in absence or presence of N-acetyl-D-glucosamine. Parasites were cultured in SCM-6 supplemented with 10 mM or 2 mM glucose in the presence or absence of 60 mM GlcNAc and density monitored by haemocytometer every 24 hours.

S3 figure: Comparative transcriptomics analysis of the electron transport chain in *T. congolense* and *T. brucei*. A heatmap of all ETC complexes based on a table generated by Zikova and colleagues [73]. Heatmaps are divided into the alternative oxidases (AOX), NADH dehydrogenase 2 (NDH2), complex I, II, III, IV and ATPase (complex V).

S4 figure: Stable isotope labelled (^{13}C)-glucose derived pyrimidine labelling. Comparative analysis of glucose-derived pyrimidine labelling in *T. congolense* and *T. brucei* (taken from [42]).

S5 figure: Effect of cysteine exclusion on *T. congolense* growth. Parasites were grown in SCM-6 supplemented with 1.5 mM, 1.0 mM or absence of L-cysteine. Cell density was monitored every 24 hours.

S6 figure: Comparison of amino acid metabolism in *T. congolense* and *T. brucei*. A) glucose-derived carbon labelling of amino acids B) Transcriptomics pathway analysis. Gene IDs: A) ARG+POLYAMINE-SYN: AdoMetDC_3193, AdoMet decarboxylase, TbTc_3193; ODC, ornithine decarboxylase, TbTc_5903; AdoMetDC_0696, AdoMet decarboxylase, TbTc_0696; SpSyn, spermidine synthase, TbTc_1034. B) ASPASN-PWY: cASAT, cytosolic aspartate aminotransferase, TbTc_0799; ASNS, asparagine synthetase, TbTc_4894; mASAT, mitochondrial aspartate aminotransferase, TbTc_5877. C) GLUCAT-PWY: OGDH-E1, 2-oxoglutarate dehydrogenase E1, TbTc_2864; GDH, glutamate dehydrogenase, TbTc_0872; SCSα, succinyl-CoA synthetase, TbTc_0813; SUCLG2, succinyl-CoA ligase, TbTc_3392; OGDH-E2, 2-oxoglutarate dehydrogenase E2, TbTc_3057. D) ILEUDEG-PWY: ECH, enoyl-CoA hydratase, TbTc_3283; BCAAT, branched-chain amino acid aminotransferase, TbTc_0559; SCP2, 3-ketoacyl-CoA thiolase, TbTc_4024. E) LEUDEG-PWY: ECH, enoyl-CoA hydratase, TbTc_3283; BCKDHα, 2-oxoisovalerate dehydrogenase α, TbTc_1182; BCKDHβ, 2-oxoisovalerate dehydrogenase β, TbTc_0682; AUH, methylglutaconyl-CoA hydratase, TbTc_5348; HMGCL, hydroxymethylglutaryl-CoA lyase, TbTc_6160; BCAAT, branched-chain amino acid aminotransferase, TbTc_0559; MCCβ, 3-methylcrotonyl-CoA carboxylase β, TbTc_5385; MCCα, 3-methylcrotonyl-CoA carboxylase α, TbTc_1670; SCP2, 3-ketoacyl-CoA thiolase, TbTc_4024; IVDH, isovaleryl-CoA dehydrogenase, TbTc_3112. F) PWY0-781: cASAT, cytosolic aspartate aminotransferase, TbTc_0799; MTR - 5-methyltetrahydropteroyltriglutamate-homocysteine S-methyltransferase, TbTc_5805; NMNAT, nicotinamide/nicotinic acid mononucleotide adenylyltransferase, TbTc_4133; NADSYN, NAD+ synthase, TbTc_2404; mASAT, mitochondrial aspartate aminotransferase, TbTc_5877; METK1, AdoMet synthase, TbTc_0178. G) PWY1V8-11: AKCT, 2-amino-3-ketobutyrate-CoA ligase, TbTc_6236; TDH, L-threonine dehydrogenase, TbTc_5991. H) VALDEG-PWY: ECH, enoyl-CoA hydratase, TbTc_3283; HOPR, 2-hydroxy-3-oxopropionate reductase, TbTc_2903; BCAAT, branched-chain amino acid aminotransferase, TbTc_0559. I) PROLINE-DEG2-PWY: P5CDH, delta-1-pyrroline-5-carboxylate dehydrogenase, TbTc1695; GDH, glutamate dehydrogenase, TbTc_0872; ProDH, proline dehydrogenase, TbTc_1591.

S7 figure: Carbon utilisation for trypanothione biosynthesis in *T. congolense*. Metabolomics and transcriptomics analyses were carried out to analyse trypanothione biosynthesis. A) A simplified map of trypanothione biosynthesis as known in *T. brucei*. Numbers refer to the following enzymes: 1, S-adenosyl-L-methionine synthase, METK1; 2, S-adenosyl-L-methionine decarboxylase, AdoMetDC; 3, spermidine synthase, SpSyn; 4, methyltransferase reaction, MTase; 5, S-adenosyl-L-homocysteine dehydrolase, AdoHycase; 6, cystathionine beta synthase, CBS; 7, cystathione gamma lyase, CTH; 8, glutaminase/amidase, AM; 9, gamma-glutamylcysteine synthetase, GCS; 10, glutathione synthetase, GSS; 11, ornithine decarboxylase, ODC; 12, spermidine synthase, SpSyn; 13, glutathionylspermidine synthase, GSP; 14, trypanothione synthetase, TRYS; 15, tryparedoxin peroxidase, TXN1b; 16, trypanothione reductase, TRYR. B) Isotopologue labelling experiments using 100% ^{13}C-L-serine, ^{13}C-L-glutamine, ^{13}C-L-methionine or ^{13}C-L-cysteine, showing the abundance of carbon labelling derived from these amino acids in components of the trypanothione biosynthesis pathway. C) Transcriptomics analysis using the following TrypanoCyc pathways: PWY1V8-6 (trypanothione biosynthesis), HOMOCYSDESGR-PWY1 (homocysteine degradation/cysteine biosynthesis) & METHIONINE-DEG1-PWY (methionine degradation I). GeneIDs: TNX1b, tryparedoxin 1b, TbTc_0324; TRYS, trypanothione synthetase, TbTc_1359; SpSyn, Spermidine synthase, TbTc_1034; TRYR, trypanothione reductase, TbTc_4239; AdoMetDC_0696, S-adenosylmethionine decarboxylase, TbTc0696; GCS, gamma-glutamylcysteine synthetase, TbTc_3424; METK1, S-adenosylmethionine synthetase, TbTc_0178; GSS, glutathione synthetase, TbTc_3678; AdoMetDC_3193, S-adenosylmethionine decarboxylase, TbTc_3193; AM, amidase, TbTc_5549; ODC, ornithine decarboxylase, TbTc_5903; CTH, cystathione gamma lyase, TbTc_1051; CBS, cystathionine beta synthase, TbTc_0413; AdoHcyase, S-adenosylhomocysteine hydrolase, TbTc_0685; METK1, S-adenosylmethionine synthase, TbTc_0178.

S8 Figure: Analysis of LC-MS utilising stable isotope labelled amino acids. Percentage total labelling of metabolites identified in data from 6 stable isotope labelling experiments using ^{13}C-L-asparagine, ^{13}C-L-cysteine, ^{13}C-L-glutamine, ^{13}C-L-methionine, ^{13}C-L-proline and ^{13}C-L-serine. Colour intensity correlates to the total fraction of the metabolite that was ^{13}C-labeled.

Supplementary Data

S1 Table: RNAseq dataset – *T. congolense ex vivo*, *T. congolense in vitro*, *T. brucei ex vivo*, *T. brucei in vitro*, Silvester *et al* dataset

S2 Table: Orthofinder output comparing *T. congolense* TriTrypDB (v34.0), *T. congolense* Liverpool pacbio, *T. brucei* TriTrypDB (v34.0) and other trypanosomatids

S3 Table: RNAseq dataset – *T. congolense* only, Pacbio assembly, single genes.

S4 Table: Supernatant metabolomics dataset for *in vitro* cultured *T. congolense* over a period of 56 hours. Metabolites highlighted in yellow were confidently predicted using a set of metabolite standards run alongside the experimental samples. Results of statistical analysis by means of a one-way repeated measures ANOVA (false discovery rate-adjusted P value, FDR) is also shown for metabolites that were taken forward for downstream analysis

S5 Table: TrypanoCyc pathways and linked Orthogroup gene IDs

S6 Table: Formulation of Steketee's congolense medium (SCM)-6 & -7

S7 table: List of primers used in this study

Compound	Target	*T. congolense* EC_{50} Mean ± SEM	*T. brucei* EC_{50} Mean ± SEM	Fold change (Tc/Tb)	P value (*t*-test)
Antimycin	Complex III	271.2 ± 143.5 µM	144.2 ± 18.1 µM	1.9	0.4295
FCCP	Uncoupling agent	12.6 ± 5.3 µM	13.0 ± 5.0 µM	1.0	0.9592
Azide	F_1-ATPase	432.3 ± 127.9 µM	235.0 ± 6.0 µM	1.8	0.1982
Oligomycin	Complex V (F_0 ATPase)	33.9 ± 14.1 nM	197.6 ± 39.0 nM	0.2	0.0169
Rotenone	Complex I	27.4 ± 1.4 µM	7.4 ± 0.9 µM	3.7	0.0003
SHAM	TAO	14.4 ± 0.5 µM	26.0 ± 1.5 µM	0.6	0.0004
UK5099	Pyruvate transport	82.1 ± 8.8 µM	130.0 ± 5.0 µM	0.6	0.0091
ACS inhibitor	Acetyl-CoA synthetase	57.7 ± 15.2 µM	7.1 ± 2.4 µM	8.1	0.0304
Orlistat	Fatty acid synthase/lipases	15.6 ± 2.5 µM	0.02 ± 0.01 µM	780.0	0.0033
Diminazene	Kinetoplast	50.0 ± 5.6 nM	32.0 ± 0.5 nM	1.6	0.0425

Table 1: Comparative analysis of sensitivity to metabolic inhibitors in *T. congolense* and *T. brucei*. Abbreviations: SHAM, salicylhydroxamic acid; LCFA, long-chain fatty acid

References

1. Morrison LJ, Vezza L, Rowan T, Hope JC. Animal African Trypanosomiasis: Time to Increase Focus on Clinically Relevant Parasite and Host Species. Trends Parasitol. 2016;32(8): 599-607. doi: 10.1016/j.pt.2016.04.012.
2. Auty H, Torr SJ, Michoel T, Jayaraman S, Morrison LJ. Cattle trypanosomosis: the diversity of trypanosomes and implications for disease epidemiology and control. Rev Sci Tech. 2015;34(2): 587-98.
3. Giordani F, Morrison LJ, Rowan TG, HP DEK, Barrett MP. The animal trypanosomiases and their chemotherapy: a review. Parasitology. 2016;143(14): 1862-89. doi: 10.1017/S0031182016001268.
4. Shaw AP, Cecchi G, Wint GR, Mattioli RC, Robinson TP. Mapping the economic benefits to livestock keepers from intervening against bovine trypanosomosis in Eastern Africa. Prev Vet Med. 2014;113(2): 197-210. doi: 10.1016/j.prevetmed.2013.10.024.
5. Chitanga S, Marcotty T, Namangala B, Van den Bossche P, Van Den Abbeele J, Delespaux V. High prevalence of drug resistance in animal trypanosomes without a history of drug exposure. PLoS Negl Trop Dis. 2011;5(12): e1454. doi: 10.1371/journal.pntd.0001454.
6. Delespaux V, Dinka H, Masumu J, Van den Bossche P, Geerts S. Five-fold increase in Trypanosoma congolense isolates resistant to diminazene aceturate over a seven-year period in Eastern Zambia. Drug Resist Updat. 2008;11(6): 205-9. doi: 10.1016/j.drup.2008.10.002.
7. Geerts S, Holmes PH, Eisler MC, Diall O. African bovine trypanosomiasis: the problem of drug resistance. Trends Parasitol. 2001;17(1): 25-8.
8. Diall O, Cecchi G, Wanda G, Argiles-Herrero R, Vreysen MJB, Cattoli G, et al. Developing a Progressive Control Pathway for African Animal Trypanosomosis. Trends Parasitol. 2017;33(7): 499-509. doi: 10.1016/j.pt.2017.02.005.
9. Barrett MP, Burchmore RJ, Stich A, Lazzari JO, Frasch AC, Cazzulo JJ, et al. The trypanosomiases. Lancet. 2003;362(9394): 1469-80. doi: 10.1016/S0140-6736(03)14694-6.
10. Alsford S, Kawahara T, Glover L, Horn D. Tagging a T. brucei RRNA locus improves stable transfection efficiency and circumvents inducible expression position effects. Mol Biochem Parasitol. 2005;144(2): 142-8. doi: 10.1016/j.molbiopara.2005.08.009.
11. Rico E, Jeacock L, Kovarova J, Horn D. Inducible high-efficiency CRISPR-Cas9-targeted gene editing and precision base editing in African trypanosomes. Sci Rep. 2018;8(1): 7960. doi: 10.1038/s41598-018-26303-w.

12. Gibson W. The origins of the trypanosome genome strains Trypanosoma brucei brucei TREU 927, T. b. gambiense DAL 972, T. vivax Y486 and T. congolense IL3000. Parasit Vectors. 2012;5: 71. doi: 10.1186/1756-3305-5-71.
13. Kay C, Peacock L, Gibson W. Trypanosoma congolense: In Vitro Culture and Transfection. Curr Protoc Microbiol. 2019;53(1): e77. doi: 10.1002/cpmc.77.
14. Coustou V, Guegan F, Plazolles N, Baltz T. Complete in vitro life cycle of Trypanosoma congolense: development of genetic tools. PLoS Negl Trop Dis. 2010;4(3): e618. doi: 10.1371/journal.pntd.0000618.
15. Hirumi H, Hirumi K. In vitro cultivation of Trypanosoma congolense bloodstream forms in the absence of feeder cell layers. Parasitology. 1991;102 Pt 2: 225-36.
16. Rotureau B, Van Den Abbeele J. Through the dark continent: African trypanosome development in the tsetse fly. Front Cell Infect Microbiol. 2013;3: 53. doi: 10.3389/fcimb.2013.00053.
17. Silvester E, Young J, Ivens A, Matthews KR. Interspecies quorum sensing in co-infections can manipulate trypanosome transmission potential. Nat Microbiol. 2017;2(11): 1471-9. doi: 10.1038/s41564-017-0014-5.
18. Jackson AP, Allison HC, Barry JD, Field MC, Hertz-Fowler C, Berriman M. A cell-surface phylome for African trypanosomes. PLoS Negl Trop Dis. 2013;7(3): e2121. doi: 10.1371/journal.pntd.0002121.
19. Jackson AP, Berry A, Aslett M, Allison HC, Burton P, Vavrova-Anderson J, et al. Antigenic diversity is generated by distinct evolutionary mechanisms in African trypanosome species. Proc Natl Acad Sci U S A. 2012;109(9): 3416-21. doi: 10.1073/pnas.1117313109.
20. Silva Pereira S, Casas-Sanchez A, Haines LR, Ogugo M, Absolomon K, Sanders M, et al. Variant antigen repertoires in Trypanosoma congolense populations and experimental infections can be profiled from deep sequence data using universal protein motifs. Genome Res. 2018;28(9): 1383-94. doi: 10.1101/gr.234146.118.
21. Silva Pereira S, de Almeida Castilho Neto KJG, Duffy CW, Richards P, Noyes H, Ogugo M, et al. Variant antigen diversity in Trypanosoma vivax is not driven by recombination. Nat Commun. 2020;11(1): 844. doi: 10.1038/s41467-020-14575-8.
22. Tihon E, Imamura H, Dujardin JC, Van Den Abbeele J, Van den Broeck F. Discovery and genomic analyses of hybridization between divergent lineages of Trypanosoma congolense, causative agent of Animal African Trypanosomiasis. Mol Ecol. 2017;26(23): 6524-38. doi: 10.1111/mec.14271.
23. Creek DJ, Barrett MP. Determination of antiprotozoal drug mechanisms by metabolomics approaches. Parasitology. 2014;141(1): 83-92. doi: 10.1017/S0031182013000814.

24. Haanstra JR, Gerding A, Dolga AM, Sorgdrager FJH, Buist-Homan M, du Toit F, et al. Targeting pathogen metabolism without collateral damage to the host. Sci Rep. 2017;7: 40406. doi: 10.1038/srep40406.
25. Vincent IM, Ehmann DE, Mills SD, Perros M, Barrett MP. Untargeted Metabolomics To Ascertain Antibiotic Modes of Action. Antimicrob Agents Chemother. 2016;60(4): 2281-91. doi: 10.1128/AAC.02109-15.
26. Bringaud F, Biran M, Millerioux Y, Wargnies M, Allmann S, Mazet M. Combining reverse genetics and nuclear magnetic resonance-based metabolomics unravels trypanosome-specific metabolic pathways. Mol Microbiol. 2015;96(5): 917-26. doi: 10.1111/mmi.12990.
27. Creek DJ, Anderson J, McConville MJ, Barrett MP. Metabolomic analysis of trypanosomatid protozoa. Mol Biochem Parasitol. 2012;181(2): 73-84. doi: 10.1016/j.molbiopara.2011.10.003.
28. Allmann S, Bringaud F. Glycosomes: A comprehensive view of their metabolic roles in T. brucei. Int J Biochem Cell Biol. 2017;85: 85-90. doi: 10.1016/j.biocel.2017.01.015.
29. Haanstra JR, van Tuijl A, Kessler P, Reijnders W, Michels PA, Westerhoff HV, et al. Compartmentation prevents a lethal turbo-explosion of glycolysis in trypanosomes. Proc Natl Acad Sci U S A. 2008;105(46): 17718-23. doi: 10.1073/pnas.0806664105.
30. Mazet M, Morand P, Biran M, Bouyssou G, Courtois P, Daulouede S, et al. Revisiting the central metabolism of the bloodstream forms of Trypanosoma brucei: production of acetate in the mitochondrion is essential for parasite viability. PLoS Negl Trop Dis. 2013;7(12): e2587. doi: 10.1371/journal.pntd.0002587.
31. Millerioux Y, Mazet M, Bouyssou G, Allmann S, Kiema TR, Bertiaux E, et al. De novo biosynthesis of sterols and fatty acids in the Trypanosoma brucei procyclic form: Carbon source preferences and metabolic flux redistributions. PLoS Pathog. 2018;14(5): e1007116. doi: 10.1371/journal.ppat.1007116.
32. Yang PY, Wang M, Liu K, Ngai MH, Sheriff O, Lear MJ, et al. Parasite-based screening and proteome profiling reveal orlistat, an FDA-approved drug, as a potential anti Trypanosoma brucei agent. Chemistry. 2012;18(27): 8403-13. doi: 10.1002/chem.201200482.
33. Lamour N, Riviere L, Coustou V, Coombs GH, Barrett MP, Bringaud F. Proline metabolism in procyclic Trypanosoma brucei is down-regulated in the presence of glucose. J Biol Chem. 2005;280(12): 11902-10. doi: 10.1074/jbc.M414274200.
34. Tielens AG, Van Hellemond JJ. Differences in energy metabolism between trypanosomatidae. Parasitol Today. 1998;14(7): 265-72.

35. van Weelden SW, Fast B, Vogt A, van der Meer P, Saas J, van Hellemond JJ, et al. Procyclic Trypanosoma brucei do not use Krebs cycle activity for energy generation. J Biol Chem. 2003;278(15): 12854-63. doi: 10.1074/jbc.M213190200.
36. van Hellemond JJ, Opperdoes FR, Tielens AG. The extraordinary mitochondrion and unusual citric acid cycle in Trypanosoma brucei. Biochem Soc Trans. 2005;33(Pt 5): 967-71. doi: 10.1042/BST20050967.
37. Villafraz O, Biran M, Pineda E, Plazolles N, Cahoreau E, Ornitz R, et al. Fly stage trypanosomes recycle glucose catabolites and TCA cycle intermediates to stimulate growth in near physiological conditions. 2020: 2020.12.17.423221. doi: 10.1101/2020.12.17.423221 %J bioRxiv.
38. Colasante C, Robles A, Li CH, Schwede A, Benz C, Voncken F, et al. Regulated expression of glycosomal phosphoglycerate kinase in Trypanosoma brucei. Mol Biochem Parasitol. 2007;151(2): 193-204. doi: 10.1016/j.molbiopara.2006.11.003.
39. Blattner J, Helfert S, Michels P, Clayton C. Compartmentation of phosphoglycerate kinase in Trypanosoma brucei plays a critical role in parasite energy metabolism. Proc Natl Acad Sci U S A. 1998;95(20): 11596-600.
40. Deramchia K, Morand P, Biran M, Millerioux Y, Mazet M, Wargnies M, et al. Contribution of pyruvate phosphate dikinase in the maintenance of the glycosomal ATP/ADP balance in the Trypanosoma brucei procyclic form. J Biol Chem. 2014;289(25): 17365-78. doi: 10.1074/jbc.M114.567230.
41. van Grinsven KW, Van Den Abbeele J, Van den Bossche P, van Hellemond JJ, Tielens AG. Adaptations in the glucose metabolism of procyclic Trypanosoma brucei isolates from tsetse flies and during differentiation of bloodstream forms. Eukaryot Cell. 2009;8(8): 1307-11. doi: 10.1128/EC.00091-09.
42. Creek DJ, Mazet M, Achcar F, Anderson J, Kim DH, Kamour R, et al. Probing the metabolic network in bloodstream-form Trypanosoma brucei using untargeted metabolomics with stable isotope labelled glucose. PLoS Pathog. 2015;11(3): e1004689. doi: 10.1371/journal.ppat.1004689.
43. Agosin M, Von Brand T. Studies on the carbohydrate metabolism of Trypanosoma congolense. Exp Parasitol. 1954;3(6): 517-24.
44. Bringaud F, Baltz D, Baltz T. Functional and molecular characterization of a glycosomal PPi-dependent enzyme in trypanosomatids: pyruvate, phosphate dikinase. Proc Natl Acad Sci U S A. 1998;95(14): 7963-8.
45. Ohashi-Suzuki M, Yabu Y, Ohshima S, Nakamura K, Kido Y, Sakamoto K, et al. Differential kinetic activities of glycerol kinase among African trypanosome species: phylogenetic and therapeutic implications. J Vet Med Sci. 2011;73(5): 615-21.

46. Parker HL, Hill T, Alexander K, Murphy NB, Fish WR, Parsons M. Three genes and two isozymes: gene conversion and the compartmentalization and expression of the phosphoglycerate kinases of Trypanosoma (Nannomonas) congolense. Mol Biochem Parasitol. 1995;69(2): 269-79.
47. Vickerman K. The fine structure of Trypanosoma congolense in its bloodstream phase. J Protozool. 1969;16(1): 54-69.
48. Bienen EJ, Webster P, Fish WR. Trypanosoma (Nannomonas) congolense: changes in respiratory metabolism during the life cycle. Exp Parasitol. 1991;73(4): 403-12.
49. Ebiloma GU, Ayuga TD, Balogun EO, Gil LA, Donachie A, Kaiser M, et al. Inhibition of trypanosome alternative oxidase without its N-terminal mitochondrial targeting signal (DeltaMTS-TAO) by cationic and non-cationic 4-hydroxybenzoate and 4-alkoxybenzaldehyde derivatives active against T. brucei and T. congolense. Eur J Med Chem. 2018;150: 385-402. doi: 10.1016/j.ejmech.2018.02.075.
50. Fueyo Gonzalez FJ, Ebiloma GU, Izquierdo Garcia C, Bruggeman V, Sanchez Villamanan JM, Donachie A, et al. Conjugates of 2,4-Dihydroxybenzoate and Salicylhydroxamate and Lipocations Display Potent Antiparasite Effects by Efficiently Targeting the Trypanosoma brucei and Trypanosoma congolense Mitochondrion. J Med Chem. 2017;60(4): 1509-22. doi: 10.1021/acs.jmedchem.6b01740.
51. Steiger RF, Steiger E, Trager W, Schneider I. Trypanosoma congolense: partial cyclic development in a Glossina cell system and oxygen consumption. J Parasitol. 1977;63(5): 861-7.
52. Hsu HH, Araki M, Mochizuki M, Hori Y, Murata M, Kahar P, et al. A Systematic Approach to Time-series Metabolite Profiling and RNA-seq Analysis of Chinese Hamster Ovary Cell Culture. Sci Rep. 2017;7: 43518. doi: 10.1038/srep43518.
53. Wagner GP, Kin K, Lynch VJ. Measurement of mRNA abundance using RNA-seq data: RPKM measure is inconsistent among samples. Theory Biosci. 2012;131(4): 281-5. doi: 10.1007/s12064-012-0162-3.
54. Emms DM, Kelly S. OrthoFinder: solving fundamental biases in whole genome comparisons dramatically improves orthogroup inference accuracy. Genome Biol. 2015;16: 157. doi: 10.1186/s13059-015-0721-2.
55. Silvester E, Ivens A, Matthews KR. A gene expression comparison of Trypanosoma brucei and Trypanosoma congolense in the bloodstream of the mammalian host reveals species-specific adaptations to density-dependent development. PLoS Negl Trop Dis. 2018;12(10): e0006863. doi: 10.1371/journal.pntd.0006863.
56. Creek DJ, Nijagal B, Kim DH, Rojas F, Matthews KR, Barrett MP. Metabolomics guides rational development of a simplified cell culture medium for drug screening against

Trypanosoma brucei. Antimicrob Agents Chemother. 2013;57(6): 2768-79. doi: 10.1128/AAC.00044-13.

57. Kim DH, Achcar F, Breitling R, Burgess KE, Barrett MP. LC-MS-based absolute metabolite quantification: application to metabolic flux measurement in trypanosomes. Metabolomics. 2015;11(6): 1721-32. doi: 10.1007/s11306-015-0827-2.
58. Nok AJ, Esievo KA, Ibrahim S, Ukoha AI, Ikediobi CO. Phospholipase A2 from Trypanosoma congolense: characterization and haematological properties. Cell Biochem Funct. 1993;11(2): 125-30. doi: 10.1002/cbf.290110208.
59. Duszenko M, Ferguson MA, Lamont GS, Rifkin MR, Cross GA. Cysteine eliminates the feeder cell requirement for cultivation of Trypanosoma brucei bloodstream forms in vitro. J Exp Med. 1985;162(4): 1256-63.
60. Shameer S, Logan-Klumpler FJ, Vinson F, Cottret L, Merlet B, Achcar F, et al. TrypanoCyc: a community-led biochemical pathways database for Trypanosoma brucei. Nucleic Acids Res. 2015;43(Database issue): D637-44. doi: 10.1093/nar/gku944.
61. Szoor B, Ruberto I, Burchmore R, Matthews KR. A novel phosphatase cascade regulates differentiation in Trypanosoma brucei via a glycosomal signaling pathway. Genes Dev. 2010;24(12): 1306-16. doi: 10.1101/gad.570310.
62. Mugo E, Clayton C. Expression of the RNA-binding protein RBP10 promotes the bloodstream-form differentiation state in Trypanosoma brucei. PLoS Pathog. 2017;13(8): e1006560. doi: 10.1371/journal.ppat.1006560.
63. Dean S, Marchetti R, Kirk K, Matthews KR. A surface transporter family conveys the trypanosome differentiation signal. Nature. 2009;459(7244): 213-7. doi: 10.1038/nature07997.
64. Aranda A, Maugeri D, Uttaro AD, Opperdoes F, Cazzulo JJ, Nowicki C. The malate dehydrogenase isoforms from Trypanosoma brucei: subcellular localization and differential expression in bloodstream and procyclic forms. Int J Parasitol. 2006;36(3): 295-307. doi: 10.1016/j.ijpara.2005.09.013.
65. Abbas AH, Silva Pereira S, D'Archivio S, Wickstead B, Morrison LJ, Hall N, et al. The Structure of a Conserved Telomeric Region Associated with Variant Antigen Loci in the Blood Parasite Trypanosoma congolense. Genome Biol Evol. 2018;10(9): 2458-73. doi: 10.1093/gbe/evy186.
66. Spitznagel D, Ebikeme C, Biran M, Nic a' Bhaird N, Bringaud F, Henehan GT, et al. Alanine aminotransferase of Trypanosoma brucei--a key role in proline metabolism in procyclic life forms. FEBS J. 2009;276(23): 7187-99. doi: 10.1111/j.1742-4658.2009.07432.x.

67. Natesan SK, Peacock L, Leung KF, Gibson W, Field MC. Evidence that low endocytic activity is not directly responsible for human serum resistance in the insect form of African trypanosomes. BMC Res Notes. 2010;3: 63. doi: 10.1186/1756-0500-3-63.
68. Ebikeme CE, Peacock L, Coustou V, Riviere L, Bringaud F, Gibson WC, et al. N-acetyl D-glucosamine stimulates growth in procyclic forms of Trypanosoma brucei by inducing a metabolic shift. Parasitology. 2008;135(5): 585-94. doi: 10.1017/S0031182008004241.
69. Awuah-Mensah G, McDonald J, Steketee PC, Autheman D, Whipple S, D'Archivio S, et al. Reliable, scalable functional genetics in bloodstream-form *Trypanosoma congolense* in vitro and in vivo. PLoS Pathog. 2020;Forthcoming.
70. Kovarova J, Nagar R, Faria J, Ferguson MAJ, Barrett MP, Horn D. Gluconeogenesis using glycerol as a substrate in bloodstream-form Trypanosoma brucei. PLoS Pathog. 2018;14(12): e1007475. doi: 10.1371/journal.ppat.1007475.
71. Tielens AG, van Hellemond JJ. Surprising variety in energy metabolism within Trypanosomatidae. Trends Parasitol. 2009;25(10): 482-90. doi: 10.1016/j.pt.2009.07.007.
72. Trindade S, Rijo-Ferreira F, Carvalho T, Pinto-Neves D, Guegan F, Aresta-Branco F, et al. Trypanosoma brucei Parasites Occupy and Functionally Adapt to the Adipose Tissue in Mice. Cell Host Microbe. 2016;19(6): 837-48. doi: 10.1016/j.chom.2016.05.002.
73. Zikova A, Verner Z, Nenarokova A, Michels PAM, Lukes J. A paradigm shift: The mitoproteomes of procyclic and bloodstream Trypanosoma brucei are comparably complex. PLoS Pathog. 2017;13(12): e1006679. doi: 10.1371/journal.ppat.1006679.
74. Geiger A, Hirtz C, Becue T, Bellard E, Centeno D, Gargani D, et al. Exocytosis and protein secretion in Trypanosoma. BMC Microbiol. 2010;10: 20. doi: 10.1186/1471-2180-10-20.
75. Manivel G, Meyyazhagan A, Durairaj DR, Piramanayagam S. Genome-wide analysis of Excretory/Secretory proteins in Trypanosoma brucei brucei: Insights into functional characteristics and identification of potential targets by immunoinformatics approach. Genomics. 2019;111(5): 1124-33. doi: 10.1016/j.ygeno.2018.07.007.
76. Henriques C, Sanchez MA, Tryon R, Landfear SM. Molecular and functional characterization of the first nucleobase transporter gene from African trypanosomes. Mol Biochem Parasitol. 2003;130(2): 101-10. doi: 10.1016/s0166-6851(03)00167-1.
77. Burchmore RJ, Wallace LJ, Candlish D, Al-Salabi MI, Beal PR, Barrett MP, et al. Cloning, heterologous expression, and in situ characterization of the first high affinity nucleobase transporter from a protozoan. J Biol Chem. 2003;278(26): 23502-7. doi: 10.1074/jbc.M301252200.
78. Munday JC, Rojas Lopez KE, Eze AA, Delespaux V, Van Den Abbeele J, Rowan T, et al. Functional expression of TcoAT1 reveals it to be a P1-type nucleoside transporter

with no capacity for diminazene uptake. Int J Parasitol Drugs Drug Resist. 2013;3: 69-76. doi: 10.1016/j.ijpddr.2013.01.004.

79. Al-Salabi MI, Wallace LJ, Luscher A, Maser P, Candlish D, Rodenko B, et al. Molecular interactions underlying the unusually high adenosine affinity of a novel Trypanosoma brucei nucleoside transporter. Mol Pharmacol. 2007;71(3): 921-9. doi: 10.1124/mol.106.031559.
80. de Koning HP, Bridges DJ, Burchmore RJ. Purine and pyrimidine transport in pathogenic protozoa: from biology to therapy. FEMS Microbiol Rev. 2005;29(5): 987-1020. doi: 10.1016/j.femsre.2005.03.004.
81. Papageorgiou IG, Yakob L, Al Salabi MI, Diallinas G, Soteriadou KP, De Koning HP. Identification of the first pyrimidine nucleobase transporter in Leishmania: similarities with the Trypanosoma brucei U1 transporter and antileishmanial activity of uracil analogues. Parasitology. 2005;130(Pt 3): 275-83. doi: 10.1017/s0031182004006626.
82. Gudin S, Quashie NB, Candlish D, Al-Salabi MI, Jarvis SM, Ranford-Cartwright LC, et al. Trypanosoma brucei: a survey of pyrimidine transport activities. Exp Parasitol. 2006;114(2): 118-25. doi: 10.1016/j.exppara.2006.02.018.
83. de Koning HP, Jarvis SM. A highly selective, high-affinity transporter for uracil in Trypanosoma brucei brucei: evidence for proton-dependent transport. Biochem Cell Biol. 1998;76(5): 853-8. doi: 10.1139/bcb-76-5-853.
84. Ali JA, Tagoe DN, Munday JC, Donachie A, Morrison LJ, de Koning HP. Pyrimidine biosynthesis is not an essential function for Trypanosoma brucei bloodstream forms. PLoS One. 2013;8(3): e58034. doi: 10.1371/journal.pone.0058034.
85. Johnston K, Kim DH, Kerkhoven EJ, Burchmore R, Barrett MP, Achcar F. Mapping the metabolism of five amino acids in bloodstream form Trypanosoma brucei using U-(13)C-labelled substrates and LC-MS. Biosci Rep. 2019;39(5). doi: 10.1042/BSR20181601.
86. Marchese L, Nascimento JF, Damasceno FS, Bringaud F, Michels PAM, Silber AM. The Uptake and Metabolism of Amino Acids, and Their Unique Role in the Biology of Pathogenic Trypanosomatids. Pathogens. 2018;7(2). doi: 10.3390/pathogens7020036.
87. Mantilla BS, Marchese L, Casas-Sanchez A, Dyer NA, Ejeh N, Biran M, et al. Proline Metabolism is Essential for Trypanosoma brucei brucei Survival in the Tsetse Vector. PLoS Pathog. 2017;13(1): e1006158. doi: 10.1371/journal.ppat.1006158.
88. Paul KS, Jiang D, Morita YS, Englund PT. Fatty acid synthesis in African trypanosomes: a solution to the myristate mystery. Trends Parasitol. 2001;17(8): 381-7. doi: 10.1016/s1471-4922(01)01984-5.
89. Stephens JL, Lee SH, Paul KS, Englund PT. Mitochondrial fatty acid synthesis in Trypanosoma brucei. J Biol Chem. 2007;282(7): 4427-36. doi: 10.1074/jbc.M609037200.

90. Millerioux Y, Ebikeme C, Biran M, Morand P, Bouyssou G, Vincent IM, et al. The threonine degradation pathway of the Trypanosoma brucei procyclic form: the main carbon source for lipid biosynthesis is under metabolic control. Mol Microbiol. 2013;90(1): 114-29. doi: 10.1111/mmi.12351.
91. Millerioux Y, Morand P, Biran M, Mazet M, Moreau P, Wargnies M, et al. ATP synthesis-coupled and -uncoupled acetate production from acetyl-CoA by mitochondrial acetate:succinate CoA-transferase and acetyl-CoA thioesterase in Trypanosoma. J Biol Chem. 2012;287(21): 17186-97. doi: 10.1074/jbc.M112.355404.
92. Surve SV, Jensen BC, Heestand M, Mazet M, Smith TK, Bringaud F, et al. NADH dehydrogenase of Trypanosoma brucei is important for efficient acetate production in bloodstream forms. Mol Biochem Parasitol. 2017;211: 57-61. doi: 10.1016/j.molbiopara.2016.10.001.
93. Stafkova J, Mach J, Biran M, Verner Z, Bringaud F, Tachezy J. Mitochondrial pyruvate carrier in Trypanosoma brucei. Mol Microbiol. 2016;100(3): 442-56. doi: 10.1111/mmi.13325.
94. Comerford SA, Huang Z, Du X, Wang Y, Cai L, Witkiewicz AK, et al. Acetate dependence of tumors. Cell. 2014;159(7): 1591-602. doi: 10.1016/j.cell.2014.11.020.
95. Riviere L, Moreau P, Allmann S, Hahn M, Biran M, Plazolles N, et al. Acetate produced in the mitochondrion is the essential precursor for lipid biosynthesis in procyclic trypanosomes. Proc Natl Acad Sci U S A. 2009;106(31): 12694-9. doi: 10.1073/pnas.0903355106.
96. Lee SH, Stephens JL, Paul KS, Englund PT. Fatty acid synthesis by elongases in trypanosomes. Cell. 2006;126(4): 691-9. doi: 10.1016/j.cell.2006.06.045.
97. Danaei G, Finucane MM, Lu Y, Singh GM, Cowan MJ, Paciorek CJ, et al. National, regional, and global trends in fasting plasma glucose and diabetes prevalence since 1980: systematic analysis of health examination surveys and epidemiological studies with 370 country-years and 2.7 million participants. Lancet. 2011;378(9785): 31-40. doi: 10.1016/S0140-6736(11)60679-X.
98. Cozzi G, Ravarotto L, Gottardo F, Stefani AL, Contiero B, Moro L, et al. Short communication: reference values for blood parameters in Holstein dairy cows: effects of parity, stage of lactation, and season of production. J Dairy Sci. 2011;94(8): 3895-901. doi: 10.3168/jds.2010-3687.
99. Jackson PGG, Cockcroft PD. Appendix 2: Laboratory Reference Values: Haematology. Clinical Examination of Farm Animals2002. p. 302-.
100. Mair B, Drillich M, Klein-Jobstl D, Kanz P, Borchardt S, Meyer L, et al. Glucose concentration in capillary blood of dairy cows obtained by a minimally invasive lancet

technique and determined with three different hand-held devices. BMC Vet Res. 2016;12: 34. doi: 10.1186/s12917-016-0662-3.

101. Nafikov RA, Beitz DC. Carbohydrate and lipid metabolism in farm animals. J Nutr. 2007;137(3): 702-5. doi: 10.1093/jn/137.3.702.

102. Puppel K, Kuczynska B. Metabolic profiles of cow's blood; a review. J Sci Food Agric. 2016;96(13): 4321-8. doi: 10.1002/jsfa.7779.

103. Bochud-Allemann N, Schneider A. Mitochondrial substrate level phosphorylation is essential for growth of procyclic Trypanosoma brucei. J Biol Chem. 2002;277(36): 32849-54. doi: 10.1074/jbc.M205776200.

104. Mochizuki K, Inaoka DK, Mazet M, Shiba T, Fukuda K, Kurasawa H, et al. The ASCT/SCS cycle fuels mitochondrial ATP and acetate production in Trypanosoma brucei. Biochim Biophys Acta Bioenerg. 2020;1861(11): 148283. doi: 10.1016/j.bbabio.2020.148283.

105. Verner Z, Skodova I, Polakova S, Durisova-Benkovicova V, Horvath A, Lukes J. Alternative NADH dehydrogenase (NDH2): intermembrane-space-facing counterpart of mitochondrial complex I in the procyclic Trypanosoma brucei. Parasitology. 2013;140(3): 328-37. doi: 10.1017/S003118201200162X.

106. Fang J, Beattie DS. Novel FMN-containing rotenone-insensitive NADH dehydrogenase from Trypanosoma brucei mitochondria: isolation and characterization. Biochemistry. 2002;41(9): 3065-72. doi: 10.1021/bi015989w.

107. Dewar CE, MacGregor P, Cooper S, Gould MK, Matthews KR, Savill NJ, et al. Mitochondrial DNA is critical for longevity and metabolism of transmission stage Trypanosoma brucei. PLoS Pathog. 2018;14(7): e1007195. doi: 10.1371/journal.ppat.1007195.

108. Tizard IR, Mellors A, Holmes WL, Nielsen K. The generation of phospholipase A and hemolytic fatty acids by autolysing suspensions of Trypanosoma congolense. Tropenmed Parasitol. 1978;29(1): 127-33.

109. Field MC, Horn D, Fairlamb AH, Ferguson MAJ, Gray DW, Read KD, et al. Anti-trypanosomatid drug discovery: an ongoing challenge and a continuing need. Nat Rev Microbiol. 2017;15(7): 447. doi: 10.1038/nrmicro.2017.69.

110. Hirumi H, Hirumi K. Axenic culture of African trypanosome bloodstream forms. Parasitol Today. 1994;10(2): 80-4.

111. Vassella E, Kramer R, Turner CM, Wankell M, Modes C, van den Bogaard M, et al. Deletion of a novel protein kinase with PX and FYVE-related domains increases the rate of differentiation of Trypanosoma brucei. Mol Microbiol. 2001;41(1): 33-46.

112. Hirumi H, Hirumi K. Continuous cultivation of Trypanosoma brucei blood stream forms in a medium containing a low concentration of serum protein without feeder cell layers. J Parasitol. 1989;75(6): 985-9.

113. Herbert WJ, Lumsden WH. Trypanosoma brucei: a rapid "matching" method for estimating the host's parasitemia. Exp Parasitol. 1976;40(3): 427-31. doi: 10.1016/0014-4894(76)90110-7.

114. Lanham SM, Godfrey DG. Isolation of salivarian trypanosomes from man and other mammals using DEAE-cellulose. Exp Parasitol. 1970;28(3): 521-34. doi: 10.1016/0014-4894(70)90120-7.

115. Schumann Burkard G, Jutzi P, Roditi I. Genome-wide RNAi screens in bloodstream form trypanosomes identify drug transporters. Mol Biochem Parasitol. 2011;175(1): 91-4. doi: 10.1016/j.molbiopara.2010.09.002.

116. Raz B, Iten M, Grether-Buhler Y, Kaminsky R, Brun R. The Alamar Blue assay to determine drug sensitivity of African trypanosomes (T.b. rhodesiense and T.b. gambiense) in vitro. Acta Trop. 1997;68(2): 139-47. doi: 10.1016/s0001-706x(97)00079-x.

117. Untergasser A, Cutcutache I, Koressaar T, Ye J, Faircloth BC, Remm M, et al. Primer3--new capabilities and interfaces. Nucleic Acids Res. 2012;40(15): e115. doi: 10.1093/nar/gks596.

118. Tihon E, Imamura H, Van den Broeck F, Vermeiren L, Dujardin JC, Van Den Abbeele J. Genomic analysis of Isometamidium Chloride resistance in Trypanosoma congolense. Int J Parasitol Drugs Drug Resist. 2017;7(3): 350-61. doi: 10.1016/j.ijpddr.2017.10.002.

119. Livak KJ, Schmittgen TD. Analysis of relative gene expression data using real-time quantitative PCR and the 2(-Delta Delta C(T)) Method. Methods. 2001;25(4): 402-8. doi: 10.1006/meth.2001.1262.

120. Smith CA, Want EJ, O'Maille G, Abagyan R, Siuzdak G. XCMS: processing mass spectrometry data for metabolite profiling using nonlinear peak alignment, matching, and identification. Anal Chem. 2006;78(3): 779-87. doi: 10.1021/ac051437y.

121. Scheltema RA, Jankevics A, Jansen RC, Swertz MA, Breitling R. PeakML/mzMatch: a file format, Java library, R library, and tool-chain for mass spectrometry data analysis. Anal Chem. 2011;83(7): 2786-93. doi: 10.1021/ac2000994.

122. Creek DJ, Jankevics A, Burgess KE, Breitling R, Barrett MP. IDEOM: an Excel interface for analysis of LC-MS-based metabolomics data. Bioinformatics. 2012;28(7): 1048-9. doi: 10.1093/bioinformatics/bts069.

123. Chokkathukalam A, Jankevics A, Creek DJ, Achcar F, Barrett MP, Breitling R. mzMatch-ISO: an R tool for the annotation and relative quantification of isotope-labelled

mass spectrometry data. Bioinformatics. 2013;29(2): 281-3. doi: 10.1093/bioinformatics/bts674.

124. Chong J, Xia J. Using MetaboAnalyst 4.0 for Metabolomics Data Analysis, Interpretation, and Integration with Other Omics Data. Methods Mol Biol. 2020;2104: 337-60. doi: 10.1007/978-1-0716-0239-3_17.

125. Kim D, Langmead B, Salzberg SL. HISAT: a fast spliced aligner with low memory requirements. Nat Methods. 2015;12(4): 357-60. doi: 10.1038/nmeth.3317.

126. Aslett M, Aurrecoechea C, Berriman M, Brestelli J, Brunk BP, Carrington M, et al. TriTrypDB: a functional genomic resource for the Trypanosomatidae. Nucleic Acids Res. 2010;38(Database issue): D457-62. doi: 10.1093/nar/gkp851.

127. Li H, Handsaker B, Wysoker A, Fennell T, Ruan J, Homer N, et al. The Sequence Alignment/Map format and SAMtools. Bioinformatics. 2009;25(16): 2078-9. doi: 10.1093/bioinformatics/btp352.

128. Team. RC. R: A language and environment for statistical computing.: R Foundation for Statistical Computing, Vienna, Austria.; 2013.

129. Gu Z, Eils R, Schlesner M. Complex heatmaps reveal patterns and correlations in multidimensional genomic data. Bioinformatics. 2016;32(18): 2847-9. doi: 10.1093/bioinformatics/btw313.

130. Dolezelova E, Teran D, Gahura O, Kotrbova Z, Prochazkova M, Keough D, et al. Evaluation of the Trypanosoma brucei 6-oxopurine salvage pathway as a potential target for drug discovery. PLoS Negl Trop Dis. 2018;12(2): e0006301. doi: 10.1371/journal.pntd.0006301.

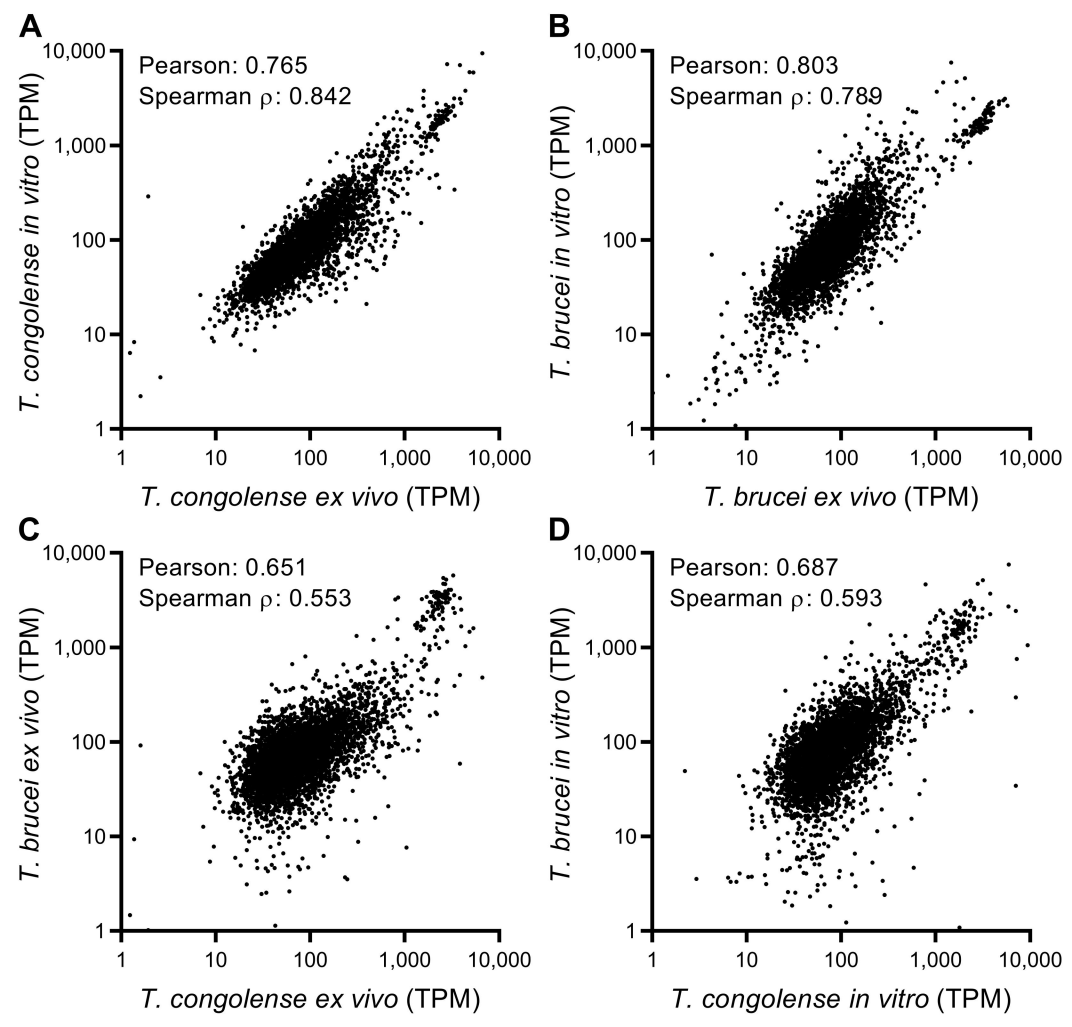
A
Pearson: 0.765
Spearman ρ: 0.842
T. congolense in vitro (TPM)
T. congolense ex vivo (TPM)
B
Pearson: 0.803
Spearman ρ: 0.789
T. brucei in vitro (TPM)
T. brucei ex vivo (TPM)
C
Pearson: 0.651
Spearman ρ: 0.553
T. brucei ex vivo (TPM)
T. congolense ex vivo (TPM)
D
Pearson: 0.687
Spearman ρ: 0.593
T. brucei in vitro (TPM)
T. congolense in vitro (TPM)
1
10
100
1,000
10,000

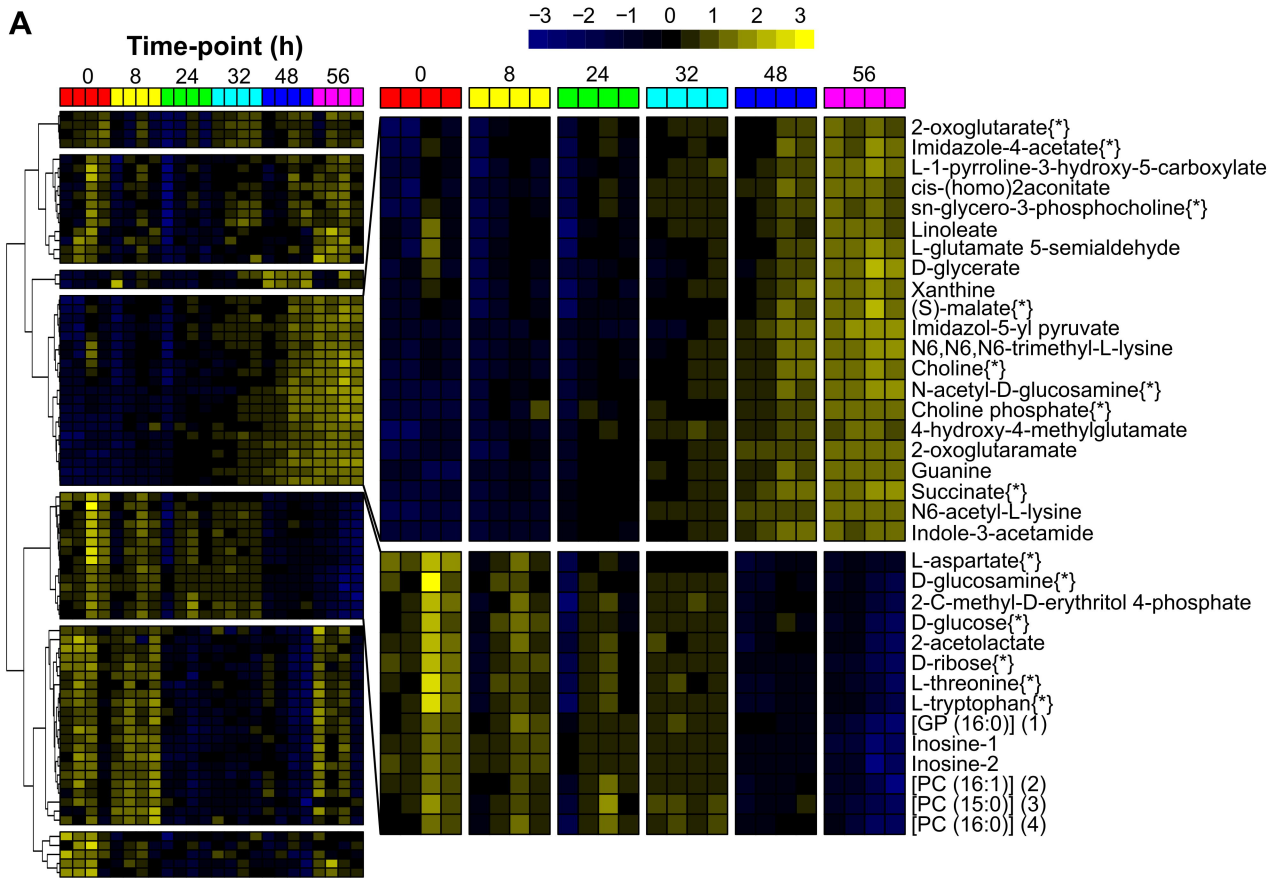

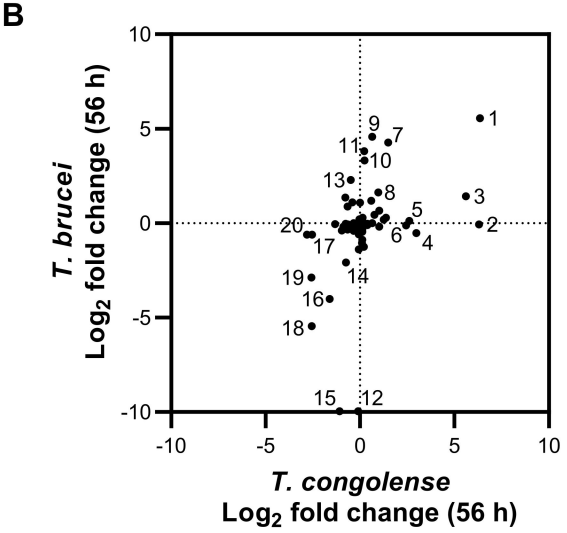

1. Guanine
2. N6-acetyl-L-lysine
3. Succinate
4. 4-hydroxy-4-methylglutamate
5. N6,N6,N6-trimethyl-L-lysine
6. Choline
7. 2-oxoglutarate
8. L-1-pyrroline-3-hydroxy-5-carboxylate
9. D-glycerate
10. Pyruvate
11. 12-hydroxydodecanoic acid
12. L-cystine
13. Diacetyl
14. PC(18:0)
15. LysoPC(17:0)
16. PC(16:0)
17. Inosine
18. PC(16:1)
19. FA trihydroxyl(18:1)
20. Inosine

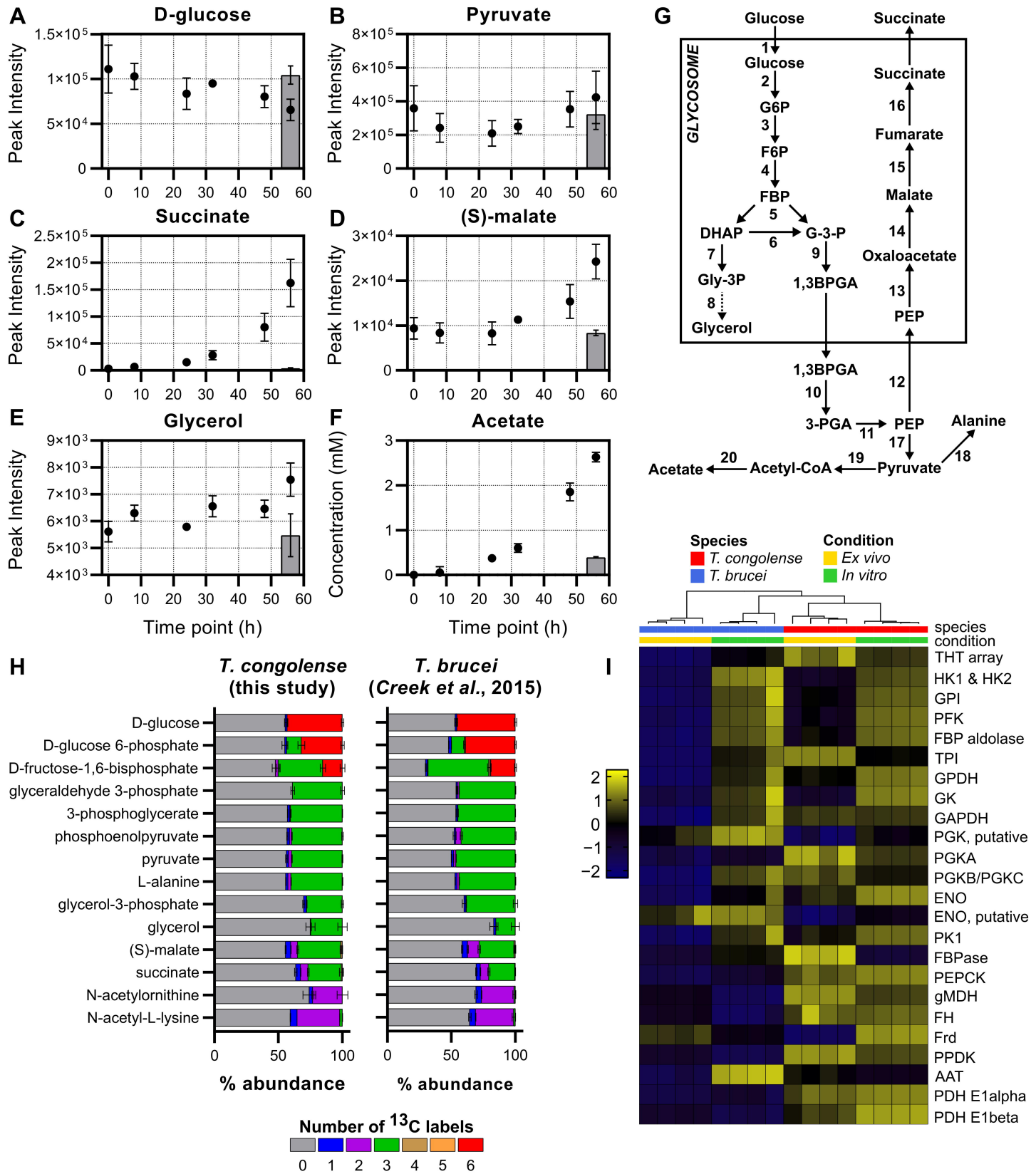
A
D-glucose
Peak Intensity
B
Pyruvate
C
Succinate
D
(S)-malate
E
Glycerol
F
Acetate
Concentration (mM)
Time point (h)
G
GLYCOSOME
Glucose
Glucose
G6P
F6P
FBP
DHAP
G-3-P
Gly-3P
Glycerol
1,3BPGA
3-PGA
PEP
Pyruvate
Acetyl-CoA
Acetate
Succinate
Succinate
Fumarate
Malate
Oxaloacetate
PEP
Alanine
Species
T. congolense
T. brucei
Condition
Ex vivo
In vitro
species
condition
H
T. congolense (this study)
T. brucei (Creek et al., 2015)
D-glucose
D-glucose 6-phosphate
D-fructose-1,6-bisphosphate
glyceraldehyde 3-phosphate
3-phosphoglycerate
phosphoenolpyruvate
pyruvate
L-alanine
glycerol-3-phosphate
glycerol
(S)-malate
succinate
N-acetylornithine
N-acetyl-L-lysine
% abundance
Number of 13C labels
I
THT array
HK1 & HK2
GPI
PFK
FBP aldolase
TPI
GPDH
GK
GAPDH
PGK, putative
PGKA
PGKB/PGKC
ENO
ENO, putative
PK1
FBPase
PEPCK
gMDH
FH
Frd
PPDK
AAT
PDH E1alpha
PDH E1beta

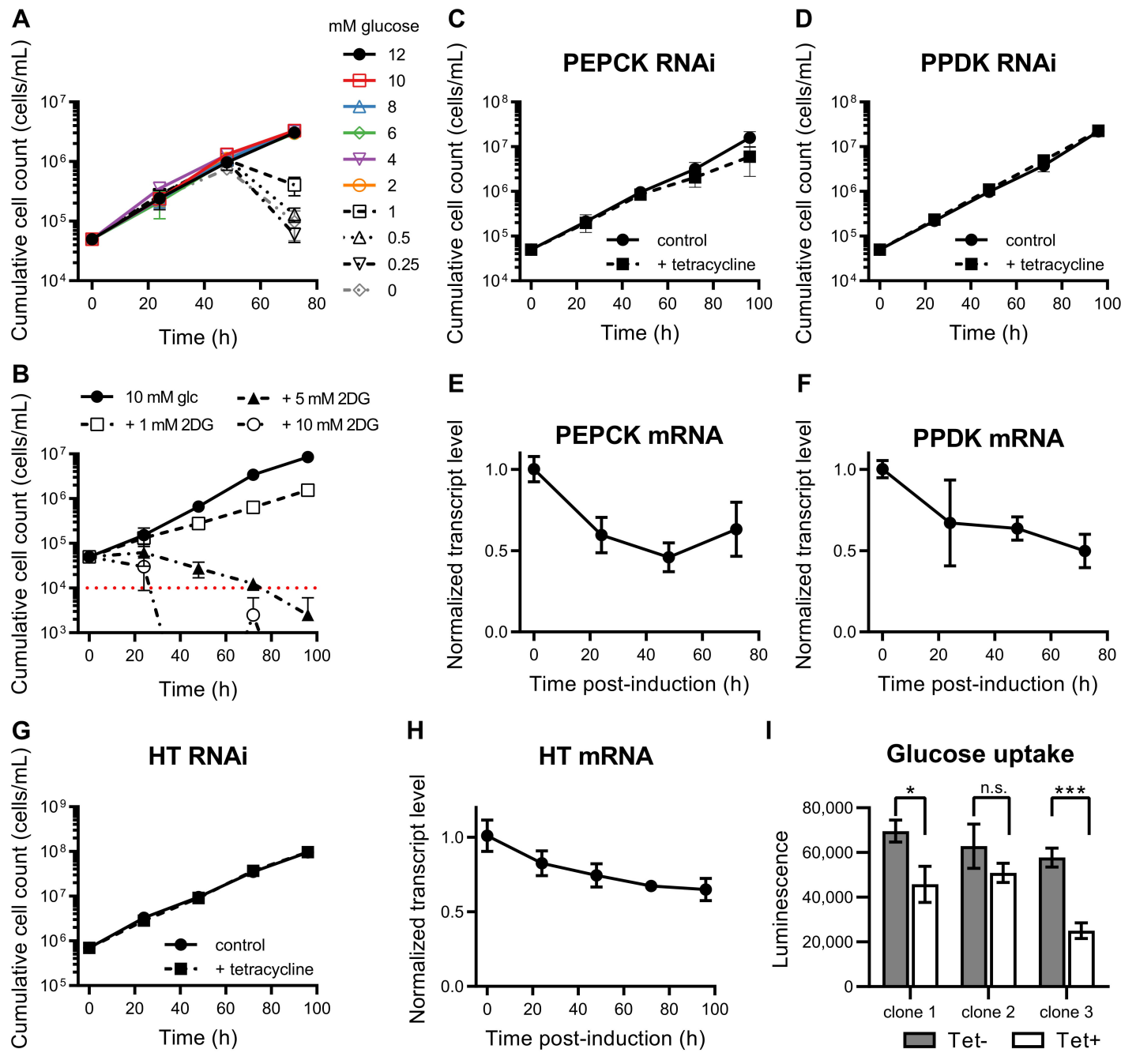
A
mM glucose
12
10
8
6
4
2
1
0.5
0.25
0
Cumulative cell count (cells/mL)
Time (h)
B
10 mM glc
+ 1 mM 2DG
+ 5 mM 2DG
+ 10 mM 2DG
Cumulative cell count (cells/mL)
Time (h)
C
PEPCK RNAi
control
+ tetracycline
Cumulative cell count (cells/mL)
Time (h)
D
PPDK RNAi
control
+ tetracycline
Cumulative cell count (cells/mL)
Time (h)
E
PEPCK mRNA
Normalized transcript level
Time post-induction (h)
F
PPDK mRNA
Normalized transcript level
Time post-induction (h)
G
HT RNAi
control
+ tetracycline
Cumulative cell count (cells/mL)
Time (h)
H
HT mRNA
Normalized transcript level
Time post-induction (h)
I
Glucose uptake
*
n.s.
***
Luminescence
clone 1
clone 2
clone 3
Tet-
Tet+

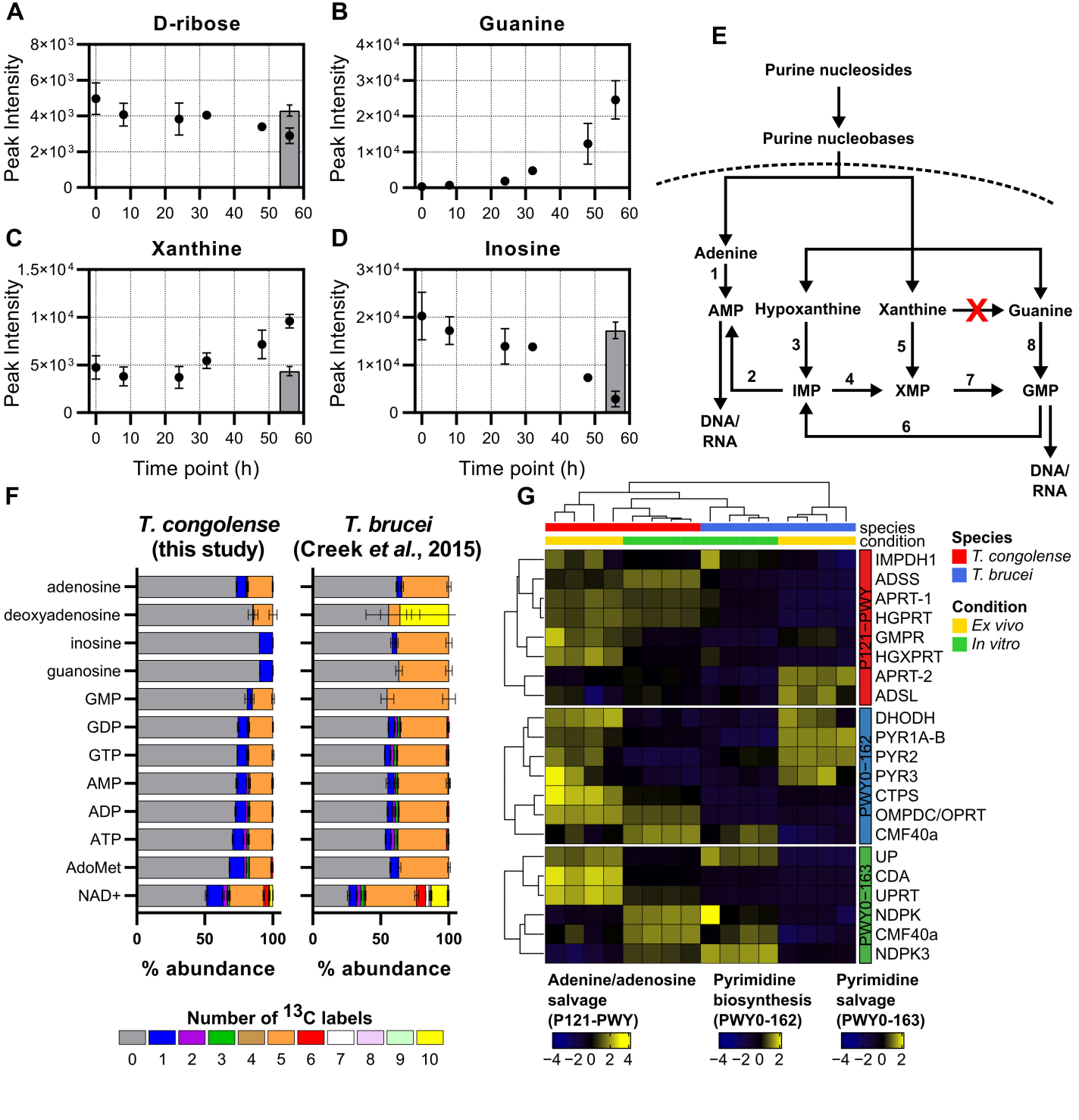
A
D-ribose
B
Guanine
C
Xanthine
D
Inosine
Peak Intensity
Time point (h)
E
Purine nucleosides
Purine nucleobases
Adenine
AMP
Hypoxanthine
Xanthine
Guanine
IMP
XMP
GMP
DNA/
RNA
F
T. congolense
(this study)
T. brucei
(Creek et al., 2015)
adenosine
deoxyadenosine
inosine
guanosine
GMP
GDP
GTP
AMP
ADP
ATP
AdoMet
NAD+
% abundance
Number of 13C labels
G
species
condition
Species
T. congolense
T. brucei
Condition
Ex vivo
In vitro
IMPDH1
ADSS
APRT-1
HGPRT
GMPR
HGXPRT
APRT-2
ADSL
P121−PWY
DHODH
PYR1A-B
PYR2
PYR3
CTPS
OMPDC/OPRT
CMF40a
PWY0−162
UP
CDA
UPRT
NDPK
CMF40a
NDPK3
PWY0−163
Adenine/adenosine
salvage
(P121-PWY)
Pyrimidine
biosynthesis
(PWY0-162)
Pyrimidine
salvage
(PWY0-163)

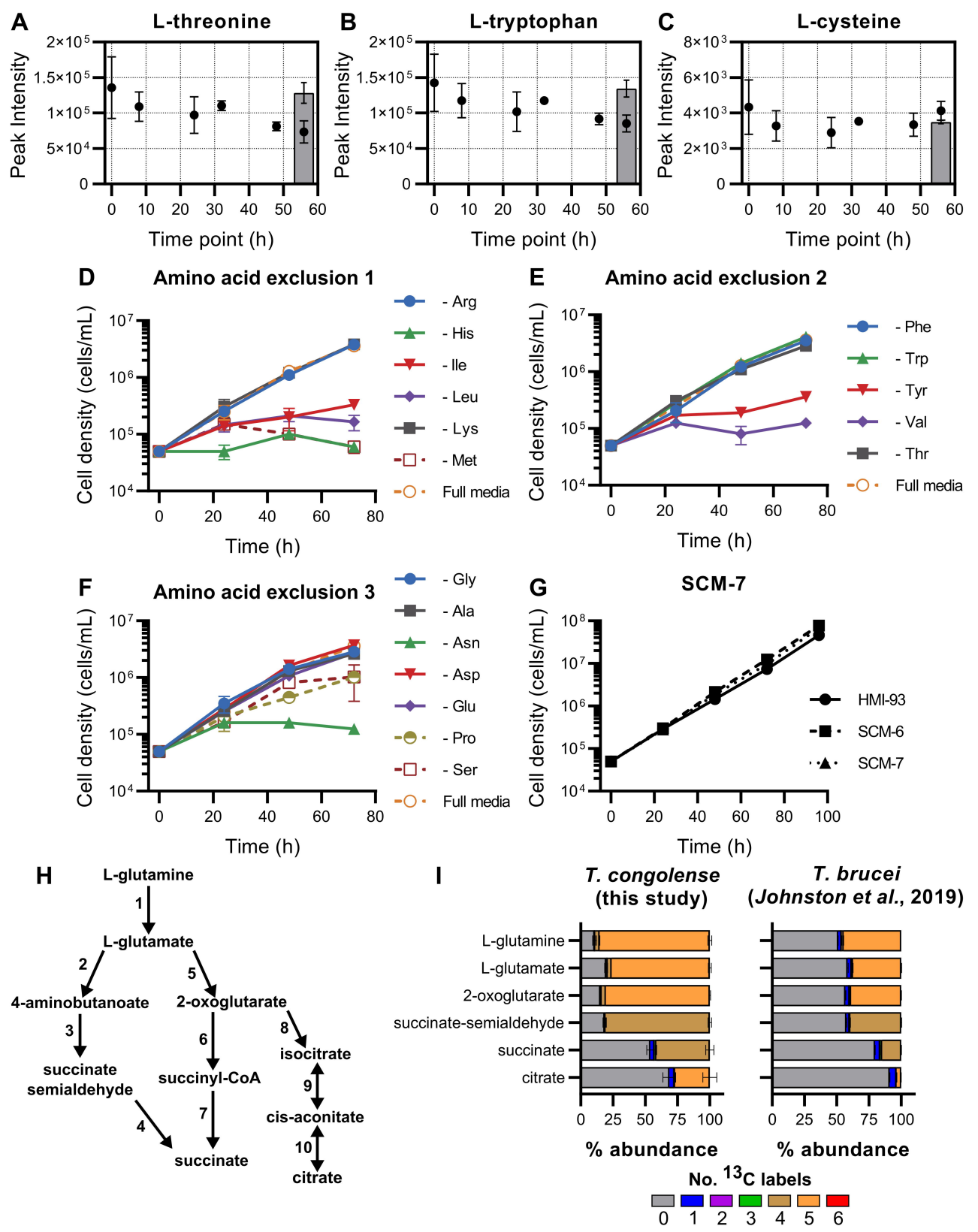
A
L-threonine
Peak Intensity
Time point (h)
B
L-tryptophan
Peak Intensity
Time point (h)
C
L-cysteine
Peak Intensity
Time point (h)
D
Amino acid exclusion 1
Cell density (cells/mL)
Time (h)
- Arg
- His
- Ile
- Leu
- Lys
- Met
Full media
E
Amino acid exclusion 2
Cell density (cells/mL)
Time (h)
- Phe
- Trp
- Tyr
- Val
- Thr
Full media
F
Amino acid exclusion 3
Cell density (cells/mL)
Time (h)
- Gly
- Ala
- Asn
- Asp
- Glu
- Pro
- Ser
Full media
G
SCM-7
Cell density (cells/mL)
Time (h)
HMI-93
SCM-6
SCM-7
H
L-glutamine
1
L-glutamate
2
4-aminobutanoate
3
succinate semialdehyde
4
5
2-oxoglutarate
6
succinyl-CoA
7
succinate
8
isocitrate
9
cis-aconitate
10
citrate
I
T. congolense (this study)
T. brucei (Johnston et al., 2019)
L-glutamine
L-glutamate
2-oxoglutarate
succinate-semialdehyde
succinate
citrate
% abundance
% abundance
No. 13C labels
0 1 2 3 4 5 6

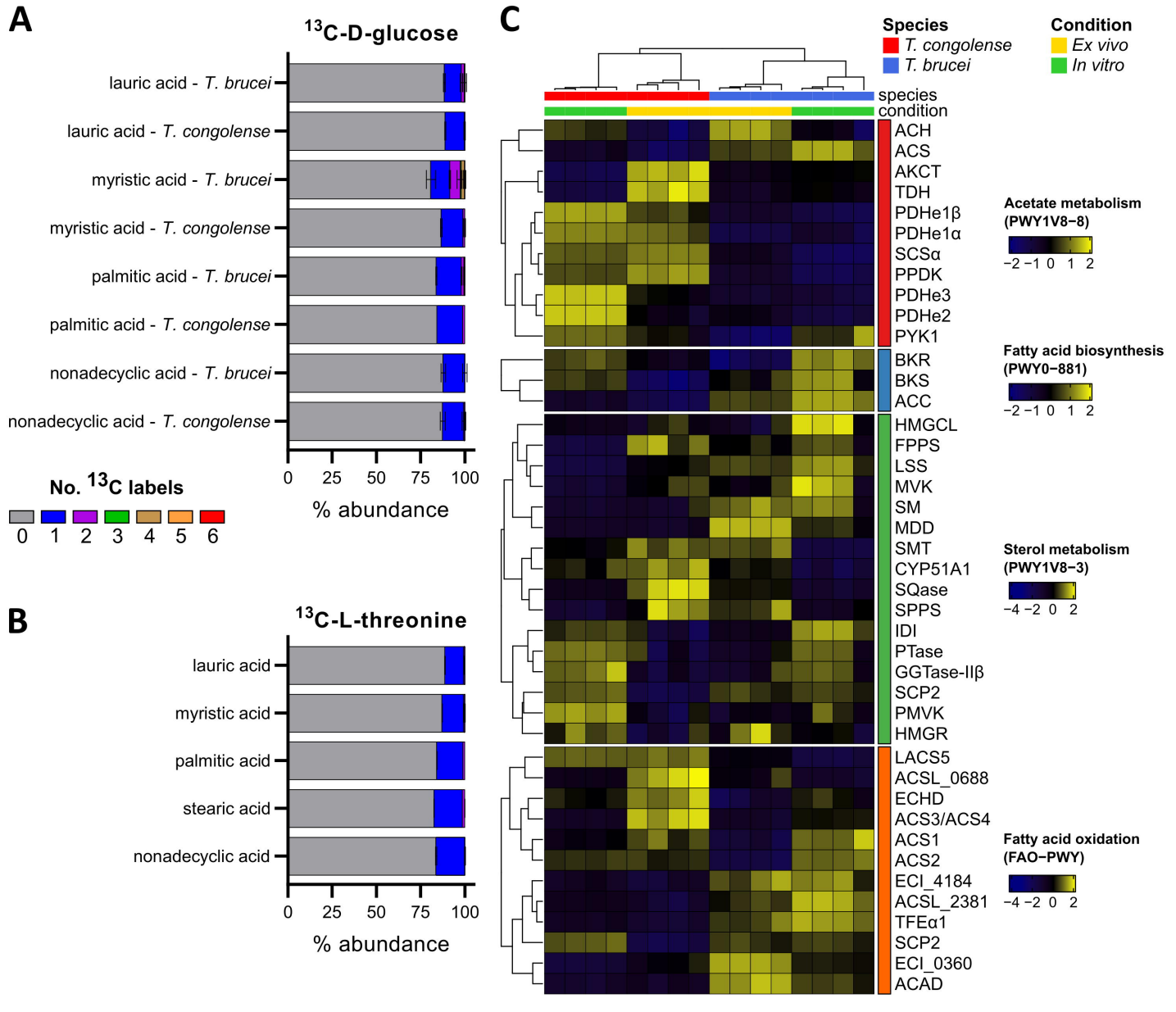
A
^{13}C-D-glucose
lauric acid - T. brucei
lauric acid - T. congolense
myristic acid - T. brucei
myristic acid - T. congolense
palmitic acid - T. brucei
palmitic acid - T. congolense
nonadecyclic acid - T. brucei
nonadecyclic acid - T. congolense
0 25 50 75 100
% abundance
No. ^{13}C labels
0 1 2 3 4 5 6
B
^{13}C-L-threonine
lauric acid
myristic acid
palmitic acid
stearic acid
nonadecyclic acid
0 25 50 75 100
% abundance
C
Species
T. congolense
T. brucei
Condition
Ex vivo
In vitro
species
condition
ACH
ACS
AKCT
TDH
PDHe1β
PDHe1α
SCSα
PPDK
PDHe3
PDHe2
PYK1
BKR
BKS
ACC
HMGCL
FPPS
LSS
MVK
SM
MDD
SMT
CYP51A1
SQase
SPPS
IDI
PTase
GGTase-IIβ
SCP2
PMVK
HMGR
LACS5
ACSL_0688
ECHD
ACS3/ACS4
ACS1
ACS2
ECI_4184
ACSL_2381
TFEα1
SCP2
ECI_0360
ACAD
Acetate metabolism
(PWY1V8−8)
−2 −1 0 1 2
Fatty acid biosynthesis
(PWY0−881)
−2 −1 0 1 2
Sterol metabolism
(PWY1V8−3)
−4 −2 0 2
Fatty acid oxidation
(FAO−PWY)
−4 −2 0 2

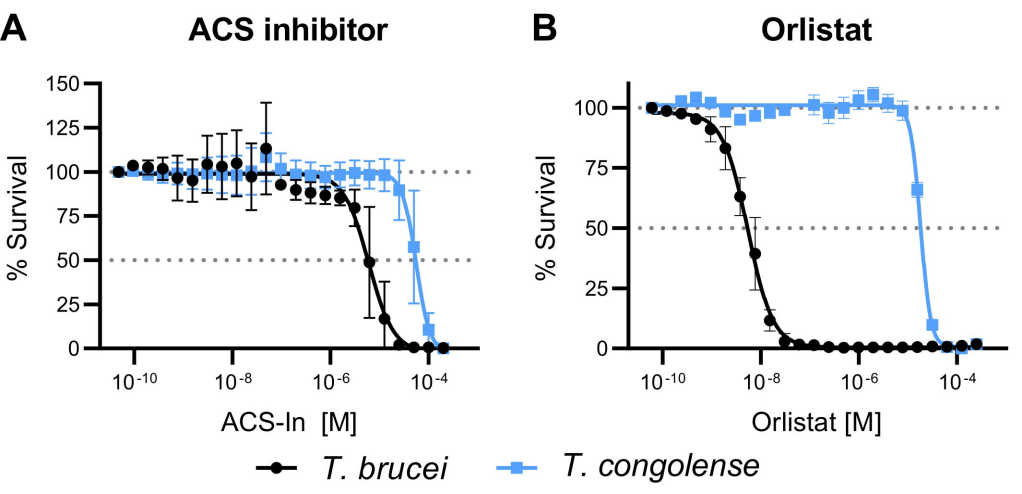
A
ACS inhibitor
% Survival
150
125
100
75
50
25
0
10-10
10-8
10-6
10-4
ACS-In [M]
B
Orlistat
% Survival
100
75
50
25
0
10-10
10-8
10-6
10-4
Orlistat [M]
T. brucei
T. congolense

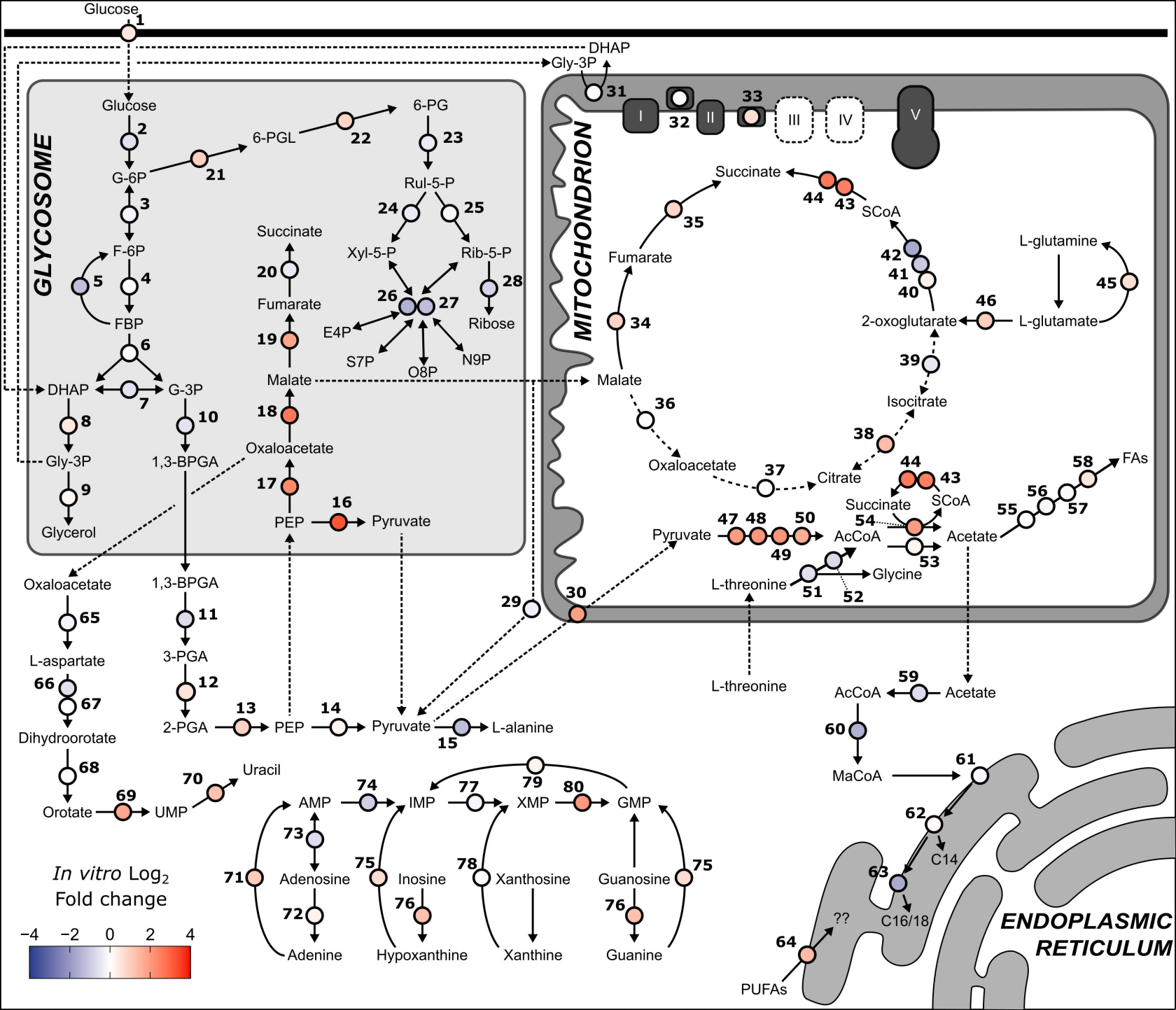
Glucose
1
DHAP
Gly-3P
31
I
32
II
33
III
IV
V
GLYCOSOME
MITOCHONDRION
Glucose
2
G-6P
21
6-PGL
22
6-PG
23
3
F-6P
5
4
FBP
6
24
25
Rul-5-P
Xyl-5-P
Rib-5-P
28
26
27
E4P
S7P
O8P
N9P
Ribose
Succinate
20
Fumarate
19
Malate
18
Oxaloacetate
17
PEP
16
Pyruvate
DHAP
7
G-3P
8
10
Gly-3P
9
Glycerol
1,3-BPGA
Succinate
44
43
SCoA
35
Fumarate
34
42
41
40
2-oxoglutarate
46
L-glutamine
45
L-glutamate
39
Isocitrate
Malate
36
38
Oxaloacetate
37
Citrate
44
43
SCoA
Succinate
58
FAs
56
57
55
54
47
48
50
Pyruvate
AcCoA
Acetate
49
53
L-threonine
51
52
Glycine
29
30
Oxaloacetate
65
1,3-BPGA
11
L-aspartate
66
67
3-PGA
12
Dihydroorotate
68
2-PGA
13
PEP
14
Pyruvate
15
L-alanine
L-threonine
AcCoA
59
Acetate
60
MaCoA
61
62
C14
63
C16/18
??
64
PUFAs
ENDOPLASMIC
RETICULUM
Orotate
69
UMP
70
Uracil
AMP
74
IMP
77
XMP
79
80
GMP
73
71
Adenosine
75
Inosine
78
Xanthosine
Guanosine
75
72
76
76
Adenine
Hypoxanthine
Xanthine
Guanine
In vitro Log2
Fold change
−4
−2
0
2
4

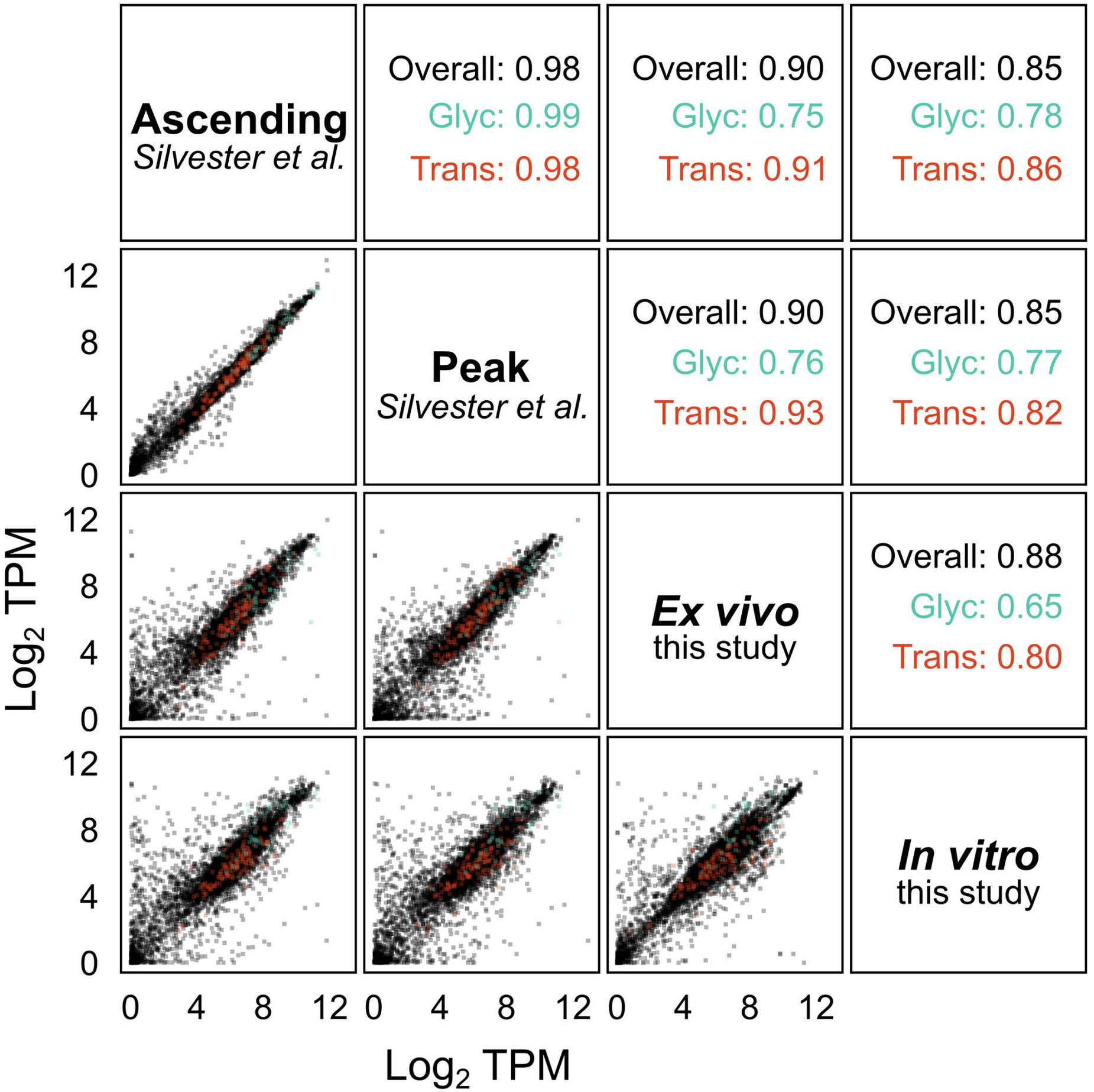
Ascending
Silvester et al.
Overall: 0.98
Glyc: 0.99
Trans: 0.98
Overall: 0.90
Glyc: 0.75
Trans: 0.91
Overall: 0.85
Glyc: 0.78
Trans: 0.86
Peak
Silvester et al.
Overall: 0.90
Glyc: 0.76
Trans: 0.93
Overall: 0.85
Glyc: 0.77
Trans: 0.82
Ex vivo
this study
Overall: 0.88
Glyc: 0.65
Trans: 0.80
In vitro
this study
Log2 TPM
Log2 TPM
0
4
8
12

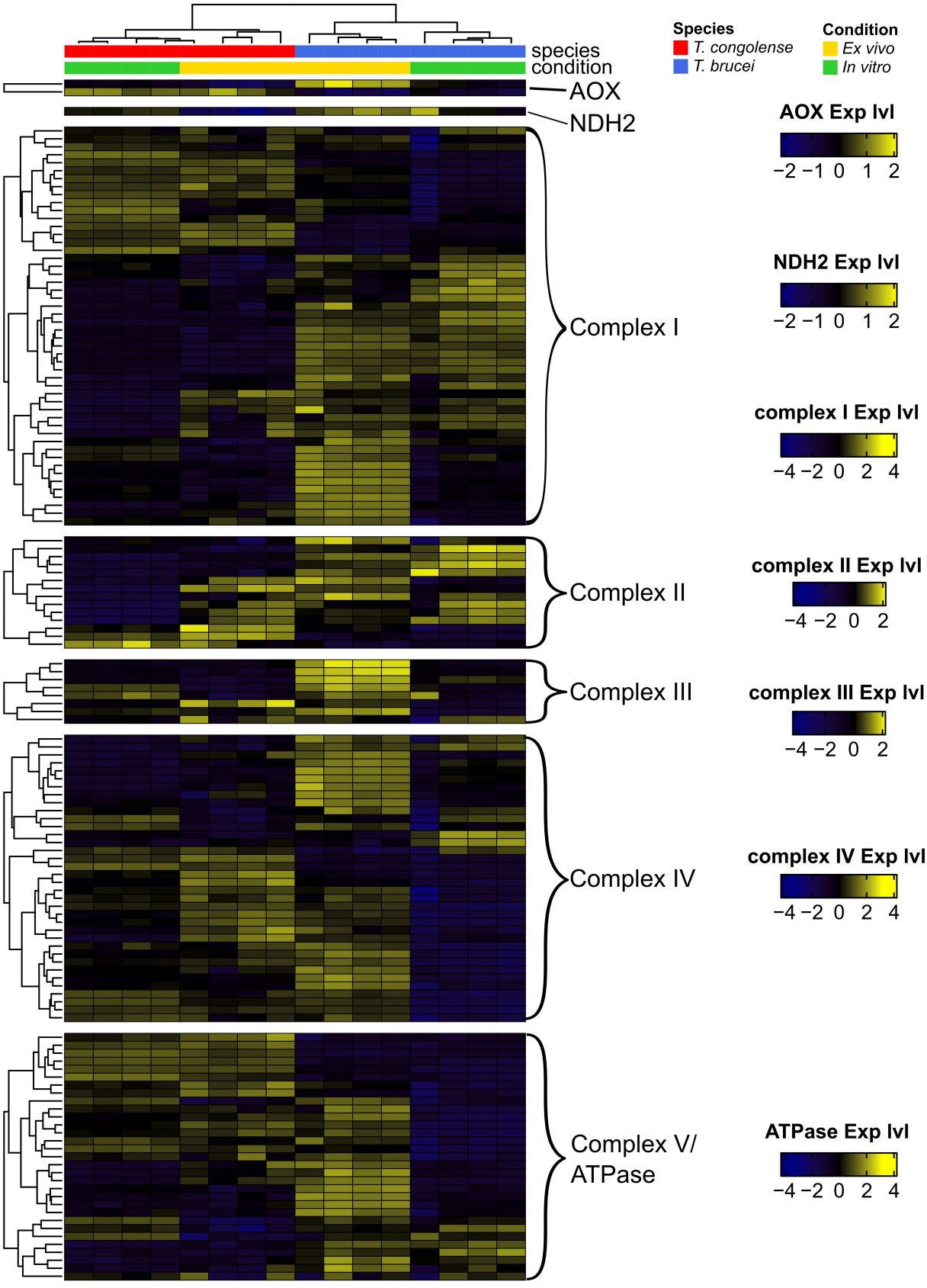
Species
T. congolense
T. brucei
Condition
Ex vivo
In vitro
species
condition
AOX
NDH2
AOX Exp lvl
−2 −1 0 1 2
NDH2 Exp lvl
−2 −1 0 1 2
Complex I
complex I Exp lvl
−4 −2 0 2 4
Complex II
complex II Exp lvl
−4 −2 0 2
Complex III
complex III Exp lvl
−4 −2 0 2
Complex IV
complex IV Exp lvl
−4 −2 0 2 4
Complex V/
ATPase
ATPase Exp lvl
−4 −2 0 2 4

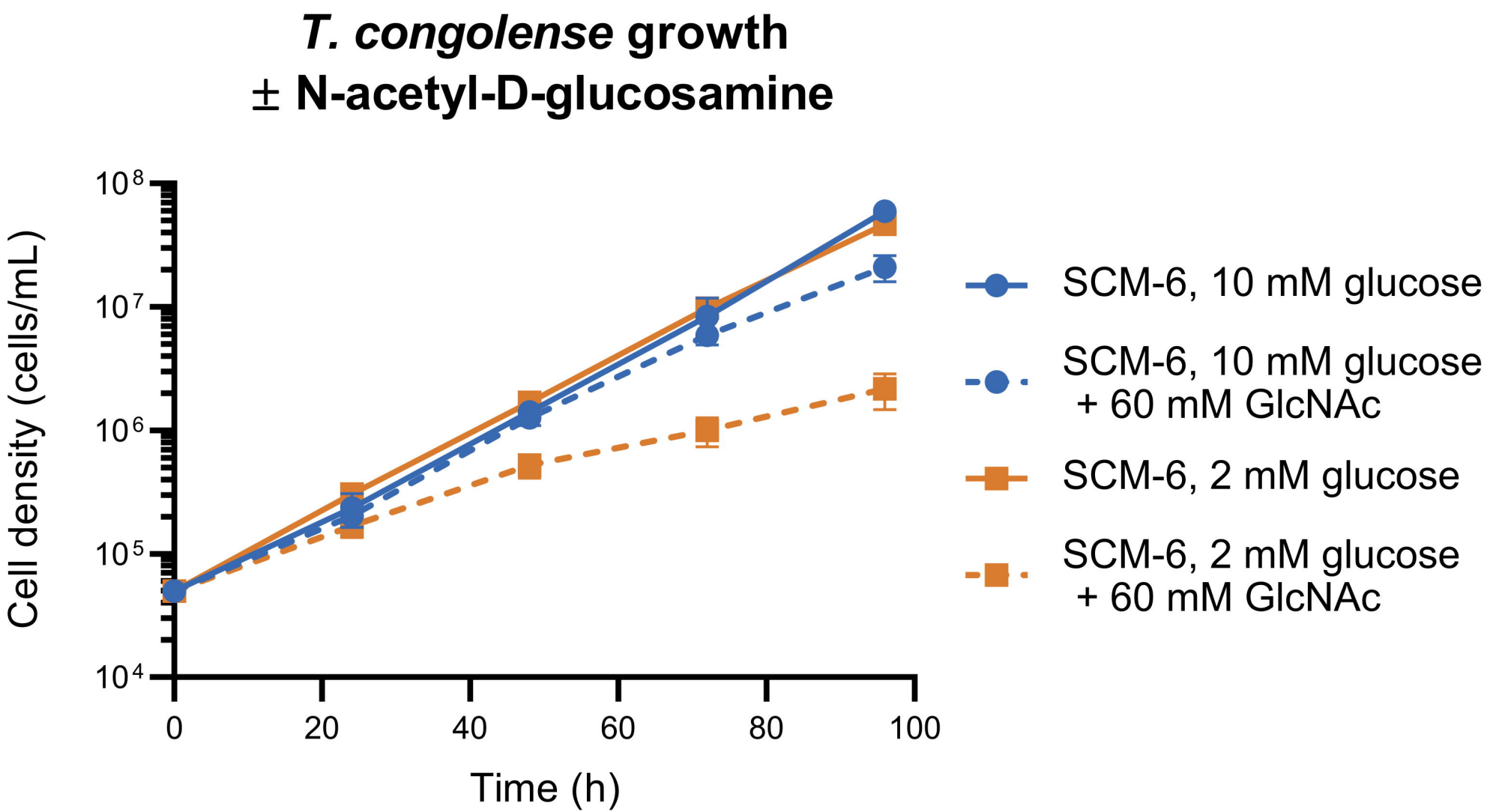
T. congolense growth
± N-acetyl-D-glucosamine
Cell density (cells/mL)
10^8
10^7
10^6
10^5
10^4
0
20
40
60
80
100
Time (h)
SCM-6, 10 mM glucose
SCM-6, 10 mM glucose + 60 mM GlcNAc
SCM-6, 2 mM glucose
SCM-6, 2 mM glucose + 60 mM GlcNAc

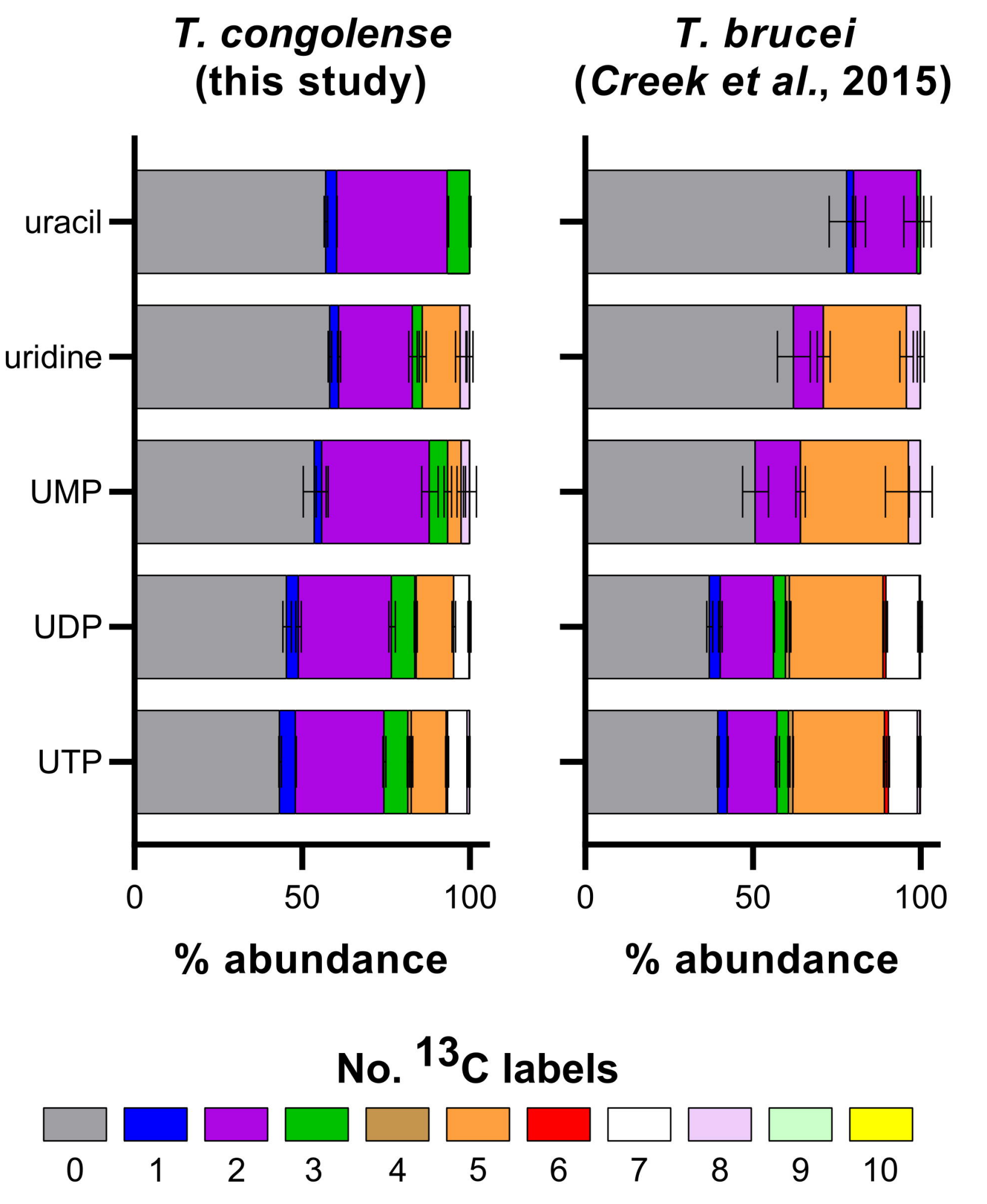
T. congolense
(this study)
T. brucei
(Creek et al., 2015)
uracil
uridine
UMP
UDP
UTP
0
50
100
% abundance
No. 13C labels
0
1
2
3
4
5
6
7
8
9
10

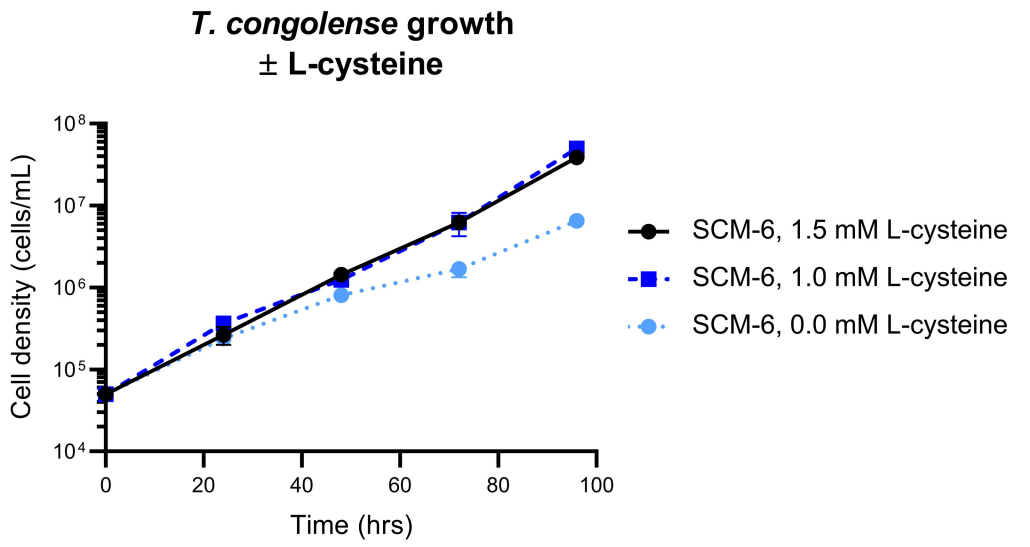
T. congolense growth
± L-cysteine
Cell density (cells/mL)
10^8
10^7
10^6
10^5
10^4
0
20
40
60
80
100
Time (hrs)
SCM-6, 1.5 mM L-cysteine
SCM-6, 1.0 mM L-cysteine
SCM-6, 0.0 mM L-cysteine

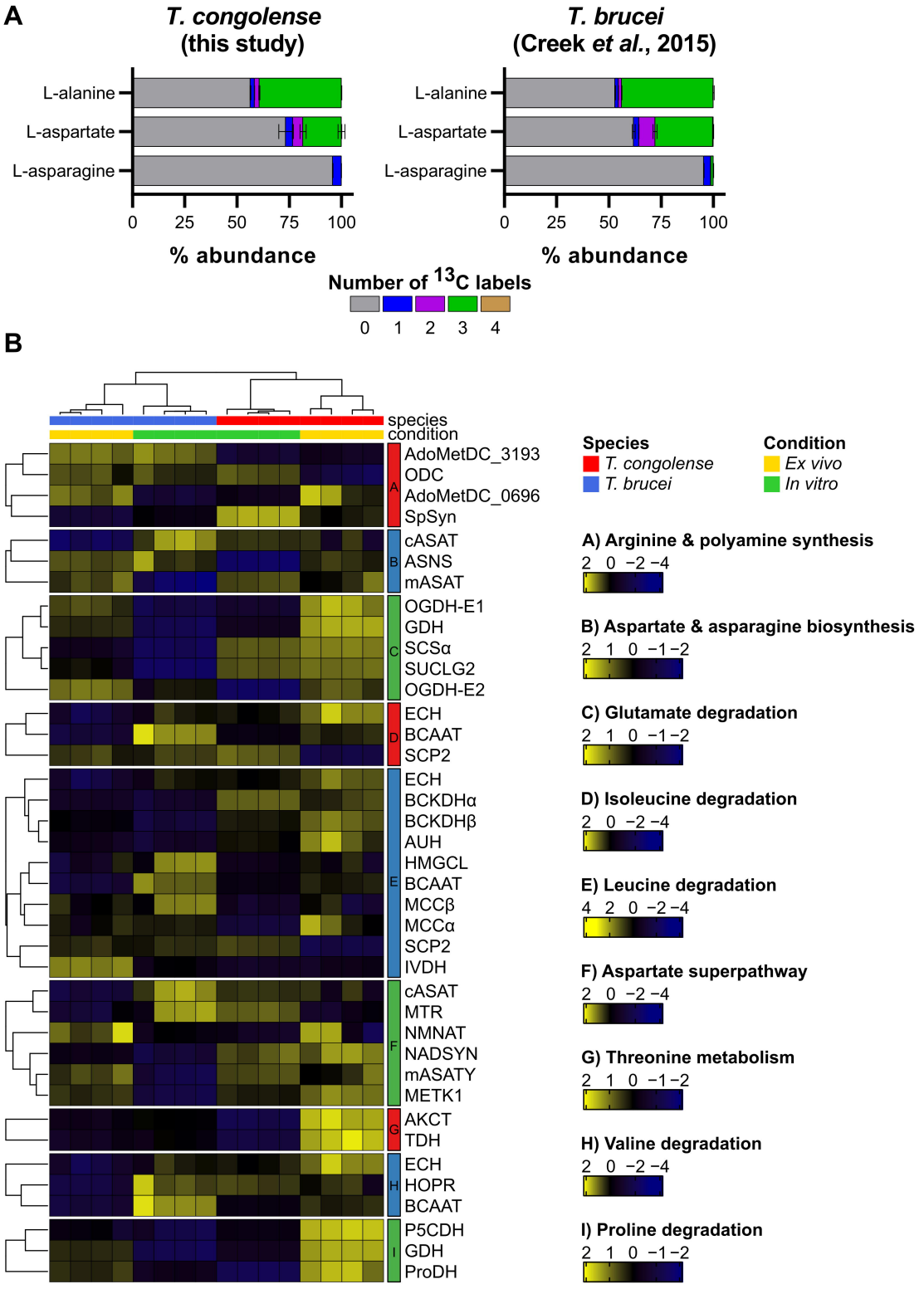
A
T. congolense
(this study)
T. brucei
(Creek et al., 2015)
L-alanine
L-aspartate
L-asparagine
0
25
50
75
100
% abundance
Number of 13C labels
0 1 2 3 4
B
species
condition
AdoMetDC_3193
ODC
AdoMetDC_0696
SpSyn
cASAT
ASNS
mASAT
OGDH-E1
GDH
SCSα
SUCLG2
OGDH-E2
ECH
BCAAT
SCP2
ECH
BCKDHα
BCKDHβ
AUH
HMGCL
BCAAT
MCCβ
MCCα
SCP2
IVDH
cASAT
MTR
NMNAT
NADSYN
mASATY
METK1
AKCT
TDH
ECH
HOPR
BCAAT
P5CDH
GDH
ProDH
Species
T. congolense
T. brucei
Condition
Ex vivo
In vitro
A) Arginine & polyamine synthesis
2 0 −2 −4
B) Aspartate & asparagine biosynthesis
2 1 0 −1 −2
C) Glutamate degradation
2 1 0 −1 −2
D) Isoleucine degradation
2 0 −2 −4
E) Leucine degradation
4 2 0 −2 −4
F) Aspartate superpathway
2 0 −2 −4
G) Threonine metabolism
2 1 0 −1 −2
H) Valine degradation
2 0 −2 −4
I) Proline degradation
2 1 0 −1 −2

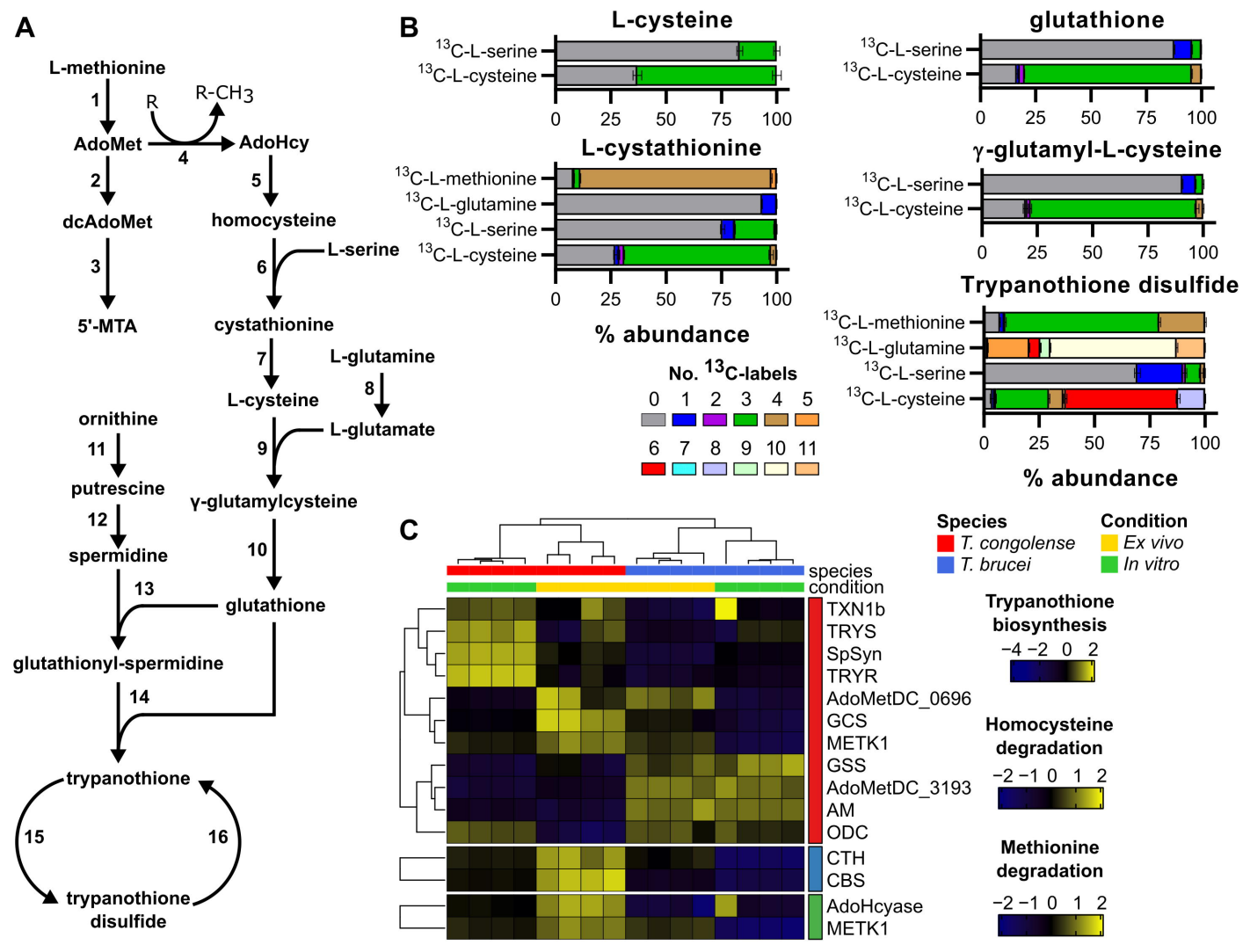
A
L-methionine
1
R
R-CH3
AdoMet
AdoHcy
4
2
5
dcAdoMet
homocysteine
3
6
L-serine
5'-MTA
cystathionine
7
L-glutamine
8
L-cysteine
ornithine
11
9
L-glutamate
putrescine
γ-glutamylcysteine
12
10
spermidine
13
glutathione
glutathionyl-spermidine
14
trypanothione
15
16
trypanothione disulfide
B
L-cysteine
13C-L-serine
13C-L-cysteine
0 25 50 75 100
L-cystathionine
13C-L-methionine
13C-L-glutamine
13C-L-serine
13C-L-cysteine
0 25 50 75 100
% abundance
No. 13C-labels
0 1 2 3 4 5
6 7 8 9 10 11
glutathione
13C-L-serine
13C-L-cysteine
0 25 50 75 100
γ-glutamyl-L-cysteine
13C-L-serine
13C-L-cysteine
0 25 50 75 100
Trypanothione disulfide
13C-L-methionine
13C-L-glutamine
13C-L-serine
13C-L-cysteine
0 25 50 75 100
% abundance
C
species
condition
TXN1b
TRYS
SpSyn
TRYR
AdoMetDC_0696
GCS
METK1
GSS
AdoMetDC_3193
AM
ODC
CTH
CBS
AdoHcyase
METK1
Species
T. congolense
T. brucei
Condition
Ex vivo
In vitro
Trypanothione biosynthesis
−4 −2 0 2
Homocysteine degradation
−2 −1 0 1 2
Methionine degradation
−2 −1 0 1 2

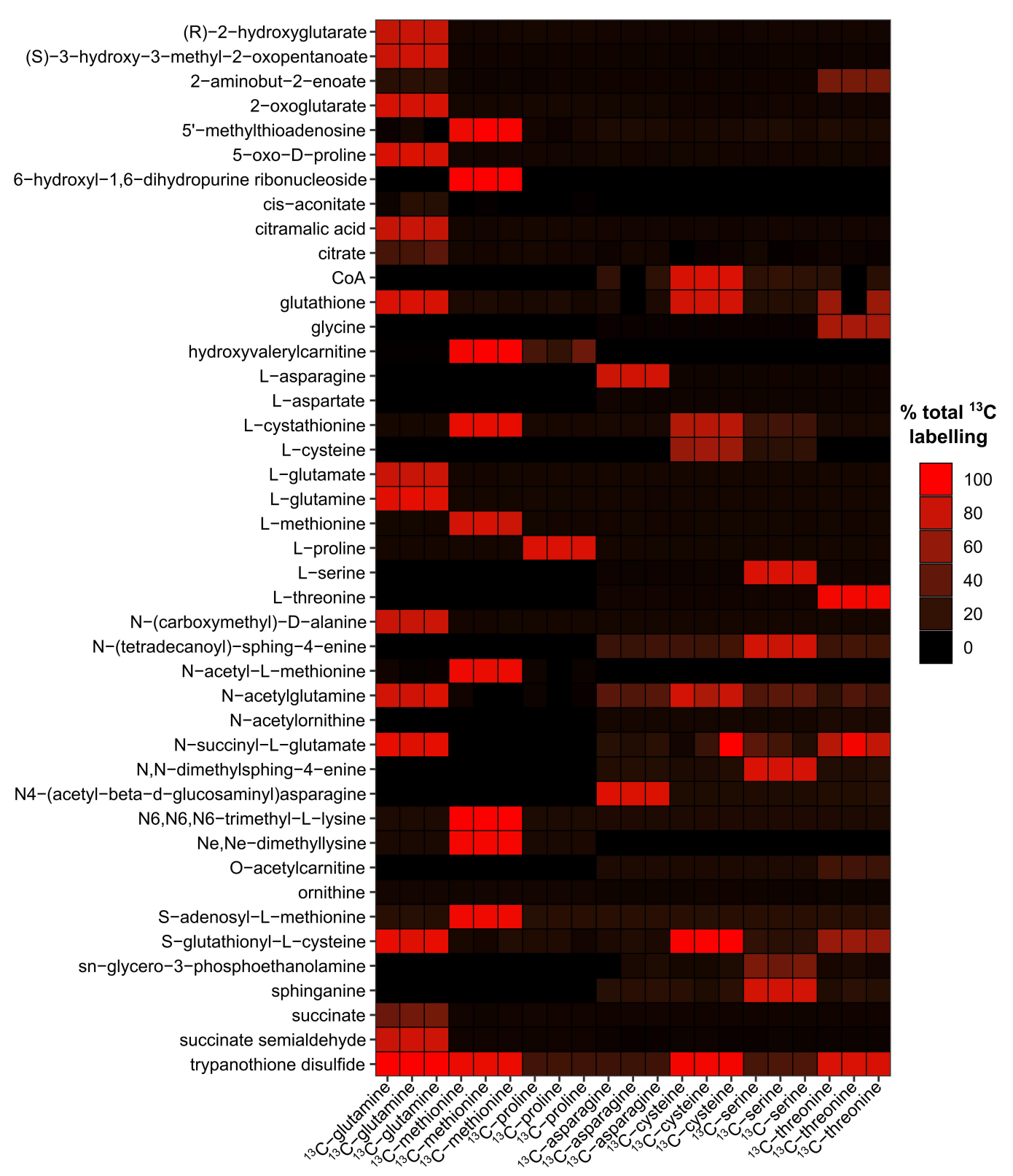
(R)−2−hydroxyglutarate
(S)−3−hydroxy−3−methyl−2−oxopentanoate
2−aminobut−2−enoate
2−oxoglutarate
5'−methylthioadenosine
5−oxo−D−proline
6−hydroxyl−1,6−dihydropurine ribonucleoside
cis−aconitate
citramalic acid
citrate
CoA
glutathione
glycine
hydroxyvalerylcarnitine
L−asparagine
L−aspartate
L−cystathionine
L−cysteine
L−glutamate
L−glutamine
L−methionine
L−proline
L−serine
L−threonine
N−(carboxymethyl)−D−alanine
N−(tetradecanoyl)−sphing−4−enine
N−acetyl−L−methionine
N−acetylglutamine
N−acetylornithine
N−succinyl−L−glutamate
N,N−dimethylsphing−4−enine
N4−(acetyl−beta−d−glucosaminyl)asparagine
N6,N6,N6−trimethyl−L−lysine
Ne,Ne−dimethyllysine
O−acetylcarnitine
ornithine
S−adenosyl−L−methionine
S−glutathionyl−L−cysteine
sn−glycero−3−phosphoethanolamine
sphinganine
succinate
succinate semialdehyde
trypanothione disulfide
% total 13C labelling
100
80
60
40
20
0
13C−glutamine
13C−glutamine
13C−glutamine
13C−methionine
13C−methionine
13C−methionine
13C−proline
13C−proline
13C−proline
13C−asparagine
13C−asparagine
13C−asparagine
13C−cysteine
13C−cysteine
13C−cysteine
13C−serine
13C−serine
13C−serine
13C−threonine
13C−threonine
13C−threonine